Development and application of spin dependent van der Waals density functional method

Doctoral Thesis

Development and application of spin dependent van der Waals density functional method

Division of Mathematical and Physical Sciences

Graduated School of Science and Technology,

Kanazawa University

Student ID Number : 1424012003

Name : Masao Obata

Chief supervisor : Prof. Tatsuki Oda

July 1st, 2016

Contents

List of Figures

List of Tables

Chapter 1

Introduction

Computational science, as the computer performance develops, has become an essential approach in the scientific field. Exploitation and improvement in the calculation method such as algorithm, not only in the development of the computer performance have progressed continuously. In the filed of condensed matter physics, computational science, in particularly, first-principles approach has been recognized as a useful tool of for investigating the electronic state of material. Since explanation of experimental facts is emphasized, the differences between experiments and theory are not taken care so much, meaning that computational science had a role to understand the rough electronic state. This role is also important for computational science but society, in particular environmental or energy issues that require innovation, expect further results from computational science, in additional to the description of the experiment.

One of important roles is a highly accurate prediction of physical properties on uninvestigated or unidentified materials in experience, and it is necessary to perform a quantitative predictions rather than qualitative. This is because the investigation of these substances by first-principles approach is very useful to material development, leading to material design. There are many developments of high-performance materials using a complex substance in recent years, and the importance of theoretical calculation is increasing year by year because these crystals and molecules have complicated structures which could not be obtained in detail in experiment. For such purposes, some methods that can predict physics quantity in reasonable computational cost are highly desirable. However, in general, computational cost increases for increasing computational accuracy, requiring a reduced computational system size. For example, configuration interaction method which is one of the most accurate method to solve Schrödinger equation, could

handle relatively small molecules.

Density functional theory (DFT) approach, in fact, Kohn and Sham approach based on DFT, has been proposed by the researchers of K. Hohenberg, W. Kohn, and L. J. Sham, is one of promising methods achieving many successes[5, 6]. And it can also treat relatively large system size compared with the other electronic state calculations. The calculations of more than 1000 atoms were already carried out using highly massive parallel computing although the system size depends on the calculation methods or conditions, namely basis set, number of Kohn-Sham orbitals, handling of core electrons, magnetism, and relativistic effect, etc. Since the calculations of 1000-order atoms can handle the relatively complex molecular and crystal, DFT approach seems to be suitable for materials design. Of course, computable system size should be increase and some algorithms, such as the linear-scaling or order-N schemes (N is number of Kohn-Sham orbitals), are ready for practical use [7]. The detail of DFT and Kohn-Sham approach will be reviewed in Chapter 2.

However it is known to general DFT approach have some problems for accuracy, for example, band gap underestimation and disregard of van der Waals (vdW) force are well known problem. In particular vdW force is important to predict the crystal and molecular structure in weakly bound systems e.g.: layered material, protein system, neutral molecule systems. vdW force is famous interaction, and we already know that vdW potential (V_{disp}), at a distance r from the atom on appropriate distance, can be written as

$$V_{\mathrm{disp}} = -\frac{C_6}{r^6}, \tag{1.1}$$

where C_6 is vdW coefficient which is parameter depending on atomic or molecular species. But it is not as simple as it seem because the origin is interaction between instantaneously induce dipoles caused by quantum fluctuation and C_6 coefficient exactly depends on electronic state. These facts indicate that vdW force should be estimated by electron electronic state calculation.

Since DFT is an exact theory for a ground state, all of the problems for accuracy in ground state which lies in an approximation of exchange-correlation energy functional that describes the quantum-mechanical effect. Exchange energy is obtained from

Hartree-Fock theory and correlation energy is defined as all of the leftover effects. vdW force is classified in correlation effect because it is quantum effect, not exchange. Local density approximation (LDA) or generalized gradient approximation (GGA) are used for approximation of exchange-correlation energy and these approaches having a lot of success despite the rough approximation. LDA exchange-correlation energy is as follows:

$$E_{\rm xc}^{\rm LDA} = \int d\mathbf{r} n \epsilon_{\rm xc}(n), \tag{1.2}$$

where n is electron density and $\epsilon_{\rm xc}$ is free electron exchange-correlation energy on density n. In the GGA, $\epsilon_{\rm xc}$ is estimated from electron density and its gradient. Therefore nonlocal effect, like vdW force, can not be taken into account in LDA/GGA. For the material design, this problem must be solved.

M. Dion et al. have proposed vdW-DF approach and introduced nonempirical and nonlocal correlation energy functional to describe nonlocal electron correlation effect such as the vdW force.[8] They had succeeded the development of nonlocal correlation kernel depending on electron charge density by using some approximations. The detail of vdW-DF is reviewed in Chapter 3. We introduced the method to our DFT code, and show some applications in Chapter 6.

Applications of vdW-DF remain with in nonmagnetic systems. The extension of its approach to the magnetism is important in increasing the range of applications of the DFT, supporting material design. For example, the interface between magnetic surface and organic molecules is investigated as a candidate of organic-spintronics devices [9]. Therefore, we proposed the extension for spin polarized system named vdW-DF-SGC explained in Chapter 5 and some applications will be described in Chapter 6. In Chapter 7, we will show that the possibility for improvement of vdW-DF-SGC method in oxygen systems.

Since vdW-DF approach employs GGA exchange functional, the error of exchange energy is not be corrected the vdW-DF approach. Sometimes electron correlation effect, such as on-site Coulomb play an important role in magnetic system. Therefore we will also introduce *GW* approximation reviewed in Chapter 4 as more accurate electronic state calculation. This method need to be investigated, and is helpful to improve the vdW-DF approach.

Chapter 2

Overview of first-principles calculation based on density function theory

In this chapter, the basic theory on the first-principles calculation method of density functional theory will be reviewed [10, 11]. Consequently, the difficulty of local density approximation or generalized gradient approximation will be described.

2.1 Density functional theory

As it is well known that density functional theory (DFT) approach is one of fully promising methods has been achieving a lot of successes in not only solid material physics. Owing to the expansion of the computational sources, it has been applied to not only solid material but also to cluster system such as a protein.

2.2 Hohenberg and Kohn theorem

Density functional theory is based on Hohenberg and Kohn theorem [5]. Here we consider the system has the electron potential of ions written as follows:

$$v_{\text{ext}} = \sum_{\mathbf{R}_I} v_I(\mathbf{r} - \mathbf{R}_I). \tag{2.1}$$

Assuming that there is no degeneracy on the ground state, it can be determined on uniquely by using the external potential. There is a one-to-one correspondence between

the one-electron density and the external potential v_{ext}. If the external potential which provide a one-electron density of the ground state is determined uniquely, the ground state of the system will be uniquely determined by the one-electron density.

P. Hohenberg and W. Kohn demonstrate that the external potential v_{ext} can be determined on uniquely for given electron density. Here we assumed the existence of v_{ext} with respect to given one particle electron density (v representation). This assumption is specious, but it is unproven. Therefore, a weaker constraint (N representation) of one particle electron density that can be constructed by antisymmetric wave function ψ^n was considered;

$$n(\mathbf{r}) = N \int d\xi_1 dx_2 \cdots dx_n |\psi^n(x_1, x_2, \cdots, x_n)|^2. \tag{2.2}$$

where x is composite index for position $\mathbf{r}$ and spin coordinate ζ. N representation is weaker construction than v representation. If the v representation is realized, the external potential v_{ext} with respect to ground state electron density $n(\mathbf{r})$ can be exist, and the ground state wave function can be determined. Therefore N representation is satisfied. However there is no uniquely for wave function that can express the one particle electron density $n(\mathbf{r})$. Now we consider the antisymmetric wave function ψ^n_{min} satisfied with the following conditions.

- Give the electron density $n(\mathbf{r})$
- Give the minimum expected value of sum of the kinetic and electron-electron interaction V_{ee}

The expected value of sum of kinetic and electron-electron interaction by using ψ^n_{min} $F[n] = \langle \psi^n_{min} | \, T + V_{ee} \, | \psi^n_{min} \rangle$ is functional of electron density, because ψ^n_{min} is determined by the electron density n. Since F is functional of $n(\mathbf{r})$, it is independent on external potential (independent on material). Hohenberg and Kohn's theorem by using $F[n]$ is as follows:

- Variational principle for the energy functional on ground state : the energy functional depending one particle electron density $n(\mathbf{r})$ satisfied with N-representation

defined as follows:

$$E[n] = \int d\mathbf{r} v_{\text{ext}}(\mathbf{r}) n(\mathbf{r}) + F[n] \tag{2.3}$$

Then ground state energy of this system E_{GS} is lower limit of $E[n]$.

- The possibility of one electron density representation : the ground state energy E_{GS} can be given by the following formula as a functional of one particle electron density n_{GS};

$$E_{\text{GS}} = \int d\mathbf{r} v_{\text{ext}}(\mathbf{r}) n_{\text{GS}}(\mathbf{r}) + F[n_{\text{GS}}]. \tag{2.4}$$

The main message of this theorem is the existence of one particle electron density and universal functional $F[n]$ that can give the total energy on the ground state. In other words, the total energy on ground state can be estimated by electron density $n(\mathbf{r})$ without solving the many body Schrödinger equation.

2.3 Kohn-Sham method

Hohenberg and Kohn's theorem showed theoretical framework. However this theorem does not provide the F, we should defined F function for obtaining the total energy[6]. W. Kohn and L. J. Sham had suggested the functional formula of F as follows:

$$F[n] = T_s[n] + \frac{1}{2} \iint d\mathbf{r} d\mathbf{r}' \frac{n(\mathbf{r}) n(\mathbf{r}')}{|\mathbf{r} - \mathbf{r}'|} + E_{\text{xc}}[n]. \tag{2.5}$$

The first term on right hand side is kinetic energy with respect to ideal non interacting system having electron density n, second term is classical coulomb interaction called Hartree energy, and third term is exchange correlation energy that contains all quantum effect. By introducing of non-interacting virtual system (Kohn-Sham auxiliary system) having electron density n, many body problem can be replaced to an effective one particle

problem. Therefore Kohn-Sham auxiliary system satisfied with the following formula;

$$\left[-\frac{1}{2}\nabla^2 + v(\mathbf{r})\right]\psi_i(\mathbf{r}) = \varepsilon_i\psi_i(\mathbf{r}), \tag{2.6}$$

$$n(\mathbf{r}) = \sum_i |\psi_i(\mathbf{r})|^2. \tag{2.7}$$

where v is effective one particle potential and summation of index i go until the number of electrons. The kinetic energy can be defined as

$$T_s[n] = -\frac{1}{2}\sum_i \int d\mathbf{r}\psi_i^*(\mathbf{r})\nabla^2\psi_i(\mathbf{r}). \tag{2.8}$$

It can be also written as

$$T_s[n] = \sum_i \varepsilon_i - \int d\mathbf{r}v(\mathbf{r})n(\mathbf{r}). \tag{2.9}$$

Therefore the total energy depending on electron density n is written as

$$E[n] = \sum_i \varepsilon_i - \int d\mathbf{r}v(\mathbf{r})n(\mathbf{r}) + \int d\mathbf{r}v_{\text{ext}}(\mathbf{r})n(\mathbf{r}) + \frac{1}{2}\iint d\mathbf{r}d\mathbf{r}'\frac{n(\mathbf{r})n(\mathbf{r}')}{|\mathbf{r}-\mathbf{r}'|} + E_{\text{xc}}, \tag{2.10}$$

where $v(\mathbf{r})$ can be estimated from variational equation on the total energy with respect to electron density. Now we consider n is the grand state electron density ($\delta E[n] = 0$).

$$\begin{aligned}\delta E[n] = &\int d\mathbf{r}\delta v(\mathbf{r})n(\mathbf{r}) - \int d\mathbf{r}\delta n(\mathbf{r})v(\mathbf{r}) - \int d\mathbf{r}\delta v(\mathbf{r})n(\mathbf{r}) \\ &+ \int d\mathbf{r}\delta n(\mathbf{r})\left[v_{\text{ext}}(\mathbf{r}) + \int d\mathbf{r}'\frac{n(\mathbf{r}')}{|\mathbf{r}-\mathbf{r}'|} + \frac{\delta E_{\text{xc}}[n]}{\delta n(\mathbf{r})}\right]\end{aligned} \tag{2.11}$$

The following formula is used.

$$\sum_i \delta\varepsilon_i = \int d\mathbf{r}\delta v(\mathbf{r})n(\mathbf{r}) \tag{2.12}$$

By using the condition on conservation of the number of electrons written $\int d\mathbf{r}\delta n(\mathbf{r}) = 0$, we can get v as follows:

$$v(\mathbf{r}) = v_{\text{ext}}(\mathbf{r}) + \int d\mathbf{r}'\frac{n(\mathbf{r}')}{|\mathbf{r}-\mathbf{r}'|} + \frac{\delta E_{\text{xc}}[n]}{\delta n(\mathbf{r})} \tag{2.13}$$

The second and third terms of right hand side is Hartree potential and exchange correlation potential, respectively. Exchange correlation potential is driven by functional differential of exchange correlation energy.

$$\left[-\frac{1}{2}\nabla^2 + v_{\mathrm{ext}}(\mathbf{r}) + \int d\mathbf{r}' \frac{n(\mathbf{r}')}{|\mathbf{r}-\mathbf{r}'|} + \frac{\delta E_{\mathrm{xc}}[n]}{\delta n(\mathbf{r})}\right]\psi_i(\mathbf{r}) = \varepsilon\psi_i(\mathbf{r}) \tag{2.14}$$

This is called Kohn-Sham equation. This is nonlinear equation and should be solved on self-consistent filed. Since there is no approximation on this derivation, if we can know the exact formula of E_{xc}, this equation gave the exact one particle electron density and the total energy on ground state.

2.4 Local density approximation

The exchange correlation energy includes all quantum effect, indicating that it is important to describe it for the investigation of quantum effect e.g: magnetism, electron correlation. If this energy is neglected, we can not get the reasonable physical quantity such as crystal or molecule structure, binding energy, chemical reaction, even if it has small energy order compared with total energy. We should employ the some approximation for exchange correlation energy, because the computable exact formulation for correlation energy function can not be founded. For the exchange term, Hartree Fock exchange, however it is exact exchange formula, require a high computational resources and it is not suitable for solid material. Therefore a much simplified formula for the exchange correlation energy which called local density approximation (LDA) is employed for a long time. The LDA exchange correlation energy functional can be written as

$$E_{\mathrm{xc}} = \int d\mathbf{r}\epsilon_{\mathrm{xc}}(n(\mathbf{r}))n(\mathbf{r}). \tag{2.15}$$

Here $\epsilon_{\mathrm{xc}} = \epsilon_{\mathrm{x}} + \epsilon_{\mathrm{c}}$, which is introduced from free electron model, is one electron exchange and correlation energy. ϵ_{c} can be used some approximated formula because the exact formula of it can not be discovered [12].

The more reasonable approximation "generalized gradient approximation (GGA)" which is more mainstream than LDA has been proposed. The difference between LDA and GGA is the way of estimation for ϵ_{xc}. Is is function of the electron density on

LDA, but GGA requires not only the density but also its gradient. The GGA exchange correction energy is

$$E_{\rm xc} = \int d\mathbf{r}\epsilon_{\rm xc}(n(\mathbf{r}), |\nabla n(\mathbf{r})|)n(\mathbf{r}). \tag{2.16}$$

The potential of GGA ($v_{\rm xc}$)can be estimated by

$$\delta E_{\rm xc} = \frac{\Omega}{N_{grid}} \sum_j \frac{df_{\rm xc}}{dn(\mathbf{r}_j)}\delta n = \frac{\Omega}{N_{grid}} \sum_j v_{\rm xc}(\mathbf{r}_j)\delta n \tag{2.17}$$

$$v_{\rm xc}(\mathbf{r}_j) = \frac{\partial f_{\rm xc}}{\partial n(\mathbf{r}_j)} + \sum_k \frac{\partial f_{\rm xc}}{\partial \nabla n(\mathbf{r}_k)} \cdot \frac{d\nabla n(\mathbf{r}_k)}{dn(\mathbf{r}_j)}, . \tag{2.18}$$

where $f_{\rm xc} = n\varepsilon_{\rm xc}$, Ω is the volume of the unit cell and N_{grid} is the number of FFT grids. Here we can use the following formula.

$$\nabla n(\mathbf{r}) = \sum_{\mathbf{G}} i\mathbf{G}n(\mathbf{G})e^{i\mathbf{G}\cdot\mathbf{r}} = \frac{1}{N_{grid}} \sum_{\mathbf{G},j} i\mathbf{G}n(\mathbf{r}_j)e^{i\mathbf{G}\cdot(\mathbf{r}-\mathbf{r}_j)}. \tag{2.19}$$

Finally, the GGA potential is computed by the following formula.

$$\begin{aligned} v_{\rm xc}(\mathbf{r}_j) =& \frac{\partial f_{\rm xc}}{\partial n(\mathbf{r}_j)} + \sum_{\mathbf{G},k} i\mathbf{G} \cdot \frac{\partial f_{\rm xc}}{\partial \nabla n(\mathbf{r}_k)} e^{i\mathbf{G}\cdot(\mathbf{r}_k-\mathbf{r}_j)} \\ =& \frac{\partial f_{\rm xc}}{\partial n(\mathbf{r}_j)} - \sum_{\mathbf{G}} e^{i\mathbf{G}\cdot\mathbf{r}_j} i\mathbf{G} \cdot \left(\frac{1}{N_{grid}} \sum_k \frac{\nabla n(\mathbf{r}_k)}{|\nabla n(\mathbf{r}_k)|} \frac{\partial f_{\rm xc}}{\partial |\nabla n(\mathbf{r}_k)|} e^{-i\mathbf{G}\cdot\mathbf{r}_k} \right). \end{aligned} \tag{2.20}$$

For expression deformation, White and Bird method is employed[13]. Using Fourier transformation, the density gradient can be calculated easily and in high accuracy. The function of $\epsilon_{\rm xc}(n, |\nabla n|)$ is proposed by many researchers [14, 15, 16, 17]. Roughly speaking, these GGA functionals give similar results about electronic, molecular, and crystal structures.

2.5 Adiabatic connection and exchange-correlation hole

The correlation energy contains both electron-electron interaction and correction to KS kinetic energy. However it can be described by the interaction among electron by using adiabatic connection [18]. In this concept, Hamiltonians is function of λ which can control the strength of electron interaction.

The system becomes non-interacting on $\lambda = 0$ case, on the other hand it becomes real system on $\lambda = 1$.

$$H(\lambda) = T + V_{\text{ext}} + \lambda \frac{1}{2} \sum_{i \neq j} \frac{1}{|\mathbf{r}_i - \mathbf{r}_j|} \tag{2.21}$$

where T is the kinetic energy operator and V_{ext} is the external potential ($V_{\text{ext}} = \sum_i v(\mathbf{r}_i)$). In any λ, it has been promised that the external potential $V[n, \lambda]$, that gives the ground state density $n(\mathbf{r})$ with respect to Hamiltonian $\tilde{H}(\lambda)$ define by following formula, is exist according to Hohenberg and Kohn's theorem.

$$\tilde{H}(\lambda) = H(\lambda) + V[n, \lambda]. \tag{2.22}$$

There is no electron interaction on $\lambda = 0$. The $V[n, \lambda = 0]$ is difference between Kohn-Sham potential V_s and external potential V_{ext}, on the other hand $V[n, \lambda = 1]$ vanishes on $\lambda = 1$. The total energy of $\tilde{H}(\lambda)$ is written as

$$E(\lambda) = \langle \psi(\lambda) | \, \tilde{H}(\lambda) \, | \psi(\lambda) \rangle = \langle \tilde{H}(\lambda) \rangle_\lambda \tag{2.23}$$

where $|\psi(\lambda)\rangle$ are eigenstates with respect to $\tilde{H}(\lambda)$. The $E(\lambda)$ can be written as

$$E(\lambda) = E(0) + \int_0^\lambda d\lambda' \left\langle \frac{dV[n, \lambda']}{d\lambda'} \right\rangle_{\lambda'} + \int_0^\lambda \frac{d\lambda'}{\lambda'} E_{\text{int}}(\lambda'). \tag{2.24}$$

where

$$E_{\text{int}}(\lambda) = \left\langle \frac{\lambda}{2} \sum_{i \neq j} \frac{1}{|\mathbf{r}_i - \mathbf{r}_j|} \right\rangle_\lambda \tag{2.25}$$

The $V[n, \lambda]$ is one particle potential, $V[n, \lambda] = \sum_i V[n, \lambda; \mathbf{r}_i]$. Hence

$$\begin{aligned} \int_0^1 d\lambda \left\langle \frac{dV[n, \lambda]}{d\lambda} \right\rangle_\lambda &= \int_0^\lambda d\lambda \int d\mathbf{r} \frac{dV[n, \lambda; \mathbf{r}]}{d\lambda} n(\mathbf{r}) \\ &= - \int d\mathbf{r} V[n, 0; \mathbf{r}] n(\mathbf{r}) = - \langle V_s \rangle + \langle V_{\text{ext}} \rangle . \end{aligned} \tag{2.26}$$

The integration with respect to λ can be calculated the electron density which is independence from λ. Using $E(0) = \langle T_s \rangle + \langle V_s \rangle$(the total energy on $\lambda = 0$ state can be estimated by electron density, because it is Kohn-Sham's auxiliary system.), we get the following formula;

$$E(1) = \langle T_s \rangle + \langle V_{\rm ext} \rangle + \int_0^1 \frac{d\lambda}{\lambda} E_{\rm int}(\lambda). \tag{2.27}$$

Comparing with energy function on Kohn-Sham approach, exchange correlation energy can be written as

$$E_{\rm xc} = \int_0^1 \frac{d\lambda}{\lambda} E_{\rm int}(\lambda) - \frac{1}{2} \int d\mathbf{r} d\mathbf{r}' \frac{n(\mathbf{r}) n(\mathbf{r}')}{|\mathbf{r} - \mathbf{r}'|}. \tag{2.28}$$

Note that it is described by electron interaction, but it contains the correction of the Kohn-Sham kinetic energy. Although the above exchange correlation energy is exact formula except adiabatic connection, it is just rewriting of the formula and can not be compute on numerically. That formula can be also written by density operator. The density operator formula is $\hat{n}(\mathbf{r}) = \sum_i \delta(\mathbf{r} - \mathbf{r}_i)$, and $n(\mathbf{r}) = \langle \psi(\lambda) | \, \hat{n}(\mathbf{r}) \, | \psi(\lambda) \rangle = \langle \hat{n}(\mathbf{r}) \rangle_\lambda$. We obtain

$$\begin{aligned}
&\int d\mathbf{r} d\mathbf{r}' \frac{\langle \hat{n}(\mathbf{r}) \hat{n}(\mathbf{r}') \rangle_\lambda}{|\mathbf{r} - \mathbf{r}'|} \\
&= \int d\mathbf{r} d\mathbf{r}' \frac{1}{|\mathbf{r} - \mathbf{r}'|} \left(\sum_{i \neq j} \langle \delta(\mathbf{r} - \mathbf{r}_i) \delta(\mathbf{r}' - \mathbf{r}_j) \rangle_\lambda + \sum_i \langle \delta(\mathbf{r} - \mathbf{r}_i) \delta(\mathbf{r}' - \mathbf{r}_i) \rangle_\lambda \right) \\
&= \left\langle \sum_{i \neq j} \frac{1}{|\mathbf{r}_i - \mathbf{r}_j|} \right\rangle_\lambda + \int d\mathbf{r} d\mathbf{r}' \left\langle \sum_i \delta(\mathbf{r} - \mathbf{r}_i) \right\rangle_\lambda \frac{\delta(\mathbf{r} - \mathbf{r}')}{|\mathbf{r} - \mathbf{r}'|} \\
&= \frac{2}{\lambda} E_{\rm int}(\lambda) + \int d\mathbf{r} d\mathbf{r}' \frac{\delta(\mathbf{r} - \mathbf{r}') n(\mathbf{r})}{|\mathbf{r} - \mathbf{r}'|}.
\end{aligned} \tag{2.29}$$

$$E_{\rm int}(\lambda) = \frac{1}{2} \int d\mathbf{r} d\mathbf{r}' \frac{P_\lambda(\mathbf{r}, \mathbf{r}')}{|\mathbf{r} - \mathbf{r}'|} \tag{2.30}$$

We also defined pair density P as follows:

$$P_\lambda(\mathbf{r},\mathbf{r}') = \langle \hat{n}(\mathbf{r})\hat{n}(\mathbf{r}')\rangle_\lambda - n(\mathbf{r})\delta(\mathbf{r}-\mathbf{r}')$$
$$= N(N-1)\int d\mathbf{r}_3 d\mathbf{r}_4 \cdots d\mathbf{r}_N |\psi^\lambda(\mathbf{r},\mathbf{r}',\mathbf{r}_3,\cdots,\mathbf{r}_N)|. \tag{2.31}$$

Then another operator is difference from the average of electron density $\bar{n}(\mathbf{r}) = \hat{n}(\mathbf{r}) - n(\mathbf{r})$ is defined. Using these formulas, we obtain the exchange correlation

$$E_{\mathrm{xc}}[n] = \frac{1}{2}\int d\mathbf{r}d\mathbf{r}' \frac{1}{|\mathbf{r}-\mathbf{r}'|}\int_0^1 d\lambda[\langle \bar{n}(\mathbf{r})\bar{n}(\mathbf{r}')\rangle_\lambda - \delta(\mathbf{r}-\mathbf{r}')n(\mathbf{r})]. \tag{2.32}$$

The pair distribution function $g_\lambda(\mathbf{r},\mathbf{r}')$ can be defined as follows:

$$\langle \bar{n}(\mathbf{r})\bar{n}(\mathbf{r}')\rangle_\lambda - \delta(\mathbf{r}-\mathbf{r}')n(\mathbf{r}) = P_\lambda(\mathbf{r},\mathbf{r}') - n(\mathbf{r},\mathbf{r}') = n(\mathbf{r})n(\mathbf{r}')[g_\lambda(\mathbf{r},\mathbf{r}')-1]. \tag{2.33}$$

The relation between g_λ and P_λ is

$$g_\lambda(\mathbf{r},\mathbf{r}') = \frac{P_\lambda(\mathbf{r},\mathbf{r}')}{n(\mathbf{r})n(\mathbf{r}')}. \tag{2.34}$$

We obtain the following formulas:

$$E_{\mathrm{xc}}[n] = \frac{1}{2}\int d\mathbf{r}d\mathbf{r}' \frac{n(\mathbf{r})n_{\mathrm{xc}}(\mathbf{r},\mathbf{r}')}{|\mathbf{r}-\mathbf{r}'|} \tag{2.35}$$

and

$$n_{\mathrm{xc}}(\mathbf{r},\mathbf{r}') = n(\mathbf{r}')\left(\int_0^1 d\lambda g_\lambda(\mathbf{r},\mathbf{r}') - 1\right). \tag{2.36}$$

The $n_{\mathrm{xc}}(\mathbf{r},\mathbf{r}')$ is exchange-correlation hole, which has sum rule as well as the exchange hole on Hartree-Fock approximation. The rule is can be written as

$$\int d\mathbf{r}' n_{\mathrm{xc}}(\mathbf{r},\mathbf{r}') = -1. \tag{2.37}$$

That is demonstrated in the following formula.

$$\begin{aligned}\int d\mathbf{r}' n_{\mathrm{xc}}(\mathbf{r},\mathbf{r}') &= \int_0^1 d\lambda \int d\mathbf{r}' \frac{1}{n(\mathbf{r})} P_\lambda(\mathbf{r},\mathbf{r}') - N \\ &= \int_0^1 d\lambda (N-1) - N = -1, \end{aligned} \tag{2.38}$$

where we use the following formula;

$$n(\mathbf{r}) = \frac{1}{N-1} \int d\mathbf{r}' P_\lambda(\mathbf{r},\mathbf{r}'). \tag{2.39}$$

The exchange-correlation hole eliminate the electron around itself. We need some approximation for pair potential, because it is difficult to obtain it in real system. In the local density functional approximation (LDA) , $n_{\mathrm{xc}}(\mathbf{r},\mathbf{r}')$ approximated as free electron exchange correlation with respect to density on $n(\mathbf{r})$ and pair distribution function is obtained. Finally we can get LDA formula as follows:

$$n_{\mathrm{xc}}^{\mathrm{LDA}} = n(\mathbf{r})[g_h(|\mathbf{r}-\mathbf{r}'|; n(\mathbf{r})) - 1]. \tag{2.40}$$

2.6 Response function

We introduce the response function to represent the exchange correction energy formula in the linear response theorem.

$$v_{\mathrm{ext}}(\mathbf{r},t) = \begin{cases} v_{\mathrm{ext}}(\mathbf{r}) & t \le t_0 \\ v_{\mathrm{ext}}(\mathbf{r}) + \delta v_{\mathrm{ext}}(\mathbf{r},t) & t \ge t_0 \end{cases} \tag{2.41}$$

The external potential is zero at $t \le t_0$. The $v_{\mathrm{ext}}(\mathbf{r})$ is external potential from atom and it is non-perturbative system. This system has potential $\delta v_{\mathrm{ext}}(\mathbf{r},t)$ at $t = t_0$. The electron density $n_0(\mathbf{r})$ at $t \le t_0$ obey Kohn-Sham equation;

$$\left[-\frac{1}{2}\nabla^2 + v_{\mathrm{ext}} + \int d\mathbf{r} \frac{n(\mathbf{r}')}{|\mathbf{r}-\mathbf{r}'|} + v_{\mathrm{xc}}(\mathbf{r})\right] \psi_j(\mathbf{r}) = \varepsilon_j \psi_j(\mathbf{r}). \tag{2.42}$$

The electron density $n(\mathbf{r},t)$ at $t > t_0$ can be expanded by function of $\delta v_{\mathrm{ext}}(\mathbf{r},t)$;

$$\delta n(\mathbf{r},t) = n(\mathbf{r},t) - n_0(\mathbf{r}) = n_1(\mathbf{r},t) + n_2(\mathbf{r},t) + \cdots \tag{2.43}$$

The over 2nd order expansion can be neglected in the concept of linear response $n_1(\mathbf{r},t)$. Since the $n_1(\mathbf{r},t)$ is linear function of $\delta v_{\rm ext}$, it can be written as

$$\delta n(\mathbf{r},t) = \int dt' \int d\mathbf{r}' \chi(\mathbf{r},t,\mathbf{r}',t') \delta v_{\rm ext}(\mathbf{r}',t'). \tag{2.44}$$

where χ is response function. The functional derivative formula is as follows:

$$\chi(\mathbf{r},t,\mathbf{r}',t') = \frac{\delta n[v_{\rm ext}](\mathbf{r},t)}{\delta v_{\rm ext}(\mathbf{r}',t')}. \tag{2.45}$$

By the substitution $t_0 = 0$ that dose not lost the generality, the perturbated Hamiltonian $\delta\hat{H}(t)$ can be written as

$$\delta\hat{H} = e^{\eta t} \sum_{i=1}^{N} \delta v_{\rm ext}(\mathbf{r}_i, t) \tag{2.46}$$

where η is the positive small amount, which plays a role for introducing of perturbation on slowly. Thus $e^{\eta t} \to 0$ on $t \to -\infty$ and $e^{\eta t} \to 1$ on $t \to 0$. Introducing the electron density operator $\hat{n}(\mathbf{r}) = \sum_i \delta(\mathbf{r} - \mathbf{r}_i)$, $\delta\hat{H}$ can be written as

$$\delta\hat{H}(t) = \int d\mathbf{r} \int \frac{d\omega}{2\pi} e^{-i\tilde{\omega}t} \delta v_{\rm ext}(\mathbf{r},\omega) \hat{n}(\mathbf{r}) \tag{2.47}$$

where $\tilde{\omega} = \omega + i\eta$. Using the jth eigenstate $|\Psi_j^0\rangle$ and eigenvalue E_j^0 on the non perturbated Hamiltonian H_0 ($H_0 |\Psi_j^0\rangle = E_j^0 |\Psi_j^0\rangle$),$|\Psi(t)\rangle$ that is eigenstate at t is represented as follows by 1st order perturbation,

$$|\Psi(t)\rangle = e^{-iE_0^0 t} |\Psi_0^0\rangle + \sum_{j\neq 0} a_j(t) e^{-iE_j^0 t} |\Psi_j^0\rangle \tag{2.48}$$

$$\begin{aligned} a_j(t) &= -i \int_{-\infty}^{t} dt' e^{i\omega_{0j}t'} \langle\Psi_j^0| \delta\hat{H}(t) |\Psi_0^0\rangle \\ &= -\int d\mathbf{r}' \int \frac{d\omega}{2\pi} \delta v_{\rm ext}(\mathbf{r}',\omega) \langle\Psi_j^0| \delta\hat{H}(t) |\Psi_0^0\rangle \frac{e^{i(\omega_{0j}-\tilde{\omega})t}}{\omega_{0j}-\tilde{\omega}}, \end{aligned} \tag{2.49}$$

where $\omega_{0j} = E_j^0 - E_0^0$. The induced electron charge density by the perturbation $\delta n(\mathbf{r},t)$ is estimated from;

$$\delta n(\mathbf{r},t) = \langle\Psi(t)| \hat{n}(\mathbf{r}) |\Psi(t)\rangle - \langle\Psi_0^0| \hat{n}(\mathbf{r}) |\Psi_0^0\rangle . \tag{2.50}$$

Taking first order of $a_j(t)$, the formula of δn can be written as

$$\begin{aligned}\delta n(\mathbf{r},t) =& \sum_{j\neq 0}\left[a_j(t)\left\langle\Psi_0^0\right|\hat{n}(\mathbf{r})\left|\Psi_j^0\right\rangle e^{-i\omega_{0j}t} + a_j^*(t)\left\langle\Psi_j^0\right|\hat{n}(\mathbf{r})\left|\Psi_0^0\right\rangle e^{i\omega_{0j}t}\right] \\ =& -\int d\mathbf{r}'\int\frac{d\omega}{2\pi}\delta v_{\mathrm{ext}}(\mathbf{r}',\omega)e^{-i\tilde{\omega}t} \\ & \left[\sum_{j\neq 0}\frac{\left\langle\Psi_j^0\right|\hat{n}(\mathbf{r}')\left|\Psi_0^0\right\rangle\left\langle\Psi_0^0\right|\hat{n}(\mathbf{r})\left|\Psi_j^0\right\rangle}{\omega_{0j}-\tilde{\omega}} + \frac{\left\langle\Psi_0^0\right|\hat{n}(\mathbf{r}')\left|\Psi_j^0\right\rangle\left\langle\Psi_j^0\right|\hat{n}(\mathbf{r})\left|\Psi_0^0\right\rangle}{\omega_{0j}+\tilde{\omega}}\right] \end{aligned} \tag{2.51}$$

Comparing the definition of response function, the response function is

$$\chi(\mathbf{r},\mathbf{r}',\omega) = -\sum_{j\neq 0}\frac{\left\langle\Psi_j^0\right|\hat{n}(\mathbf{r}')\left|\Psi_0^0\right\rangle\left\langle\Psi_0^0\right|\hat{n}(\mathbf{r})\left|\Psi_j^0\right\rangle}{\omega_{0j}-\tilde{\omega}} + \frac{\left\langle\Psi_0^0\right|\hat{n}(\mathbf{r}')\left|\Psi_j^0\right\rangle\left\langle\Psi_j^0\right|\hat{n}(\mathbf{r})\left|\Psi_0^0\right\rangle}{\omega_{0j}+\tilde{\omega}}. \tag{2.52}$$

The many body wave function $\Psi(\mathbf{r}_1,\cdots,\mathbf{r}_N)$ can be divided to one particle orbital in non interacting system;

$$\Psi(\mathbf{r}_1,\cdots,\mathbf{r}_N) = \psi_1(\mathbf{r}_1)\cdots\psi_N(\mathbf{r}_N) \tag{2.53}$$

The $\left\langle\Psi_j^0\right|\hat{n}(\mathbf{r}')\left|\Psi_0^0\right\rangle$ are estimated from Eq. 2.53 To get excitation jth state, we should consider just one electron excitation because $\hat{n}(\mathbf{r})$ is one electron operator. When occupied state $n(n\leq N)$ excite to mth $(m>N)$ state, we get the following formula:

$$\begin{aligned}&\sum_k\left\langle\psi_1,\cdots,\psi_n,\cdots,\psi_N\right|\delta(\mathbf{r}-\mathbf{r}_k)\left|\psi_1,\cdots,\psi_m,\cdots,\psi_N\right\rangle \\ =&\sum_k\int d\mathbf{r}_1\cdots d\mathbf{r}_N\delta(\mathbf{r}-\mathbf{r}_k)\psi_1^*(\mathbf{r}_1)\psi_1(\mathbf{r}_1)\cdots\psi_n^*(\mathbf{r}_i)\psi_m(\mathbf{r}_i)\cdots\psi_N^*(\mathbf{r}_N)\psi_N(\mathbf{r}_N) \\ =&\psi_n^*(\mathbf{r})\psi_m(\mathbf{r}).\end{aligned} \tag{2.54}$$

The summation of jth exited state is sum of occupied and unoccupied states. Using $\omega_{0j} = E_j^0 - E_0^0 = \varepsilon_m - \varepsilon_n$, the χ can be written as

$$\chi(\mathbf{r},\mathbf{r}',\omega) = -\sum_n^{\text{occ.}}\sum_m^{\text{unocc.}}\frac{\psi_m^*(\mathbf{r}')\psi_n(\mathbf{r}')\psi_n^*(\mathbf{r})\psi_m(\mathbf{r})}{\varepsilon_m-\varepsilon_n-\tilde{\omega}} + \frac{\psi_n^*(\mathbf{r}')\psi_m(\mathbf{r}')\psi_m^*(\mathbf{r})\psi_n(\mathbf{r})}{\varepsilon_m-\varepsilon_n+\tilde{\omega}}. \tag{2.55}$$

It can be also written as

$$\chi(\mathbf{r},\mathbf{r}',\omega)=\sum_{i,j}(f_i-f_j)\frac{\psi_i^*(\mathbf{r}')\psi_j(\mathbf{r}')\psi_i(\mathbf{r})\psi_j^*(\mathbf{r})}{\tilde{\omega}-(\varepsilon_i-\varepsilon_j)}. \tag{2.56}$$

where f_i, f_j is distribution function which has one (zero) value in occupied (unoccupied) state. When ψ and ε are Kohn-Sham eigenfunctions and eigenvalues, respectively, it called Kohn-Sham response function, because the non-interacting system is same with Kohn-Sham auxiliary system ($\chi_{\lambda=0}=\chi_0=\chi^{\mathrm{KS}}$). We introduce other formulation for response function. It can be written as follows using linear response theory framework:

$$\delta n(\mathbf{r},\omega)=\int d\mathbf{r}'\chi(\mathbf{r},\mathbf{r}',\omega)\delta\phi_{\mathrm{ext}}(\mathbf{r}',\omega). \tag{2.57}$$

For simplify, we use short formula $\delta n=\chi\delta\phi_{\mathrm{ext}}$. χ is described the change of electron density δn when the external potential change to $\phi_{\mathrm{ext}}+\delta\phi_{\mathrm{ext}}$. The charge of electron density cause a change of total potential. To describe it, we also introduce response function $\tilde{\chi}$ as follows:

$$\delta n=\tilde{\chi}\delta\phi. \tag{2.58}$$

Then the relation between χ and $\tilde{\chi}$ is as follows:

$$\begin{aligned}
\chi\delta\phi_{\mathrm{ext}} =&\tilde{\chi}\delta\phi \\
=&\tilde{\chi}(\delta\phi_{\mathrm{ext}}+\delta\phi_{\mathrm{ind}}) \\
=&\tilde{\chi}(\delta\phi_{\mathrm{ext}}+V\delta n) \\
=&\tilde{\chi}(\delta\phi_{\mathrm{ext}}+V\chi\delta\phi_{\mathrm{ext}}) \qquad (2.59)\\
\rightarrow&\ \chi=\tilde{\chi}+\tilde{\chi}V\chi. \qquad (2.60)
\end{aligned}$$

The induced electron density by the external electronic field related to electronic polarization moment $\mathbf{P}$ ($\delta n=-\nabla\cdot\mathbf{P}$). It also can be written as $\mathbf{P}=\frac{\epsilon-1}{4\pi}\delta\mathbf{E}$ because induced electronic filed is written as $\delta\mathbf{E}=-\nabla\delta\phi$. Therefore we obtain

$$\delta n=-\nabla\cdot\left(\frac{\epsilon-1}{4\pi}\delta\mathbf{E}\right)=\nabla_{\mathbf{r}'}\cdot\left(\frac{\epsilon-1}{4\pi}\nabla_{\mathbf{r}}\right)\delta\phi. \tag{2.61}$$

Using above relation, the $\tilde{\chi}$ using by dielectric function can be written as follows:

$$\tilde{\chi} = \nabla_{\mathbf{r}'} \cdot \frac{\epsilon - 1}{4\pi} \nabla_{\mathbf{r}}. \tag{2.62}$$

These formulations can extend to adiabatic connection framework that have a parameter λ which adjust the strength of interactions.

$$\delta n^{\lambda} = \chi_0 \delta \phi^{\lambda}_{\text{eff}} \tag{2.63}$$

According to Kohn-Sham approach, this effective potential can be written as

$$\delta \phi^{\lambda}_{\text{eff}} = \delta \phi_{\text{ext}} + (V_{\lambda} + f^{\lambda}_{\text{xc}}) \delta n^{\lambda}. \tag{2.64}$$

Although the response function on the some λ state have interacting electron in the system, it can be estimated by Kohn-Sham response function owing to the replacement of λ state to Kohn-Sham auxiliary system. Note that there is difference between many body wave function and Kohn-Sham wave function even if non-interacting system, however, response function can be estimated using same formula, because the these wave function gave same charge density. Finally we get

$$\chi_{\lambda} = \chi_0 (V_{\lambda} + f^{\lambda}_{\text{xc}}) \chi_{\lambda}. \tag{2.65}$$

This formula can be rewriting using following formulas;

$$\chi_{\lambda} = \tilde{\chi}_{\lambda} + \tilde{\chi}_{\lambda} V_{\lambda} \chi_{\lambda} \tag{2.66}$$

$$\tilde{\chi}_{\lambda} = \chi_0 + \tilde{\chi}_0 f^{\lambda}_{\text{xc}} \tilde{\chi}_{\lambda} \tag{2.67}$$

2.7 Exchange correction energy formula

There is no computable strict formula for exchange correction energy, however we can make the formula by using fluctuation dissipation theorem. This approach can give a starting point for an approximation of exchange correction energy even if it is impossible

to be solved. To get exchange-correlation formula, we start from the following formulas:

$$\begin{aligned}
&\int_0^\infty d\omega\chi(\mathbf{r},\mathbf{r}',i\omega)+\chi(\mathbf{r}',\mathbf{r},i\omega)\\
&=-\sum_{j\neq 0}\int_0^\infty d\omega(\langle\Psi_j^0|\,\hat{n}(\mathbf{r}')\,|\Psi_0^0\rangle\,\langle\Psi_0^0|\,\hat{n}(\mathbf{r})\,|\Psi_j^0\rangle+\langle\Psi_0^0|\,\hat{n}(\mathbf{r}')\,|\Psi_j^0\rangle\,\langle\Psi_j^0|\,\hat{n}(\mathbf{r})\,|\Psi_0^0\rangle)\\
&\quad\times\left(\frac{1}{\omega_{0j}-i\omega}+\frac{1}{\omega_{0j}+i\omega}\right)\\
&=-\pi(\langle\Psi_0^0|\,\hat{n}(\mathbf{r}')\hat{n}(\mathbf{r})\,|\Psi_0^0\rangle+\langle\Psi_0^0|\,\hat{n}(\mathbf{r})\hat{n}(\mathbf{r}')\,|\Psi_0^0\rangle)+2\pi n(\mathbf{r})n(\mathbf{r}').
\end{aligned}\tag{2.68}$$

The above integration with respect to ω could be performed using the following formula:

$$\int_0^\infty d\omega\frac{1}{\omega_{0j}-i\omega}+\frac{1}{\omega_{0j}+i\omega}=\int_0^\infty d\omega\frac{2\omega_{0j}}{\omega_{0j}^2+\omega^2}=\pi,\ \sum_{j\neq 0}|\Psi_j^0\rangle\,\langle\Psi_j^0|=1-|\Psi_0^0\rangle\,\langle\Psi_0^0|\tag{2.69}$$

Therefore, exchange-correction energy formula using response function can be written as

$$\begin{aligned}
E_{\mathrm{xc}}&=-\frac{1}{2}\int_0^1\frac{d\lambda}{\lambda}\int d\mathbf{r}d\mathbf{r}'\frac{\lambda}{|\mathbf{r}-\mathbf{r}'|}\int_0^\infty\frac{d\omega}{\pi}\chi_\lambda(\mathbf{r},\mathbf{r}',i\omega)-\frac{1}{2}\int d\mathbf{r}d\mathbf{r}'\frac{n(\mathbf{r})\delta(\mathbf{r}-\mathbf{r}')}{|\mathbf{r}-\mathbf{r}'|}\\
&=-\int_0^1\frac{d\lambda}{\lambda}\int_0^\infty\frac{d\omega}{2\pi}\mathrm{Tr}[\chi_\lambda V_\lambda]-E_{\mathrm{self}},
\end{aligned}\tag{2.70}$$

where the E_{self} is defined as follows:

$$E_{\mathrm{self}}=\frac{1}{2}\int d\mathbf{r}d\mathbf{r}'\frac{n(\mathbf{r})\delta(\mathbf{r}-\mathbf{r}')}{|\mathbf{r}-\mathbf{r}'|}.\tag{2.71}$$

Exactly, $\lambda=0$ part expresses exchange energy as follows:

$$-\frac{1}{2\pi}\int d\mathbf{r}d\mathbf{r}'\int_0^\infty d\omega\chi_{\lambda=0}(\mathbf{r},\mathbf{r}',i\omega)-\frac{1}{2}\int d\mathbf{r}d\mathbf{r}'\frac{n(\mathbf{r})\delta(\mathbf{r}-\mathbf{r}')}{|\mathbf{r}-\mathbf{r}'|}.\tag{2.72}$$

The first term and second term are as follows:

$$-\frac{1}{2\pi}\sum_{n}^{\text{occ.}}\sum_{m}^{\text{unocc.}}\int d\mathbf{r}d\mathbf{r}'\frac{\psi_m^*(\mathbf{r}')\psi_n(\mathbf{r}')\psi_n^*(\mathbf{r})\psi_m(\mathbf{r})}{|\mathbf{r}-\mathbf{r}'|}\int_0^\infty d\omega\left(\frac{2\omega_{nm}}{\omega_{nm}^2+\omega^2}\right)$$
$$=\frac{1}{2}\sum_{n}^{\text{occ.}}\sum_{m}^{\text{unocc.}}\int d\mathbf{r}d\mathbf{r}'\frac{\psi_m^*(\mathbf{r}')\psi_n(\mathbf{r}')\psi_n^*(\mathbf{r})\psi_m(\mathbf{r})}{|\mathbf{r}-\mathbf{r}'|} \tag{2.73}$$

$$-\frac{1}{2}\int d\mathbf{r}d\mathbf{r}'\frac{n(\mathbf{r})\delta(\mathbf{r}-\mathbf{r}')}{|\mathbf{r}-\mathbf{r}'|}=\frac{1}{2}\sum_{n}^{\text{occ.}}\sum_{m}\int d\mathbf{r}d\mathbf{r}'\frac{\psi_m^*(\mathbf{r}')\psi_n(\mathbf{r}')\psi_n^*(\mathbf{r})\psi_m(\mathbf{r})}{|\mathbf{r}-\mathbf{r}'|}. \tag{2.74}$$

Regarding second term, the integrity condition for wave function ($\sum_m \psi_m^*(\mathbf{r}')\psi_m(\mathbf{r}) = \delta(\mathbf{r}-\mathbf{r}')$) and the definition of electron density ($n(\mathbf{r}) = \sum_n^{\text{occ.}} \psi_n^*(\mathbf{r})\psi_n(\mathbf{r})$) are used. Therefore $\lambda = 0$ part becomes same with the exchange energy formula as follows:

$$-\frac{1}{2}\sum_{n}^{\text{occ.}}\sum_{m}^{\text{occ.}}\int d\mathbf{r}d\mathbf{r}'\frac{\psi_m^*(\mathbf{r}')\psi_n(\mathbf{r}')\psi_n^*(\mathbf{r})\psi_m(\mathbf{r})}{|\mathbf{r}-\mathbf{r}'|} \tag{2.75}$$

On the other hand, the non-zero λ part express correlation energy.

2.8 Recent trends of DFT

We showed that density functional approach is exact theory, but we should employ some approximations for the exchange-correlation functional. Although using Hartree-Fock exchange seems better, this attempt does not work well in solid materials because the screened effect which reduced exchange interaction could not be taken into account. And a computational cost of the Hartree-Fock approximation is much larger than LDA/GGA. These are the reasons why LDA/GGA are used for solid materials even if nonlocal effect, such as vdW interaction, can not be taken into account. To solve this problem, various methods have been developed and applied, such as random phase approximation (RPA), semi-empirical approach (DFT-D), and nonlocal correlation approach [19, 20, 21, 22]. The RPA approach has high computational cost and semi-empirical approach used empirical parameter depending on materials, indicating that these methods are not suitable for material design. Therefore we focus on nonlocal correlation approach (vdW-DF) in Chap. 3.

Chapter 3

Overview of van der Waals density functional

According to literatures, van der Waals force is defined as interactive or repulsive force between atoms, ions, and molecules that is caused by permanent dipoles and instantaneously induce dipoles in the wide sense. In this thesis, van der Waals (vdW) force indicates the later one which is called London dispersion force. Although vdW force is quantum and nonlocal effect, LDA/GGA method can not described its effect. Therefore I should introduce nonlocal correlation energy formula to describe vdW force. vdW-DF method, which can calculate non empirical nonlocal correlation energy by using electron density, has been proposed by Dion et al. In this chapter, I review vdW-DF approach.

3.1 Nonlocal correlation energy

A starting point to obtain the nonlocal correlation energy on vdW-DF method is exchange correlation formula using response function;

$$E_{\rm xc} = -\int_0^\infty \frac{d\lambda}{\lambda}\int_0^\infty \frac{d\omega}{2\pi}{\rm Tr}[\chi_\lambda V_\lambda] - E_{\rm self} \tag{3.1}$$

where $V_\lambda = \frac{\lambda}{|\mathbf{r}-\mathbf{r}'|}$. The response functions with respect to chaining of electron density are already introduced;

$$\chi_\lambda = \tilde{\chi}_\lambda + \tilde{\chi}_\lambda V_\lambda \chi_\lambda, \tag{3.2}$$

$$\tilde{\chi}_\lambda = \chi_0 + \chi_0 f_{\rm xc}^\lambda \chi_\lambda. \tag{3.3}$$

They use an approximation ($\tilde{\chi}_\lambda \simeq \tilde{\chi}_{\lambda=1}$) that is called full potential approximation (FPA), owing to overcoming the difficulty of λ dependency of the response function.

$$\chi_\lambda = (1 - \lambda\tilde{\chi}_{\lambda=1}V)^{-1}\tilde{\chi}_{\lambda=1} \tag{3.4}$$

The FPA can is correct for description of long-range interaction. Therefore another approximation ($\tilde{\chi}_\lambda \simeq \tilde{\chi}_{\lambda=0}$) which is random phase approximation is carried out in general. However that problem is well overcome on vdW-DF approach. Using FPA, the λ integration can be solved analytically.

$$\int_0^1 d\lambda(1 - \lambda\tilde{\chi}_{\lambda=1}V)^{-1} = \Big[\ln(1 - \lambda\tilde{\chi}_{\lambda=1}V)\Big]_0^1(\tilde{\chi}_{\lambda=1}V)^{-1} = -\ln(1 - \tilde{\chi}_{\lambda=1}V)(\tilde{\chi}_{\lambda=1}V)^{-1} \tag{3.5}$$

The exchange-correlation energy on FPA can be written as:

$$\begin{aligned} E_{\rm xc}^{\rm FPA} &= \int_0^\infty \frac{d\omega}{2\pi}{\rm Tr}[\ln(1 - \tilde{\chi}_{\lambda=1}V)] - E_{\rm self} \\ &= \int_0^\infty \frac{d\omega}{2\pi}{\rm Tr}\left[\ln\left(1 - \nabla\cdot\frac{\epsilon}{4\pi}\nabla V + \frac{1}{4\pi}\nabla^2 V\right)\right] - E_{\rm self} \\ &= \int_0^\infty \frac{d\omega}{2\pi}{\rm Tr}\left[\ln\left(\nabla\cdot\epsilon\nabla\frac{-V}{4\pi}\right)\right] - E_{\rm self} \end{aligned} \tag{3.6}$$

Here $V = 4\pi/r$ and $\nabla^2 V = -4\pi$ are used. The definition of nonlocal correlation energy $E_{\rm c}^{\rm nl}$ is an energy difference between FPA exchange-correlation energy and homogeneous electron gas (HEG) its.

$$E_{\rm c}^{\rm nl} = E_{\rm xc}^{\rm FPA} - E_{\rm xc}^{\rm FPA}({\rm HEG}) \tag{3.7}$$

This treatment overcomes the uncertainly problem of FPA correction energy in short-range because this error is canceled by taking the energy difference from homogeneous electron gas model. Note that homogeneous electron gas system does not have nonlocal correlation effect. Here, the second term which is FPA exchange-correlation energy on homogeneous electron gas model can be written as follows:

$$E_{\rm xc}^{\rm FPA}({\rm HEG}) = \int_0^\infty \frac{d\omega}{2\pi}{\rm Tr}[\ln\epsilon_{\lambda=1}] - E_{\rm self} \tag{3.8}$$

The nonlocal correlation energy is written as

$$E_{\mathrm{c}}^{\mathrm{nl}} = \int_0^\infty \frac{d\omega}{2\pi} \mathrm{Tr}\left[\ln(1+\epsilon^{-1}(\nabla\cdot\epsilon - \epsilon\nabla\cdot)\nabla\frac{-V}{4\pi}\right] \tag{3.9}$$

$$= \int_0^\infty \frac{d\omega}{2\pi} \mathrm{Tr}\left[\ln\left(1-\left(1-\frac{1}{\epsilon}\right)-\frac{\tilde{\chi}}{\epsilon}V\right)\right]. \tag{3.10}$$

The density dielectric function ϵ is depended on one particle wave function. The relation between dielectric and polarization function is written as follows approximately:

$$S = 1 - \frac{1}{\epsilon}. \tag{3.11}$$

The nonlocal correlation energy can be expanded by polarization function S and I used until second term,

$$E_{\mathrm{c}}^{\mathrm{nl}} \simeq \int_0^\infty \frac{d\omega}{2\pi} \mathrm{Tr}\left[S^2 - \left(\nabla\cdot S\nabla\frac{-V}{4\pi}\right)\right] \tag{3.12}$$

Then they derived an approximate expression for S and carried out the integral for ω. After that nonlocal correlation energy formula can be written as

$$E_{\mathrm{c}}^{\mathrm{nl}} = \frac{1}{2}\iint d\mathbf{r}_1 d\mathbf{r}_2 n(\mathbf{r}_1)\phi(n(\mathbf{r_1}),n(\mathbf{r_2}))n(\mathbf{r}_2) \tag{3.13}$$

where the expression of nonlocal correlation kernel function is

$$\phi(\mathbf{r}_1,\mathbf{r}_2) = \frac{2}{\pi^2}\int_0^\infty daa^2\int_0^\infty dbb^2 W(a,b)T(\nu(a),\nu(b),\nu'(a),\nu'(b)) \tag{3.14}$$

$$T(w,x,y,z) = \frac{1}{2}\left[\frac{1}{w+z}+\frac{1}{y+z}\right]\left[\frac{1}{(w+y)(x+z)}+\frac{1}{(w+z)(y+x)}\right] \tag{3.15}$$

$$W(a,b) = \frac{2}{a^3b^3}[(3-a^2)b\cos b\sin a + (3-b^2)a\cos a\sin b + (a^2+b^2-3)\sin a\sin b - 3ab\cos a\cos b]. \tag{3.16}$$

Here $\nu(y) = \frac{y^2}{2h(y/d)}$, $\nu'(y) = \frac{y^2}{2h(y/d')}$, $h(y) = 1-e^{-4\pi y^2/9}$. The double integration of a and b correspond to the trace calculation.

3.2 Order N log N method for vdW-DF

The exchange-correlation energy in vdW-DF is given[8] by

$$E_{\rm xc} = E_{\rm x} + E_{\rm c}^{\rm loc} + E_{\rm c}^{\rm nl}, \tag{3.17}$$

where $E_{\rm x}$, $E_{\rm c}^{\rm loc}$ and $E_{\rm c}^{\rm nl}$ are exchange energy, short-range local correlation energy, and nonlocal correlation energy, respectively. $E_{\rm c}^{\rm nl}$ is expressed as a double integral of the nonlocal interaction kernel $\phi(q_1, q_2, r_{12})$[8] over spatial coordinate $\mathbf{r}_1$ and $\mathbf{r}_2$ as

$$E_{\rm c}^{\rm nl} = \frac{1}{2}\iint n(\mathbf{r}_1)\phi(q_1, q_2, r_{12})n(\mathbf{r}_2)d\mathbf{r}_1 d\mathbf{r}_2, \tag{3.18}$$

where $r_{12} = |\mathbf{r}_1 - \mathbf{r}_2|$, $q_1 = q_0(\mathbf{r}_1)$, $q_2 = q_0(\mathbf{r}_2)$, and $q_0(\mathbf{r})$ is a function of the charge density $n(\mathbf{r})$ and its gradient $|\nabla n(\mathbf{r})|$. Román-Pérez and Soler (RPS)[23] proposed an efficient method to evaluate $E_{\rm c}^{\rm nl}$, as the direct computation of the double integral in Eq. (3.18) is extremely time consuming. In the RPS scheme, the vdW kernel ϕ is expanded in terms of interpolating function $p_\alpha(q)$, which satisfies $p_\alpha(q_\beta) = \delta_{\alpha\beta}$, so that ϕ is a fixed value at a given q_β point, allowing the use of the fast Fourier transform (FFT) in the evaluation of $E_{\rm c}^{\rm nl}$. However, ϕ has a divergence when $q_\alpha, q_\beta \to 0$, which makes the interpolation near the origin difficult, and thus, RPS replaced ϕ with the soft form and employed LDA-like approximation to $E_{\rm c}^{\rm nl}$ near the origin. Alternatively, Wu and Gygi (WG)[24] proposed a simplified implementation to avoid the divergence in ϕ as follows. The nonlocal interaction kernel, multiplied by q_1 and q_2, is expanded as

$$q_1 q_2 \phi(q_1, q_2, r_{12}) \simeq \sum_{\alpha\beta} q_\alpha p_\alpha(q_1) q_\beta p_\beta(q_2) \phi_{\alpha\beta}(r_{12}), \tag{3.19}$$

so that the divergence at $q_\alpha, q_\beta \to 0$ can be avoided. Introducing the function $\eta_\alpha(\mathbf{r}) = q_\alpha n(\mathbf{r}) p_\alpha(q_0(\mathbf{r}))/q_0(\mathbf{r})$, the nonlocal correlation is calculated in the reciprocal space as

$$\begin{aligned} E_{\rm c}^{\rm nl} &= \frac{1}{2}\sum_{\alpha\beta}\iint \eta_\alpha(\mathbf{r}_1)\eta_\beta(\mathbf{r}_2)\phi_{\alpha\beta}(r_{12})d\mathbf{r}_1 d\mathbf{r}_2 \\ &= \frac{\Omega}{2}\sum_{\mathbf{G}}\sum_{\alpha\beta}\eta_\alpha^*(\mathbf{G})\eta_\beta(\mathbf{G})\phi_{\alpha\beta}(G), \end{aligned} \tag{3.20}$$

where $\mathbf{G}$ is reciprocal lattice vector $G = |\mathbf{G}|$, $\eta_\alpha(\mathbf{G})$ and $\phi_{\alpha\beta}(G)$ are the Fourier components of $\eta_\alpha(\mathbf{r})$ and $\phi_{\alpha\beta}(r_{12})$, respectively, and Ω is the volume of unit cell. The Fourier component $\phi_{\alpha\beta}(G)$ is calculated as

$$\phi_{\alpha\beta}(G) = \frac{1}{q_\alpha^3} F_{\alpha\beta}\left(\frac{G}{q_\alpha}\right), \tag{3.21}$$

where

$$F_{\alpha\beta}(k) = \frac{4\pi}{k}\int_0^\infty u\phi\left(u, \frac{q_\beta}{q_\alpha}u\right)\sin(ku)du. \tag{3.22}$$

This is procedure of our vdW-DF. The kernel table $\phi(D, \delta)$ is make preparations in advance and, $\phi_{\alpha\beta}(G)$ is etimated in DFT code. Note that the $\mathbf{G} = 0$ term in Eq. (3.20) vanishes when $\alpha = \beta$. The nonlocal correlation potential within the White-Bird algorithm[13] is given by

$$\begin{aligned} v_{\mathrm{c}}^{\mathrm{nl}}(\mathbf{r}_i) &= \frac{\delta E_{\mathrm{c}}^{\mathrm{nl}}}{\delta n(\mathbf{r}_i)} \\ &\simeq \frac{N}{\Omega}\frac{dE_{\mathrm{c}}^{\mathrm{nl}}}{dn(\mathbf{r}_i)} \\ &= \sum_\alpha \left(u_\alpha(\mathbf{r}_i)\frac{\partial\eta_\alpha(\mathbf{r}_i)}{\partial n(\mathbf{r}_i)} + \sum_j u_\alpha(\mathbf{r}_j)\frac{\partial\eta_\alpha(\mathbf{r}_j)}{\partial\nabla n(\mathbf{r}_j)}\frac{\partial\nabla n(\mathbf{r}_j)}{\partial n(\mathbf{r}_i)} \right) \\ &= \sum_\alpha \left(u_\alpha(\mathbf{r}_i)\frac{\partial\eta_\alpha(\mathbf{r}_i)}{\partial n(\mathbf{r}_i)} - \sum_{\mathbf{G}} e^{i\mathbf{G}\cdot\mathbf{r}_i} i\mathbf{G}\cdot\left(\frac{1}{N_{\mathrm{grid}}}\sum_j u_\alpha(\mathbf{r}_j)\frac{\nabla n(\mathbf{r}_j)}{|\nabla n(\mathbf{r}_j)|}\frac{\partial\eta_\alpha(\mathbf{r}_j)}{\partial|\nabla n(\mathbf{r}_j)|}e^{-i\mathbf{G}\cdot\mathbf{r}_j} \right) \right) \end{aligned} \tag{3.23}$$

where

$$u_\alpha(\mathbf{r}_i) = \frac{\Omega}{N}\sum_{\beta j}\phi_{\alpha\beta}(r_{ij})\eta_\beta(\mathbf{r}_j) = \sum_{\beta\mathbf{G}}\phi_{\alpha\beta}(G)\eta_\beta(\mathbf{G})e^{i\mathbf{G}\cdot\mathbf{r}_i}, \tag{3.24}$$

with N being the number of the FFT grid. In our formulation, an additional contribution to the pressure tensor $\Pi_{k\ell}, (k, \ell = x, y, z)$ is calculated as

$$(\Pi_{\rm c}^{\rm nl})_{k\ell} = -\frac{1}{\Omega}\sum_m \frac{\partial E_{\rm c}^{\rm nl}}{\partial h_{km}}(h^t)_{m\ell} \tag{3.25}$$

$$\begin{aligned}
&= -\frac{1}{\Omega}E_{\rm c}^{\rm nl}\delta_{k\ell} \\
&\quad - \frac{1}{N}\sum_m\sum_j\sum_\alpha u_\alpha(\mathbf{r}_j)\frac{\partial\eta_\alpha(\mathbf{r}_j)}{\partial n(\mathbf{r}_j)}\frac{\partial n(\mathbf{r}_j)}{\partial h_{km}}(h^t)_{m\ell} \\
&\quad + \frac{1}{N}\sum_j\sum_\alpha u_\alpha(\mathbf{r}_j)\frac{\partial\eta_\alpha(\mathbf{r}_j)}{\partial|\nabla n(\mathbf{r}_j)|}\frac{(\nabla n(\mathbf{r}_j))_k(\nabla n(\mathbf{r}_j))_\ell}{|\nabla n(\mathbf{r}_j)|} \\
&\quad - \frac{1}{N}\sum_m\sum_j\sum_\alpha u_\alpha(\mathbf{r}_j)\frac{\partial\eta_\alpha(\mathbf{r}_j)}{\partial|\nabla n(\mathbf{r}_j)|}\frac{\nabla n(\mathbf{r}_j)}{|\nabla n(\mathbf{r}_j)|}\cdot\sum_{\mathbf{G}}\frac{\partial n(\mathbf{G})}{\partial h_{km}}(h^t)_{m\ell}(i\mathbf{G})e^{i\mathbf{G}\cdot\mathbf{r}_j} \\
&\quad + \frac{1}{2}\sum_{\alpha\beta}\sum_{\mathbf{G}}\eta_\alpha^*(\mathbf{G})\eta_\beta(\mathbf{G})\frac{\partial\phi_{\alpha\beta}(G)}{\partial|\mathbf{G}|}\frac{G_kG_\ell}{|\mathbf{G}|},
\end{aligned} \tag{3.26}$$

where the matrix $h = (\mathbf{a}_1, \mathbf{a}_2, \mathbf{a}_3)$ is a set of primitive lattice vectors $\mathbf{a}_k$ $(k = 1, 2, 3)$ and h^t is the inverse of h.

3.3 Fourier component of the kernel function $\phi_{\alpha\beta}(G)$

In the present implementation, the Fourier components of the kernel function $\phi_{\alpha\beta}(G)$ are calculated from the tabulated data for $\phi(d_1, d_2)$ ($d_1\phi(d_1, d_2)$ in the case of WG implementation) using Eq. (3.21). The typical functions of $\phi_{\alpha\beta}(G)$ are presented in Fig. 3.1. For the small q_α's, $\phi_{\alpha\alpha}(G)$ deviates slightly from zero at $G = 0$ in the present computation, which may cause a numerical error. However, the error in the absolute value of $E_{\rm c}^{\rm nl}$ associated with the deviation is typically $\sim$0.5 meV in fcc argon and negligible in the estimation of the cohesive energies.

3.4 rVV10 with the Wu-Gygi implementation

The rVV10 functional has been proposed[25] to implement the VV10 functional[26] with the efficient RPS algorithm.[23] I note that very recently the original VV10 is implemented using the WG scheme by Corsetti *et al.*[27] Here, I briefly describe our implementation of rVV10 with the algorithm proposed by WG.[24] The rVV10 nonlocal

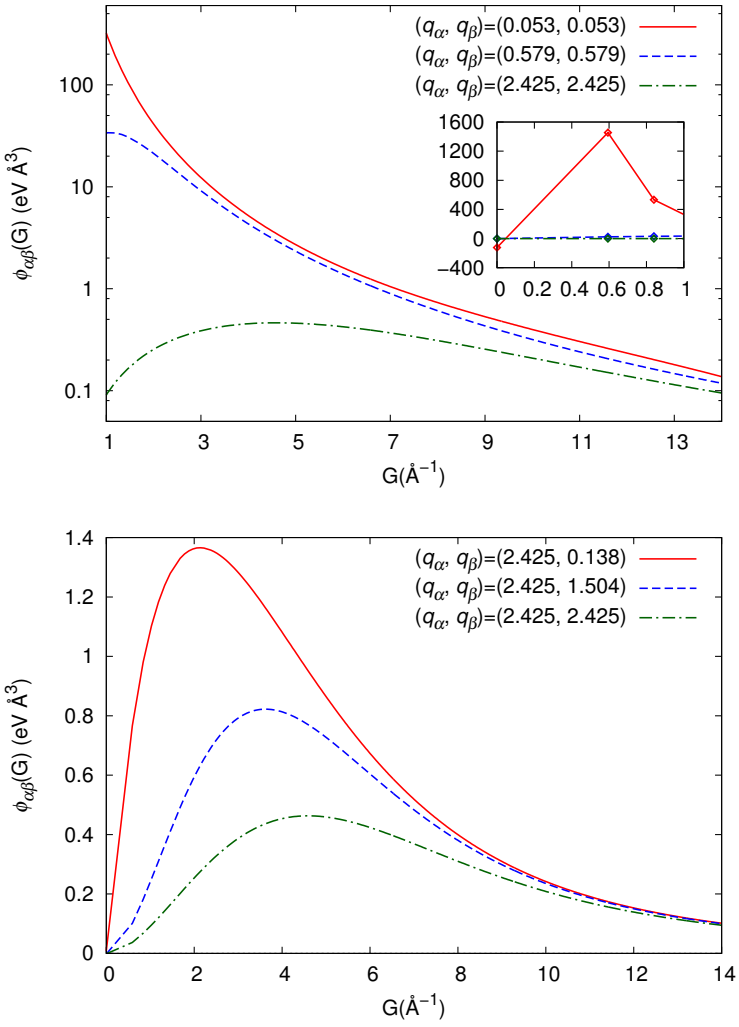

FIGURE 3.1: Fourier component of the kernel function $\phi_{\alpha\beta}(G)$, for several set of q_α and q_β. Diagonal (upper panel) and off diagonal (lower panel) components are shown.

correlation functional is given by

$$E_{\mathrm{c}}^{\mathrm{nl}} = \frac{1}{2} \iint \frac{n(\mathbf{r}_1)}{k^{3/2}(\mathbf{r}_1)} \phi^{\mathrm{rVV10}}(\tilde{q}_1, \tilde{q}_2, r_{12}) \frac{n(\mathbf{r}_2)}{k^{3/2}(\mathbf{r}_2)} d\mathbf{r}_1 d\mathbf{r}_2, \tag{3.27}$$

where $\phi^{\mathrm{rVV10}}(\tilde{q}_1, \tilde{q}_2, r_{12})$ is the rVV10 nonlocal correlation kernel,[25] $\tilde{q}_1 = \tilde{q}(\mathbf{r}_1)$, $\tilde{q}_2 = \tilde{q}(\mathbf{r}_2)$ and $k(n(\mathbf{r})) = 3\pi b(n/9\pi)^{1/6}/2$. $\tilde{q}_i$ is defined as $\tilde{q}(\mathbf{r}_i) = \omega_0(n(\mathbf{r}_i), |\nabla n(\mathbf{r}_i)|)/k(n(\mathbf{r}_i))$ with ω_0 defined in Ref. [26]. The parameter b is an adjustable parameter, which is determined by fitting on a training set (see Refs. [26, 25] for detail). By expanding the nonlocal correlation kernel in the same manner as Eq. (3.19), the nonlocal correlation energy is written as

$$E_{\mathrm{c}}^{\mathrm{nl}} = \frac{\Omega}{2} \sum_{\mathbf{G}} \sum_{\alpha\beta} \tilde{\eta}_\alpha^*(\mathbf{G}) \tilde{\eta}_\beta(\mathbf{G}) \phi_{\alpha\beta}^{\mathrm{rVV10}}(G), \tag{3.28}$$

where $\tilde{\eta}_\alpha(\mathbf{G})$ is the Fourier component of $\tilde{\eta}_\alpha(\mathbf{r})$, which is defined by

$$\tilde{\eta}_\alpha(\mathbf{r}) = q_\alpha n(\mathbf{r}) p_\alpha(\tilde{q}(\mathbf{r}))/k^{3/2}(\mathbf{r}) \tilde{q}(\mathbf{r}), \tag{3.29}$$

and the Fourier transform of the nonlocal correlation kernel ϕ^{rVV10} is given by

$$\phi_{\alpha\beta}^{\mathrm{rVV10}}(G) = \frac{1}{{q_\alpha}^{3/2}} F_{\alpha\beta}^{\mathrm{rVV10}}\left(\frac{G}{\sqrt{q_\alpha}}\right), \tag{3.30}$$

$$F_{\alpha\beta}^{\mathrm{rVV10}}(k) = \frac{4\pi}{k} \int_0^\infty u \sin(ku) \phi^{\mathrm{rVV10}}\left(u, \sqrt{\frac{q_\beta}{q_\alpha}} u\right) du. \tag{3.31}$$

The nonlocal correlation potential is calculated in the same way with vdW-DF.

3.5 Technicalities

I have implemented vdW-DF into our in-house DFT code,[28, 29, 30] which uses a plane-wave basis set and ultrasoft pseudopotentials.[31, 32] In the construction of the pseudopotentials, I neglected the nonlocal correlation ($E_{\mathrm{c}}^{\mathrm{nl}}$) and employed the semilocal exchange and correlation functionals, which are consistent with the solid state calculation. For instance, pseudopotential constructed using the refit Perdew Wang (PW86R)[33, 34] exchange and the LDA correlation was used in vdW-DF2 calculation. Use of the pseudopotential generated using the semilocal exchange correlation functional has been

justified.[35, 36] In the present vdW-DF calculations, I have used relatively large energy cutoffs for wave functions and electron density in the plane wave expansions, compared with those used in the LDA or GGA, to achieve the convergence of the pressure tensor, because the vdW forces are very weak, and potential energy surface is very sluggish. In the present work, I employed the Perdew-Zunger exchange-correlation for LDA [37] , and the PBE functional for GGA[14].

For the vdW-DF calculations, I employed the following functionals; the original vdW-DF with the revPBE[38] exchange and LDA correlation, second version of the vdW-DF (vdW-DF2), which uses PW86R[34] exchange, vdW-DF paired with the Cooper's (C09)[39] exchange (vdW-DF$^{\mathrm{C09x}}$),vdW-DF2 paired with C09 exchange (vdW-DF2$^{\mathrm{C09x}}$), vdW-DF2 paired with revised b86[36] exchange (rev-vdW-DF2). I also implemented the revised Vydrov-Van Voorhis functional (rVV10)[26, 25] with the WG[24] implementation , which uses the PW86R exchange, PBE correlation, and the nonlocal correlation. The functional is designed to give accurate C_6 coefficients and to vanish in the uniform electron gas limit.

To evaluate ϕ in the vicinity of $q_\alpha = 0$, I use a linear mesh up to $q = q_m$ with N^{lin} grid points, and the logarithmic mesh is used from q_m to q_c with N^{log} grid points, where q_c is the cutoff for the q-mesh. I use $q_c = 8$ a.u., $q_m = 0.01$ a.u., $N^{\mathrm{lin}} = 3, N^{\mathrm{log}} = 28$, except for rVV10, in which $q_c = 3$ a.u., $q_m = 0.005$ a.u. are used. I confirmed that the cutoff q_c is sufficiently large, by monitoring the distribution of q_0 and the nonlocal correlation energy as a function of q_0 function.

Chapter 4

Overview of GW method

We have some choices for exchange and local correlation energy functional on vdW-DF because this method just defines a nonlocal correlation energy except these functionals. Some combinations of exchange and local correlation energy functions have been suggested, and some researchers modified these functionals to be suitable for nonlocal correlation energy functionals. Almost methods use LDA/GGA exchange and local correlation energy, as it is well known, these treatment can not describe some electron correlation effect including an error of exchange energy. It is important to access more accurate electronic state than LDA/GGA and vdW-DF, for analyzing results obtained by those functionals and improving vdW-DF approach. Although there are some methods to access electron correlation effect, gw approximation based on many-body theory is one of promising methods for solid state physics. In this chapter we overview GW method, some problems, and beyond GW method.

4.1 1shot-GW method

GW method is based on many-body problem and quasi-particle equation is given by

$$\left[-\frac{1}{2}\nabla^2 + V_{\rm ion}(\mathbf{r}) + V^{\rm H}(\mathbf{r})\right]\psi_i(\mathbf{r},\omega) + \int \mathrm{d}\mathbf{r}'\Sigma_{\rm xc}(\mathbf{r},\mathbf{r}';\omega) = E_i\psi_i(\mathbf{r},\omega), \tag{4.1}$$

where $V_{\rm ion}$ is electronic potential from the ions, $V^{\rm H}$ is electrostatic potential (Hartree potential). The many-body effect is described by through the self-energy $\Sigma_{\rm xc}$. It is nonlinear equation because self-energy is nonlocal function and depends on eigen value of quasi-particle. According to Hedin theorem, there are some equations among the green function G, three point vertex function Γ, screened exchange W, and polarization

function Π and self-energy $\Sigma_{\mathbf{xc}}$ [40]. Since Γ is approximated as delta function by the GW approximation, self energy can be written as;

$$\Sigma_{\mathrm{xc}}(\mathbf{r},\mathbf{r}',\omega) = \frac{i}{2\pi}\int d\omega' G(\mathbf{r},\mathbf{r}',\omega-\omega')W(\mathbf{r},\mathbf{r}',\omega')e^{-i\delta\omega'}. \tag{4.2}$$

Here green function is given by

$$G(\mathbf{r},\mathbf{r}',\omega) = \sum_i \frac{\psi_i(\mathbf{r})\psi_i^*(\mathbf{r}')}{\omega-\epsilon_i \pm i\delta}. \tag{4.3}$$

The relation between W and Π is $W = v + \frac{v}{1-v\Pi}v\Pi$, and polarization function is $\Pi = -iG \times G$. In general, GW approximation indicates one-shot GW method. In this method, G is made from LDA or GGA wave functions and eigenvalues. The G, Π, W, and σ_{xc} can be calculated in order. Quasi-particle eigenvalues using self energy are estimated from following formula:

$$E_i = \epsilon_i + Z_i\left[\langle\psi_i|\Sigma_{\mathrm{xc}}(\epsilon_i) - V_{\mathrm{xc}}|\psi_i\rangle\right]. \tag{4.4}$$

Here Z_n is renormalized factor and as follows:

$$Z_n = \left[1 - \langle\psi_n|\frac{\partial}{\partial\omega}\Sigma_{\mathrm{xc}}(\mathbf{r},\mathbf{r}',\epsilon_n)|\psi_n\rangle\right]^{-1}. \tag{4.5}$$

Many researchers reported that GW approach gave more reasonable band gap on insulators.

4.2 Beyond GW method

As we showed in the last section, one shot GW approach is based on perturbation theory. For one shot GW approach is a good approximation, it is necessary that the perturbation is not large. Therefore if LDA/GGA results apart from the actual electron state, e.g: NiO, one shot GW approach does not work well. Although we can consider the different starting point for perturbation approach, such as LDA+U approach, to overcome this problem, the result of one shot GW much depends on an initial condition. Therefore the self consistent approach should be required, and self-consistent GW approach is performed. The attempt is expected to legitimate way, but it gives wrong band gap.

The neglecting of Γ function is said to be a cause of it, indicating that Γ should be must accurately calculated.

The Hedin theorem gives

$$\Sigma_{\mathrm{xc}}(x_1, x_2) = \frac{i}{2\pi} \int dx_3 x_4 G(x_1, x_3 + \delta) W(x_1, x_4) \Gamma(x_3, x_2, x_4), \tag{4.6}$$

as self energy. For successful of the self-consistent GW, the self energy would be calculated as $GW\Gamma$. However computational cost of Γ is huge, applicable systems are limited, for example a few atoms in unit cell.

4.3 QSGW approach

To overcome one shot GW problem, other self-consistent scheme that called quasi-particle self-consistent GW (QSGW) has been proposed by T. Kotani and Mark van Schilfgaarde [2]. One particle effective exchange correlation potential produced by Σ_{xc} is as follows:

$$V^{\mathrm{xc}} = \frac{1}{2} \sum_{ij} |\psi_i\rangle \, \Re[\Sigma_{\mathrm{xc}}(\epsilon_i)]_{ij} + \Re[\Sigma_{\mathrm{xc}}(\epsilon_j)]_{ij} \, \langle\psi_j| \tag{4.7}$$

LDA/GGA DFT calculation performed using this effective correlation potential, after that self energy are calculated in the same way with GW approximation. By continuing the cycle, we can get self-consistent results for effective exchange correlation potential. Although the procedure of making effective potential is not clear for theoretical background, QSGW gave more reasonable band gap compared with one shot GW approach. We refer the previous results for GW and QSGW from [1, 2] on Fig. 4.1. Figure 4.1 shows that one shot GW approach can improve band gap from LDA results, but still underestimated. On the other hand, QSGW approach reproduces experimental band gap, even though it tends to overestimate the band gap.

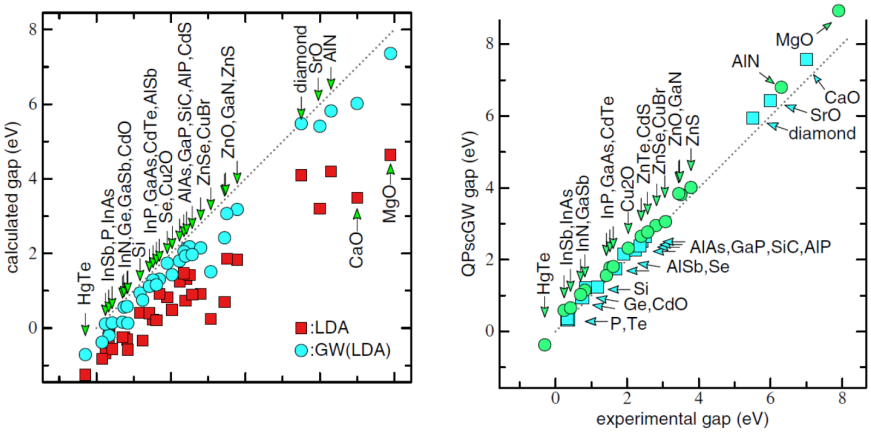

FIGURE 4.1: The comparison of band gap between experimental and theoretical values. Left figure shows LDA and one shot *GW* results and right figure shows QS*GW* results.[1, 2]

Chapter 5

Extension of vdW-DF

Since the vdW interaction is not directly related to the spin polarization, a truly spin polarized version of vdW-DF has not yet been developed, except for the one proposed by Vydrov and Van Voorhis.[41] Thus, the application of vdW-DFs to magnetic systems is quite limited. We have proposed a practical approach to magnetic system within the framework of vdW-DF, in which spin polarization dependent gradient correction is added to the local correlation energy and potential, instead of developing the spin polarized version of the nonlocal correlation [42, 43].

5.1 vdW-DF-SGC

In the original vdW-DF, LDA was employed for the short-range local correlation energy, to avoid double counting of the contribution from $|\nabla n|$ contained in $E_{\rm c}^{\rm nl}$.[8] For simplify, the exchange and local correction energy functionals can be expanded to spin polarization;

$$E_{\rm xc}[n_\uparrow, n_\downarrow] = E_{\rm x}^{\rm GGA}[n_\uparrow, n_\downarrow, |\nabla n_\uparrow|, |\nabla n_\downarrow|] + E_{\rm c}^{\rm LDA}[n_\uparrow, n_\downarrow] + E_{\rm c}^{\rm nl}[n, |\nabla n|]. \tag{5.1}$$

Here $n_\uparrow$ and $n_\downarrow$ is up and down electron density, respectively. In a spin polarized system, spin-polarization dependent gradient correction should be included in the correlation energy and potential, but such a contribution is missing in the nonlocal correlation, as it is mostly formulated for the spin unpolarized system. In this senses, we have proposed how to extent to the spin system as follows:

$$E_{\rm c}^{\rm loc} = E_{\rm c}^{\rm LSDA}[n_\uparrow, n_\downarrow] + \Delta E_{\rm c}[n, \zeta], \tag{5.2}$$

where

$$\begin{aligned}\Delta E_{\mathrm{c}}[n,\zeta] &= E_{\mathrm{c}}^{\mathrm{GGA}}[n_{\uparrow},n_{\downarrow}] - E_{\mathrm{c}}^{\mathrm{GGA}}[n/2,n/2] \\ &= \int n\left\{H(r_s,\zeta,t) - H(r_s,0,t)\right\} d\mathbf{r}, \end{aligned} \tag{5.3}$$

H, r_{s}, ζ and t are the gradient contribution, Seitz radius ($n = 3/4\pi r_s^3$), the relative spin polarization, and the dimensionless density gradient proportional to $|\nabla n|$, respectively. The $\int d\mathbf{r} n(\mathbf{r})[H(r_s,\zeta,t) - H(r_s,\zeta=0,t)]$ which is spin dependent gradient correction did not be considered in simple expansion. We use the functional form for H proposed by Perdew, Burke and Ernzerhof (PBE).[14] The present functional reduces to the original one in the absence of spin polarization. Note that SGC is not necessary for rVV10, because PBE-GGA correlation is used for the local correlation.

5.2 svdW-DF

The other extension of vdW-DF to spin polarized system (svdW-DF) has been proposed by T. Thonhauser et al.[44]. They applied svdW-DF to some magnetic molecule and the system of magnetic surface and molecule. However they did not compare between svdW-DF and vdW-DF version which has been expanded to spin polarized on exchange and local correction. Comparing with vdW-DF-SGC is also important to check the accuracy and give useful information to improve exchange-correction functional. Therefore we also implemented svdW-DF to our DFT code. In this section, we review the svdW-DF and derive energy, potential, and pressure formula using order N log N method which is proposed by Jun Wu and Fraccois Gygi to reduced the huge computational cost caused by double integral in real space. The nonlocal correlation energy in the Jun Wu and Francois Gygi method is written as follows:

$$E_{\mathrm{c}}^{\mathrm{nl}} = \frac{1}{2}\sum_{\alpha\beta}\iint d\mathbf{r}d\mathbf{r}'\eta_\alpha(\mathbf{r})\eta_\beta(\mathbf{r}')\phi_{\alpha\beta}(|\mathbf{r}-\mathbf{r}'|) \tag{5.4}$$

where

$$\eta_\alpha(\mathbf{r}) = \frac{q_\alpha n(\mathbf{r}) p_\alpha(q_0(\mathbf{r}))}{q_0(\mathbf{r})} \tag{5.5}$$

Originally, $q_0(n)$ function is composed by unspin polarized one particle exchange and correlation energy part as follows

$$q_0(\mathbf{r}) = q_{0\mathrm{x}}[n] + q_{0\mathrm{c}}[n], \tag{5.6}$$

$$q_{0\mathrm{x}}[n] = -\left(1 - \frac{Z_{ab}}{9}s^2\right)\frac{4\pi}{3}\varepsilon_{\mathrm{x}}^{\mathrm{LDA}} = \left(1 - \frac{Z_{ab}}{9}s^2\right)k_{\mathrm{F}}, \tag{5.7}$$

$$q_{0\mathrm{c}}[n] = -\frac{4\pi}{3}\varepsilon_{\mathrm{c}}^{\mathrm{LDA}}(n). \tag{5.8}$$

The $q_0(n)$ function which is related with wave number depends on charge density in vdW-DF method, but it was extended to function of spin density $n_\uparrow, n_\downarrow$ in svdW-DF. Considering the spin scaling relation, the q_0 function depending on spin density is written as follows:

$$q_0(\mathbf{r}) = \tilde{q}_{0\mathrm{x}}[n_\uparrow, n_\downarrow] + \tilde{q}_{0\mathrm{c}}[n_\uparrow, n_\downarrow], \tag{5.9}$$

$$\tilde{q}_{0\mathrm{x}}[n_\uparrow, n_\downarrow] = \frac{n_\uparrow}{n}q_{0\mathrm{x}}[2n_\uparrow] + \frac{n_\downarrow}{n}q_{0\mathrm{x}}[2n_\downarrow], \tag{5.10}$$

$$\tilde{q}_{0\mathrm{c}}[n_\uparrow, n_\downarrow] = -\frac{4\pi}{3}\varepsilon_{\mathrm{c}}^{\mathrm{LDA}}(n, \zeta). \tag{5.11}$$

The nonlocal potential depending on spin density can be written as

$$v_{\mathrm{c}\uparrow}^{\mathrm{nl}}(\mathbf{r}) \simeq \frac{\Omega}{N_{\mathrm{grid}}}\frac{dE_{\mathrm{c}}^{\mathrm{nl}}}{dn_\uparrow(\mathbf{r})} = \sum_\alpha \left(u_\alpha(\mathbf{r})\frac{\partial\eta_\alpha(\mathbf{r})}{\partial n_\uparrow(\mathbf{r})} + \sum_{\mathbf{r}'} u_\alpha(\mathbf{r}')\frac{\partial\eta_\alpha(\mathbf{r}')}{\partial\nabla n_\uparrow(\mathbf{r}')}\frac{\partial\nabla n_\uparrow(\mathbf{r}')}{\partial n_\uparrow(\mathbf{r})} \right). \tag{5.12}$$

where $u_\alpha(\mathbf{r}) = \sum_\beta \int d\mathbf{r}'\eta(\mathbf{r}')\phi_{\alpha\beta}(|\mathbf{r} - \mathbf{r}'|)$ is same with vdW-DF case. Since the nonlocal kernel function is same with vdW-DF, however q_0 function depends on spin density. In the svdW-DF approach, it is easy to expand to Wu and Gygi's order N log N method. We show the detail formulations for implementation. The spin dependent parts are calculated as follows:

$$\frac{dq_0(\mathbf{r})}{dn_\uparrow} = \frac{n_\downarrow}{n^2}(q_{0\mathrm{x}}[2n_\uparrow] - q_{0\mathrm{x}}[2n_\downarrow]) + \frac{2n_\uparrow}{n}\frac{dq_{0\mathrm{x}[n]}}{dn}|_{n=2n_\uparrow}, \tag{5.13}$$

$$\frac{dq_0(\mathbf{r})}{dn_\downarrow} = \frac{n_\uparrow}{n^2}(q_{0\mathrm{x}}[2n_\downarrow] - q_{0\mathrm{x}}[2n_\uparrow]) + \frac{2n_\downarrow}{n}\frac{dq_{0\mathrm{x}[n]}}{dn}|_{n=2n_\downarrow}. \tag{5.14}$$

Here

$$\frac{dq_{0\mathrm{x}[n]}}{dn} = \left(1 - \frac{Z_{ab}}{9}s^2\right)\frac{dk_\mathrm{F}}{dn} = \left(1 - \frac{Z_{ab}}{9}s^2\right)\frac{k_\mathrm{F}}{3n} \tag{5.15}$$

and

$$\frac{dq_0(\mathbf{r})}{d\nabla n_\uparrow} = \frac{\nabla n_\uparrow}{|\nabla n_\uparrow|}\frac{dq_0}{d|\nabla n_\uparrow|} = \frac{\nabla n_\uparrow}{|\nabla n_\uparrow|}\frac{n_\uparrow}{n}\frac{dq_{0\mathrm{x}}[2n_\uparrow]}{d|\nabla n_\uparrow|} = -\frac{Z_{ab}}{9}\frac{\nabla n_\uparrow}{2k_{\mathrm{F}\uparrow}n_\uparrow}\frac{1}{n}. \tag{5.16}$$

About the pressure tensor, it is almost some with vdW-DF case.

$$\begin{aligned}
(\Pi_\mathrm{c}^\mathrm{nl})_{k\ell} = &-\frac{1}{\Omega}E_\mathrm{c}^\mathrm{nl}\delta_{k\ell} \\
&- \frac{1}{N}\sum_m\sum_j\sum_\alpha\sum_\sigma u_\alpha(\mathbf{r}_j)\frac{\partial\eta_\alpha(\mathbf{r}_j)}{\partial n^\sigma(\mathbf{r}_j)}\frac{\partial n^\sigma(\mathbf{r}_j)}{\partial h_{km}}(h^t)_{m\ell} \\
&+ \frac{1}{N}\sum_j\sum_\alpha\sum_\sigma u_\alpha(\mathbf{r}_j)\frac{\partial\eta_\alpha(\mathbf{r}_j)}{\partial|\nabla n^\sigma(\mathbf{r}_j)|}\frac{(\nabla n^\sigma(\mathbf{r}_j))_k(\nabla n^\sigma(\mathbf{r}_j))_\ell}{|\nabla n^\sigma(\mathbf{r}_j)|} \\
&- \frac{1}{N}\sum_m\sum_j\sum_\alpha\sum_\sigma u_\alpha(\mathbf{r}_j)\frac{\partial\eta_\alpha(\mathbf{r}_j)}{\partial|\nabla n^\sigma(\mathbf{r}_j)|}\frac{\nabla n^\sigma(\mathbf{r}_j)}{|\nabla n^\sigma(\mathbf{r}_j)|}\cdot\sum_\mathbf{G}\frac{\partial n^\sigma(\mathbf{G})}{\partial h_{km}}(h^t)_{m\ell}(i\mathbf{G})e^{i\mathbf{G}\cdot\mathbf{r}_j} \\
&+ \frac{1}{2}\sum_{\alpha\beta}\sum_\mathbf{G}\eta_\alpha^*(\mathbf{G})\eta_\beta(\mathbf{G})\frac{\partial\phi_{\alpha\beta}(G)}{\partial|\mathbf{G}|}\frac{G_kG_\ell}{|\mathbf{G}|},
\end{aligned} \tag{5.17}$$

Comparing with vdW-DF, spin index σ is used in some parts. Since svdW-DF use same kernel function with vdW-DF, the last term is same with vdW-DF.

Chapter 6

Application of vdW-DF and spin dependent vdW-DF

We will show the application of vdW-DF and spin dependent vdW-DF (vdW-DF-SGC and svdW-DF). We demonstrate the usefulness of the nonlocal correaltion approach using relatively simple systems e.g.: nobel gas solid, molecular complex and molecular solid. The Results for crystal systems are summaried in [43] and oxygen molecular systems results are reported [42, 45].

6.1 Oxygen Molecule

We show the oxygen molecule results. We performed Γ point calculation which has $20 \times 20 \times 20$ Å^3 cubic unit cell using several echange-correlation functional. The energy cutoffs of 40 and 350 Ry were used for wave function and electron density, respectively. Table 6.1 shows the calculated properties of an oxygen molecule with several functionals. The calculated equilibrium bond length (b), binding energy ($E_{\rm b}^{\rm mol}$) , and vibration frequency (ω) are comparable to the experimental values. Interestingly, the data obtained with vdW-DFs shows that introduction of SGC, lowers the binding energy by 0.23 eV. $E_{\rm b}^{\rm mol}$ obtained using vdW-DF-SGC is much smaller than that obtained using PBE, and in better agreement with the experimental value, but b is overestimated. vdW-DFs with the C09 exchange tend to decrease b, leading to better agreement with the experimental value than PBE and vdW-DFs with the revPBE exchange, but overestimate $E_{\rm b}^{\rm mol}$ significantly. Nevertheless, $E_{\rm b}^{\rm mol}$'s obtained using PBE and vdW-DFs with the C09 exchange are in reasonably good agreement.

TABLE 6.1: Properties of oxygen molecule: equilibrium bond lengths (b), binding energies ($E_{\mathrm{b}}^{\mathrm{mol}}$), vibrational frequencies (ω), and HOMO-LUMO energy gaps ($\Delta\varepsilon_{\mathrm{H-L}}$).

energy functional	b (Å)	$E_{\mathrm{b}}^{\mathrm{mol}}$ (eV)	ω(THz)	$\Delta\varepsilon_{\mathrm{H-L}}$ (eV)
PBE	1.221	6.03	44.7	2.38
vdW-DF	1.233	5.50	45.7	2.26
vdW-DF-SGC	1.232	5.27	45.6	2.37
vdW-DF$^{\mathrm{C09}_x}$	1.214	6.49	48.4	2.22
vdW-DF$^{\mathrm{C09}_x}$-SGC	1.214	6.26	48.3	2.33
vdW-DF2$^{\mathrm{C09}_x}$	1.215	6.37	48.3	2.22
vdW-DF2$^{\mathrm{C09}_x}$-SGC	1.215	6.14	48.3	2.33
Exp.	1.207[a]	5.12[a]	47.39[a]	

[a] Ref. [47]

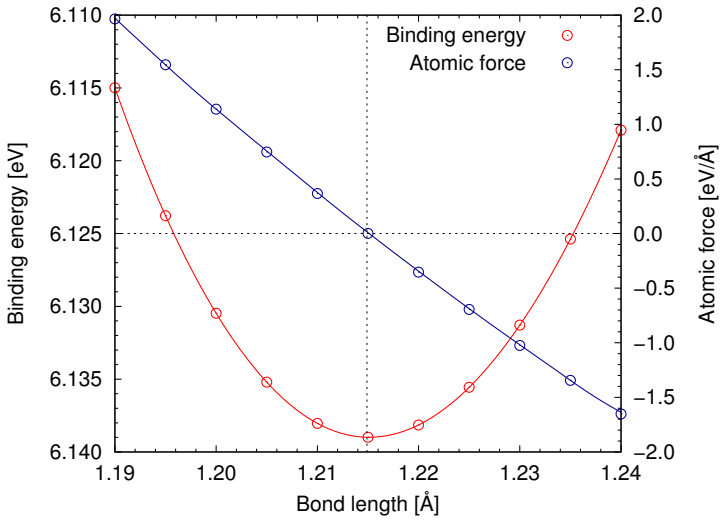

FIGURE 6.1: Binding energy and atomic force of oxygen molecule as functions of bond length. vdW-DF2$^{\mathrm{C09}_x}$-SGC was used for the calculations.

Figure 6.1 shows binding energy and atomic force as functions of bond length for the oxygen molecule calculated using vdW-DF2$^{\mathrm{C09}_x}$-SGC. The equilibrium bond length is estimated to be 1.215 Å from the energy minimum. This differs by less than 1×10^{-3} Å from the bond length determined from the atomic force. The vdW-DF approach does not drastically change the equilibrium bond length, binding energy, vibration frequency, or the energy gap between the highest occupied molecular orbital (HOMO) and the lowest unoccupied molecular orbital (LUMO) levels, compared with results of GGA (PBE). Our data is in line with the fact that the XC functional of vdW-DFs has a predictive power for small molecules similar to GGA.[46]

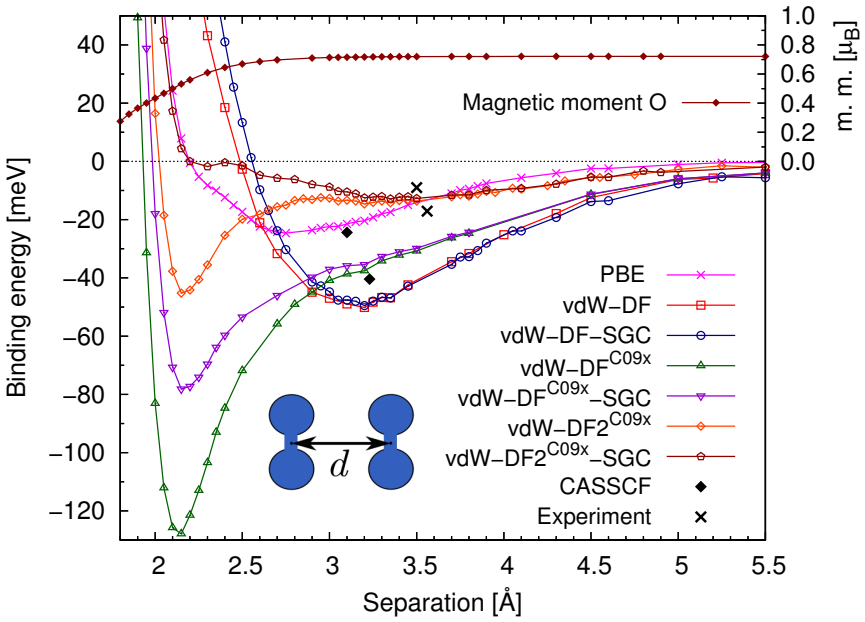

FIGURE 6.2: Intermolecular interaction energy as a function of the separation between oxygen molecules at the antiferromagnetic parallel-molecule configuration (see the inset for the configuration), together with the results from experiment and quantum chemistry calculation. The atomic magnetic moment (m.m.) is also reported in the upper part of the panel.

6.2 H-type Pair of oxygen molecules

The intermolecular interaction potential was evaluated in the parallel (H-type) molecular configuration with several functionals. In the calculation, the bond length in each molecule was fixed to its respective ground-state value listed in Table 6.1. Figure 6.2 shows the binding energy as a function of the distance between centers of molecules (d). The reference total energy was set to that of the molecular pair at d larger than 6.4 Å. This energy differs by only 0.5 meV from twice the total energy minimum of single molecule. The properties of the binding energy curve are shown in Table 6.2. The equilibrium distance and binding energy were determined by fitting the binding energy curve around the minimum to a third-order polynomial.

The potential curves from the original vdW-DF show a lower energy than those with SGC and a strong repulsive feature at distances smaller than 3.5 Å. This repulsive interaction with SGC makes the equilibrium distance larger, especially in vdW-DF2^{C09_x}. The repulsive force is attributed to the intermolecular magnetic interaction. At approximately 2.15 Å such a repulsive nature becomes weak in accordance with the decrease in

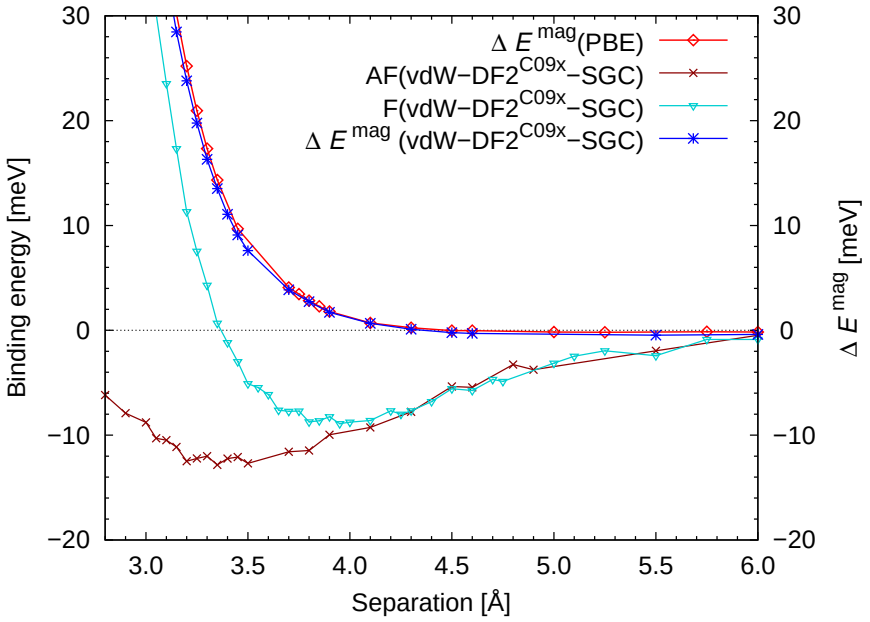

FIGURE 6.3: Magnetic interaction energies with respect to the intermolecular distance and the intermolecular interaction energies of the antiferro (AF)- and ferro (F)-magnetic coupling oxygen molecules are also shown.

magnetic moment (see upper part of Fig. 6.2, which is generally common among functionals), resulting in an energy minimum or dip in the potential curves. Note that the repulsive potential, which appears at less than 2 Å, is mainly of nonmagnetic origin.

With the original vdW-DF with SGC, the minimum is observed at 3.20 Å, with vdW-DF$^{\mathrm{C09}_x}$-SGC at 2.16 Å, and with vdW-DF2$^{\mathrm{C09}_x}$-SGC at 3.44 Å. The first and last functionals almost reproduce the distance obtained in the previous work, which employs the quantum chemistry method or experimental measurement: 3.1 Å, 3.23 Å (CASSCF),[48, 49] and 3.5 Å, 3.56 Å (experiment).[50, 3] Concerning the binding energy of the O_2 pair ($E_{\mathrm{b}}^{\mathrm{O}_4}$), the value calculated using vdW-DF2$^{\mathrm{C09}_x}$-SGC (12.9 meV) is in good agreement with experimental values; 9 meV,[50] 17.1 meV.[3] The value obtained using vdW-DF-SGC (48.0 meV) is similar to the result by CASSCF (40.4 meV), as indicated by the feature of equilibrium distance. These agreements with the more elaborate method or the recent experiment imply that vdW-DF-SGC and vdW-DF2$^{\mathrm{C09}_x}$-SGC predict a desirable potential for describing the electronic structures of larger systems, such as $(O_2)_4$ cluster and solid oxygen.

The magnetic interaction energy between molecules may be given by the energy difference ΔE^{mag} between ferro (F)- and antiferro (AF)-magnetic coupling pairs: $\Delta E^{\mathrm{mag}} =$

$E^{\mathrm{F}} - E^{\mathrm{AF}}$, where E^{F} and E^{AF} are the total energies for the F and AF states, respectively. Figure 6.3 shows ΔE^{mag} as a function of the separation d obtained using vdW-DF2$^{\mathrm{C09}_x}$. ΔE^{mag} obtained using PBE is also shown for comparison. The functional dependence of the magnetic interaction within vdW-DF was found to be small (not shown). ΔE^{mag} emerges at 4.1 Å and increases by 24 meV at 3.2 Å. Such a magnetic energy scale is comparable to the binding energy of the O_2 pair, implying that the energy minimum in the potential curve (vdW-DF-SGC or vdW-DF2$^{\mathrm{C09}_x}$-SGC) is determined not only by the balance between the Pauli repulsion and the vdW attraction, but also by an intermolecular magnetic interaction. Note that the ΔE^{mag}'s obtained using vdW-DF2$^{\mathrm{C09}_x}$ and PBE are almost identical. Because PBE lacks a long-range vdW attraction, the result suggests that our present approach (vdW-DF with SGC) describes the short-range magnetic interaction as accurate as PBE.

The tail of the interaction energy curve is characterized by the function $-C_6/d^6$. The coefficient C_6 obtained by fitting the calculated data (Table 6.2) varies from 47 to 121 eVÅ^6 in vdW-DFs. The values in the data are dispersive, but decrease in order of publication year of the functionals. These values are comparable to or larger than those of Ar (37 eV Å^6) and N_2 (47 eV Å^6) dimers.[8, 51] We note that C_6 coefficients should be identical when the same nonlocal correlation functional is used, because, in the vdW asymptote, C_6 does not depend on exchange or short-range correlation energy, but on charge density and q_0 function.[8, 41] Thus, the difference between the C_6 coefficients (for e.g., difference in those obtained with vdW-DF and vdW-DF$^{\mathrm{C09}_x}$) may be attributed to the use of a small simulation cell, and the differences (within 27 eVÅ^6) should be regarded as numerical errors. As for the Lennard-Jones potential, the hard-core diameter σ_0 of the intermolecular distance where the potential energy vanishes is worth investigating. As indicated in Table 6.2, σ_0's with vdW-DFs are equal to or less than 2.6 Å. The largest value is in agreement with those from theoretical calculations (2.7 Å, 3.0 Å)[49, 52] while the smaller value at approximately 2 Å offers a picture of smaller particles in the gas phase.

TABLE 6.2: Features of the intermolecular potential energy curve for vdW functionals (vdW-DF, vdW-DF^{C09_x}, vdW-DF2^{C09_x}) and those with gradient correction (-SGC): equilibrium distances (d), binding energies ($E_b^{O_4}$), C_6 coefficients, and hard-core diameters (σ_0). For comparison, the data of PBE, CASSCF and experimental measurement are also listed.

energy functional	d (Å)	$E_b^{O_4}$ (meV)	C_6 (eVÅ^6)	σ_0(Å)
PBE	2.77	24.6	22	2.20
vdW-DF	3.18	50.3	108	2.49
vdW-DF-SGC	3.20	48.0	121	2.56
vdW-DF^{C09_x}	2.13	128.3	95	1.93
vdW-DF^{C09_x}-SGC	2.16	78.5	94	1.98
vdW-DF2^{C09_x}	2.16	45.5	47	2.02
vdW-DF2^{C09_x}-SGC	3.44	12.9	48	2.20
CASSCF	3.1[a]	24.4[a]		
	3.23[b]	40.4[b]		2.7[b]
Exp.	3.5[c]	9[c]		
	3.56[d]	17.1[d]		

[a] Ref. [48], [b] Ref. [49], [c] Ref. [50], [d] Ref. [3]

6.3 T, X, and S type pair of oxygen molecules

Figure 6.4 shows binding energy curves of T-type and X-type configurations in ferromagnetic and antiferromagnetic states. In these configurations, the two methods gave almost the same equilibrium distance for the respective configurations, however PBE gave a weak binding energy compared with vdW-DF-SGC. This is because the PBE does not contain any explicit contribution of vdW interaction. The experimental values, equilibrium distance and binding energy, are 3.74Å, 16 meV in T-type and, are 3.63 Å and 15.3 meV in X-type [3]. These experimental values were placed between those of PBE and vdW-DF-SGC. Compared with experiment, the calculated results indicate that the nonlocal correlation energy may be overestimated.

Figure 6.5 shows binding energy curves in antiferromagnetic states. Because of kinetic super exchange, antiferromagnetic states are more stable at almost all the configurations than the respective ferromagnetic states. As reducing θ from 90 degree, decreasing the distance of the atoms belonging the other molecules, it tends to increase the equilibrium distance in either GGA and vdW-DF-SGC. However at $\theta = 90$ case (H-type), the distance was much reduced in GGA, as described in the previous study[42].

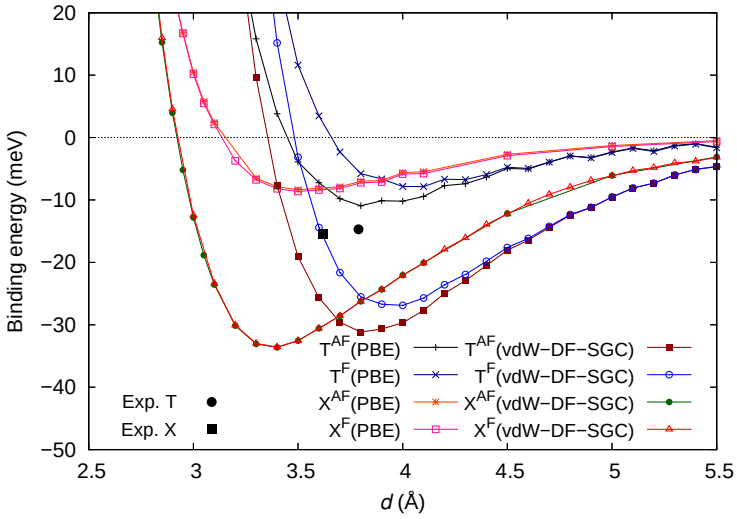

FIGURE 6.4: Binding energy curves for T-type and X-type as a function of the distance connecting the centers of molecules. The superscripts (AF, F) indicate antiferromagnetic and ferromagnetic states, respectively. The black solid circle and square are the experimental results for singlet state[3].

To understand such behavior, we check the components of total energy. The total energy ($E_{\rm tot}$) consists of Kohn-Sham kinetic energy ($T_{\rm ks} = \sum_i \langle\phi_i| - \frac{1}{2}\nabla^2|\phi_i\rangle$, where ϕ_i is Kohn-Sham wave function), electrostatic energy ($E_{\rm es}$), local and nonlocal part energies which co me from pseudopotential ($E_{\rm loc}$, $E_{\rm nl}$), and exchange correlation energy ($E_{\rm xc}$). Figure 6.6 shows each energy component in H-type configuration using PBE and vdW-DF-SGC. In the figure, vdW-DF-SGC has an attractive exchange correlation energy, on the other hand, GGA has a repulsive exchange correlation energy. This means that the origin of attractive potential is different between GGA and vdW-DF-SGC. Note that some energy components showed large differences between the two methods. As shown in Fig. 6.5, the attractive potential of vdW-DF-SGC between molecules mainly comes from exchange correlation energy.

Next, we computed magnetic interaction J defined by the energy difference between antiferromagnetic and ferromagnetic states ($J = E^{\rm F} - E^{\rm AF}$, where $E^{\rm F}$ and $E^{\rm AF}$ are the total energies of ferromagnetic and antiferromagnetic states, respectively). Figure 6.7 shows J as a function of d with using vdW-DF-SGC. As the angle θ reduces from 90 degree, the value of J reduces and, then increases. This characteristic feature may be related with an S-type structural configuration. Moreover, there are some structural parameters at which the ferromagnetic state is more stable than the antiferromagnetic

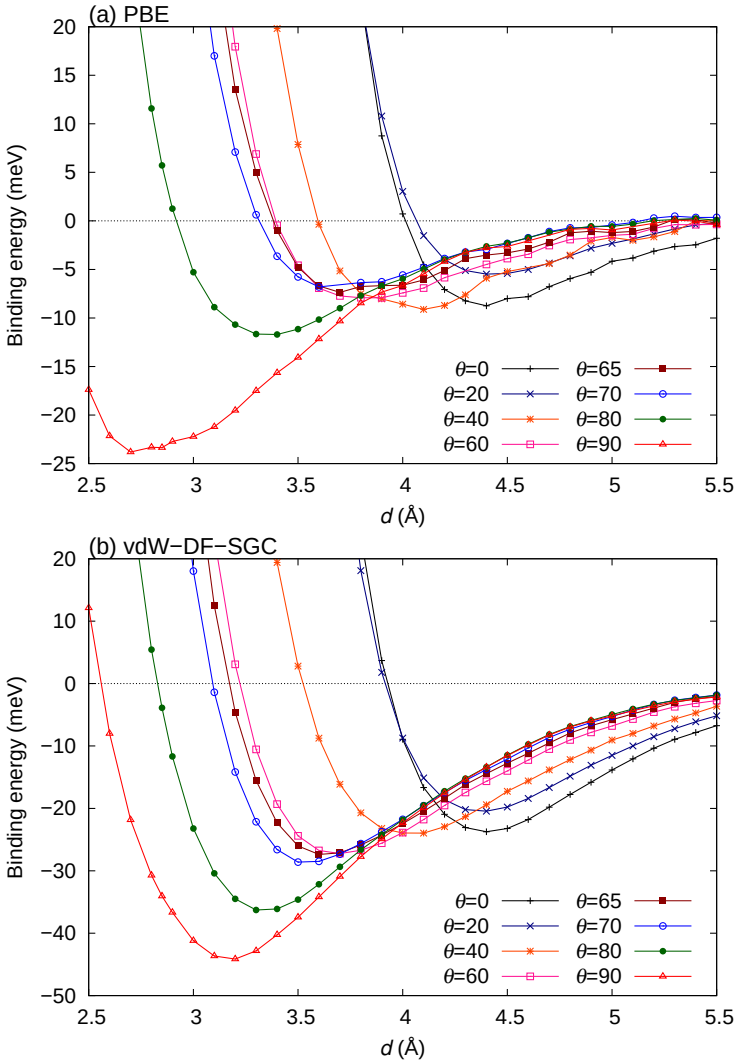

FIGURE 6.5: Binding energy curves for S-type configuration as a function of the distance connecting the centers of molecules for several configurations of θ with using (a) PBE and (b) vdW-DF-SGC.

state in a range of d ($\theta = 60 - 70$ degree). In the turning point of magnetic stability around $\theta = 70$ degree, it was found that the distance dependence of J became very weak even at the intermolecular distances longer than $d = 2.7$ Å. This is very interesting because such a structural configuration possibly passes with an tiny energy barrier at a magnetic configuration change.

As shown in Fig. 6.8, we present J as a functions of θ at $d = 3.3$ using vdW-DF-SGC. To check the accuracy of vdW-DF-SGC approach, our result is compared with the Bartolomei's result of RCCSD(T) method [4]. Both curves have a very similar behavior with respect to θ except for scale of interaction energy. Our results on J are about 5 times larger than those of RCCSD(T). The J may be proportional to $-t^2/\Delta E$, where

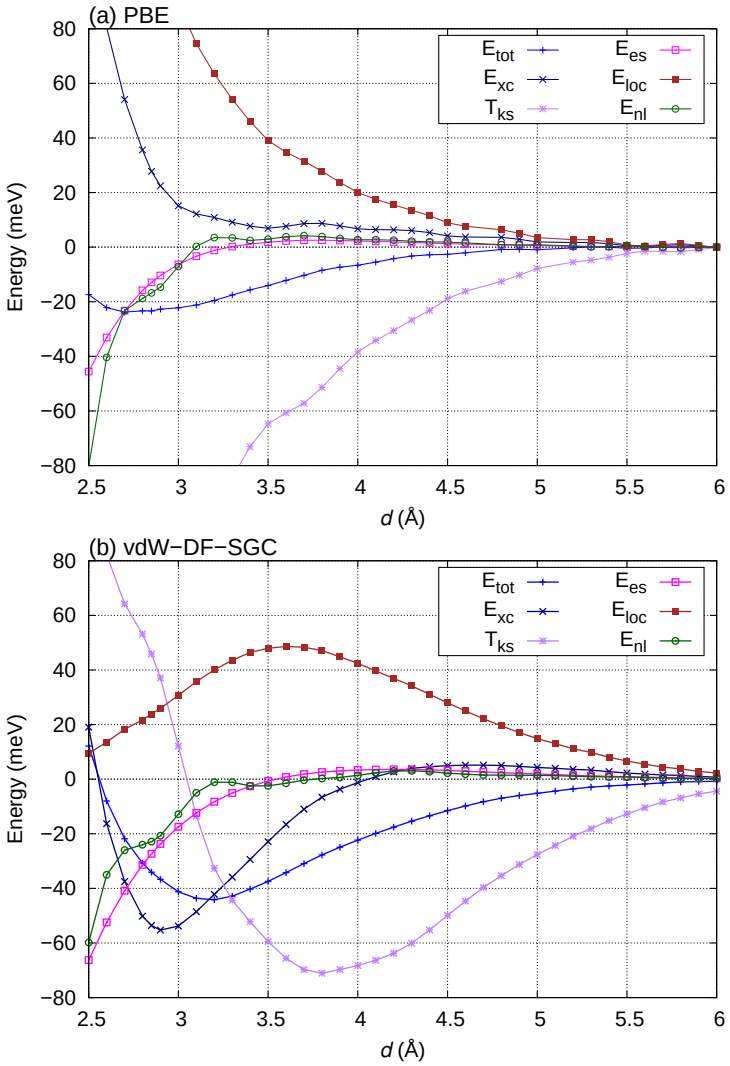

FIGURE 6.6: Components of the total energy as a function of the distance connecting the center of molecules at $\theta = 90$ (H-type) with using PBE (a) and vdW-DF-SGC (b).

t and ΔE are the transfer integral and the energy gap between spin-up and spin-down states just above and below the Fermi level. Since the GGA underestimates the energy gap in insulating or molecular system, J may be overestimated in our method. Note that, in Fig. 6.8, because there is no contribution of exchange energy at $d = 3.3$, the vdW-DF-SGC and PBE gave an identical result.

When the $|J|$ becomes zero, the transformation between antiferromagnetic and ferromagnetic states of the molecular pair occurs without any large energy change at moderate finite temperatures. There are interesting features in Fig 6.8; at $\theta = 20, 65$ degrees. The first angle corresponds to a similar value that is found in the neighboring pair of molecules when the solid oxygen transforms from α-phase to δ-phase, during which

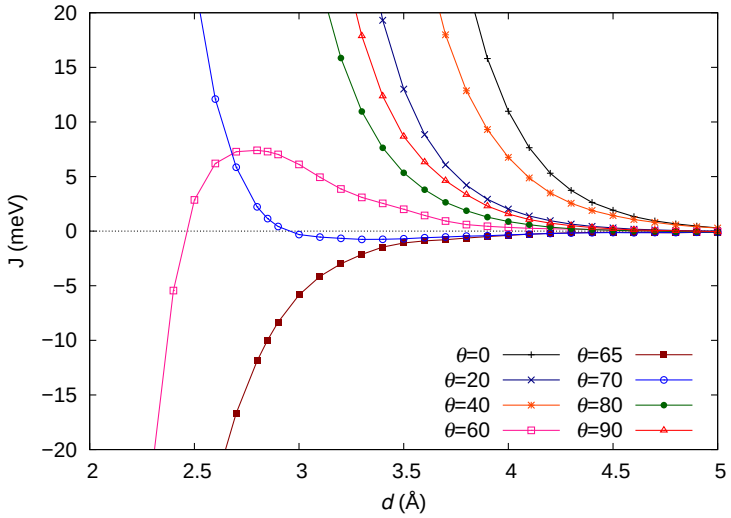

FIGURE 6.7: Magnetic interaction J as a function of the distance between molecules in S-type configuration with using vdW-DF-SGC.

the pair of spin configuration changes from antiferromagnetic coupling to ferromagnetic one[53]. The second angle may be interesting in a relation with meta-magnetic transformation under a high magnetic field. As pointed out in the experiment [54], the external field may induce a structural change in which the antiferromagnetic parallel pair (H-type) of molecules deforms to a S-type one. The structural deformation to the second angle mentioned above can much promote the induced magnetization by the external field.

6.4 Fcc and hcp argons

We begin with solid argon in the face centered cubic (fcc) and the hexagonal closed pack (hcp) structures, as a typical vdW bonded solid. It is known that at the ambient pressure, argon in the fcc structure is the most stable, while that in the hcp structure is metastable. For both phases, we optimized lattice parameters using several vdW-DFs as well as LDA and GGA. The energy cutoffs of 60 and 500 Ry were used for wave function and electron density, respectively. A $14 \times 14 \times 14$ ($8 \times 8 \times 8$) MP special k-point set was used for the fcc (hcp) phase. The optimized lattice constant and cohesive energy for fcc argon are summarized in Table 6.3, along with CCSD(T) and experimental values. The lattice constant obtained using LDA (PBE) is underestimated (overestimated), while those with vdW-DFs are improved except for vdW-DF2$^{\mathrm{C09x}}$, and most of the vdW-DFs

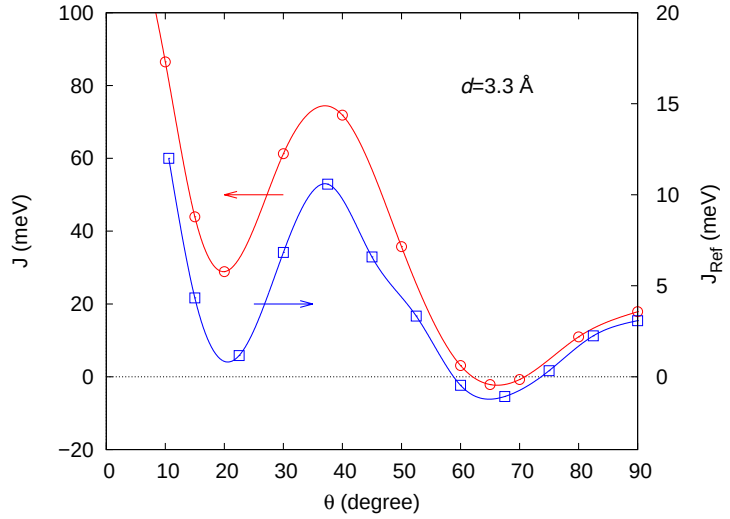

FIGURE 6.8: Magnetic interaction J as a function of θ at $d = 3.3$. The circles show the result obtained by vdW-DF-SGC and the squares the corresponding quantity reported in Ref.[4]. The curves are drawn by cubic spline.

improve the cohesive energy. Our results for fcc argon are in good agreement with the recent results by Tran and Hutter.[55]

The results for the hcp argon are summarized in Table 6.4. The difference between the cohesive energies for the fcc and hcp phases are very small (at most 2 meV/atom) and these phases are almost degenerated. The lattice parameters for the hcp structure satisfy the ideal ratio $a_{\rm fcc} \sim \sqrt{2}a_{\rm hcp}$, $c_{\rm hcp}/a_{\rm hcp} = 1.633$, where $a_{\rm fcc}$, $a_{\rm hcp}$, and $c_{\rm hcp}$ are the lattice constant for the fcc structure, in-plane lattice constant for the hcp structure, and out-of-plane-lattice constant for the hcp structure, respectively. The deviations of $a_{\rm fcc}$ from the ideal value is 0.15 Å with PBE, 0.36 Å with vdW-DF2$^{\rm C09x}$, and 0.03 Å with other functionals. Our result indicates that these two phases are almost identical, and cannot reproduce the experimentally observed stable fcc phase at an ambient pressure. This apparent discrepancy may be solved by introducing an entropic effect from phonon. Indeed, Ishikawa *et al.*[60] performed the lattice dynamics calculations and successfully predict the stable fcc argon by taking into account the entropic contributions.

In order to perform the expansion of Eq. (3.19), an appropriate cutoff q_c and mesh for q_0 function (q_α) are needed. To determine q_c and q_α, we investigated distribution of the q_0 function by sampling the values on each FFT grid point. The distribution $D(q_0)$ was calculated as a histogram; counting the number of samples while satisfying

TABLE 6.3: Optimized lattice parameter ($a_{\rm fcc}$), equilibrium volume (V_0), and cohesive energy ($\Delta E_{\rm coh}$) for solid argon in the fcc structure, obtained using different density functionals. The CCSD(T), ACFDT-RPA using PBE orbitals, and experimental values are also listed for comparison.

Functional	$a_{\rm fcc}$ (Å)	V_0 (Å^3/atom)	$\Delta E_{\rm coh}$ (meV/atom)
LDA	4.97	30.61	135
PBE	6.04	55.03	14
vdW-DF	5.53	42.34	142
vdW-DF2	5.29	37.05	116
vdW-DF$^{\rm C09x}$	5.34	38.06	105
vdW-DF2$^{\rm C09x}$	6.32	63.06	21
rVV10	5.20	35.20	99
rVV10^a	5.17	34.55	117
CCSD(T)^b	5.251	36.196	87.9
ACFDT-RPA^c	5.3	37.22	83
Expt.	5.311^d	37.451^d	80.1^e

^{a} Ref. [55]. ^{b} Ref. [56]. ^{c} Ref. [20]. ^{d} Ref. [57]. ^{e} Ref. [58].

$q_\alpha \le q_0(\mathbf{r}) < q_{\alpha+1}$. In Fig. 6.9, $D(q_0)$'s for the vdW-DF and vdW-DF2 are plotted for different lattice parameters. Furthermore, we analyzed the contribution of the nonlocal correlation energy from each q_α value, by defining

$$
\begin{aligned}
E_{\rm c}^{\rm nl} &= \sum_\alpha \varepsilon_{\rm c}^{\rm nl}(\alpha), \\
\varepsilon_{\rm c}^{\rm nl}(\alpha) &= \frac{\Omega}{2}\sum_{\mathbf{G}} \left(|\eta_\alpha(\mathbf{G})|^2 \phi_{\alpha\alpha}(G) + 2\sum_{\beta(<\alpha)} {\rm Re}(\eta_\alpha^*(\mathbf{G})\eta_\beta(\mathbf{G}))\phi_{\alpha\beta}(G) \right),
\end{aligned}
\tag{6.1}
$$

where $\varepsilon_{\rm c}^{\rm nl}(\alpha)$ is positive value. $\varepsilon_{\rm c}^{\rm nl}(\alpha)$'s for fcc argon with vdW-DF and vdW-DF2 are shown in Fig. 6.9. There is almost no contribution of the nonlocal correlation energy at the smallest q_α, although the samples of $D(q_\alpha)$ exit there. Note that the samples at the smallest q_α comes from the diluted electron density nearly zero. In the case of $a = 5.29$ Å, $\varepsilon_{\rm c}^{\rm nl}(\alpha)$'s have a peak at $q = 2.4$ and are damped rapidly as q_α increases. In the case of $a = 10.58$ Å, the shrunken electron cloud around atomic cores causes the distributions of $D(q_\alpha)$ at the larger q_α's(> 5). However there is no energy contribution from the term of $E_{\rm c}^{\rm nl}$. This is presumably because that the vdW interaction is both canceled out in the atom and fully damped at the atomic distances. From the above result, it is confirmed that the q_α mesh defined in the present work covers the energy

TABLE 6.4: Optimized lattice parameters (a_{hcp} and c_{hcp}), equilibrium volume (V_0), and cohesive energy (ΔE_{con}) for the hcp argon.

Functional	a_{hcp} (Å)	$c_{\mathrm{hcp}}/a_{\mathrm{hcp}}$	V_0 (Å^3/atom)	ΔE_{coh} (meV/atom)
LDA	3.51	1.633	30.45	135
PBE	4.16	1.633	50.92	13
vdW-DF	3.89	1.633	41.63	142
vdW-DF2	3.74	1.636	37.08	116
vdW-DF$^{\mathrm{C09x}}$	3.80	1.632	38.75	105
vdW-DF2$^{\mathrm{C09x}}$	4.19	1.632	52.81	20
rVV10	3.66	1.633	34.70	99
Expt.[a]	3.8	1.63	39	

[a] Ref. [59].

range in the system.

6.5 Graphite

Graphite consists of two-dimensional carbon allotrope, graphene, and graphene layers are bound in the out-of-plane direction with the weak vdW interaction. Graphite has been studied extensively both experimentally and theoretically, and is often used to assess the accuracy of a new method for weak interaction, as benchmark calculations with highly accurate electronic structure method such as QMC[22] and ACFDT-RPA.[61]

In our calculation, the Brillouin zone was sampled using an $8 \times 8 \times 4$ MP k-point set, and plane wave cutoffs of 80 and 480 Ry were used for wave functions and electron density, respectively. We fully optimized the lattice parameters according to the calculated internal pressure, and the binding energy was determined from the difference of the total energy at the equilibrium and that at the interlayer distance larger than 13 Å. In Table 6.5, optimized lattice parameters and binding energies obtained using different exchange-correlation functionals are summarized.

In accordance with the literature, LDA gives lattice parameters, which are in good agreement with the experiment, while GGA yields a much larger out-of-plane lattice parameter (c) and negligible binding energy, suggesting that the latter cannot predict the binding of graphite. The binding energy obtained with LDA is smaller than that from the experiment and highly accurate theoretical method. In general, our vdW-DF results are in good agreement with the previous studies, which employs different

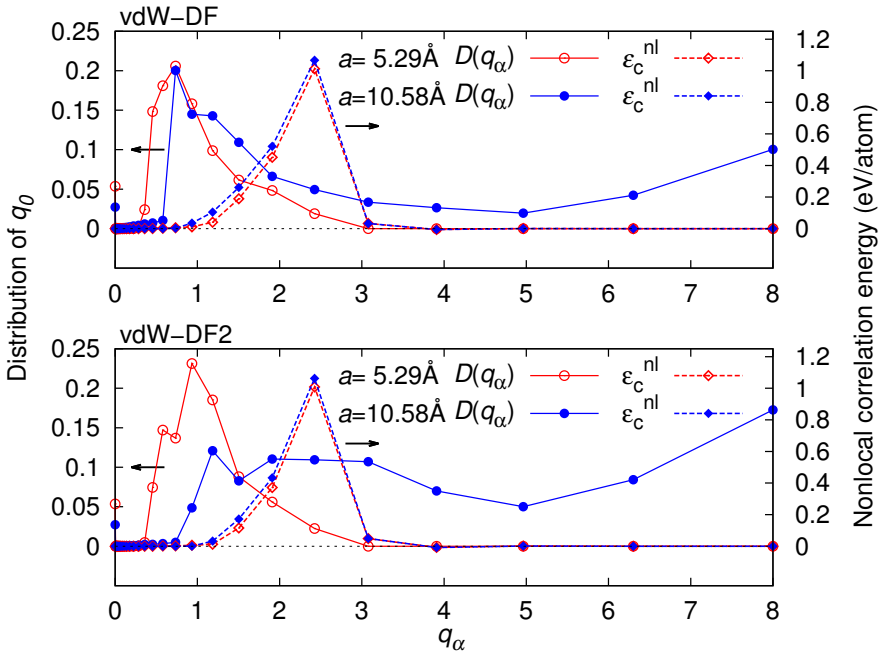

FIGURE 6.9: Distributions of q_0 function (solid curves) and $\varepsilon_c^{\rm nl}(\alpha)$ (dotted curves) for fcc argon calculated with the vdW-DF (upper panel) and vdW-DF2 (lower panel). The red-empty and blue-filled data are for the lattice parameter a of 5.29 Å and 10.58 Å, respectively.

vdW-DFs.[39, 66, 67, 68, 69, 63] The vdW-DF and vdW-DF2 predict the binding energy ($\Delta E_{\rm b}$), in good agreement with experiment. They also improve the description of structural properties, but the equilibrium volumes (V_0) are overestimated. V_0 is improved by the use of vdW-DF$^{\rm C09x}$ and rVV10, but they overestimate $\Delta E_{\rm b}$. We note that our $\Delta E_{\rm b}$ obtained using rVV10 is almost twice as large as that reported by the original authors.[25] At present, the origin of the discrepancy is yet to be clarified, but similar larger values (∼70 meV/atom) were obtained using different implementations[70, 71] of rVV10 and different potentials. On the other hand, vdW-DF2$^{\rm C09x}$ predicts lattice parameters and binding energy in good agreement with experiment, in line with the previous study.[67]

6.6 Trigonal selenium

Trigonal selenium is formed by the bundle of one-dimensional covalently bonded atomic chiral chains. As already shown in the previous works,[74, 75, 76] the gradient correction to LDA improves the description of selenium, but still less satisfactory, presumably because of the lack of the vdW interaction between the chiral chains in GGA. Bučko *et*

TABLE 6.5: In-plane lattice constant (a), out-of-plane lattice constant (c), equilibrium volume (V_0), and the binding energy ΔE_b for graphite. The numbers parentheses were obtained using the experimental value.

Functional	a (Å)	c (Å)	V_0 (Å^3/atom)	ΔE_b (meV/atom)
LDA	2.45	6.69	8.71	24
PBE	2.47	8.76	11.61	2
vdW-DF	2.49	7.18	9.61	55
vdW-DF2	2.48	7.05	9.41	53
vdW-DF$^{\mathrm{C09x}}$	2.47	6.50	8.60	76
vdW-DF2$^{\mathrm{C09x}}$	2.47	6.58	8.71	56
rVV10	2.48	6.76	8.93	68
rVV10[a]	2.46	6.72	8.80	39
VV10[b]	(2.46)	6.777	(8.88)	71
vdW-DF-cx[c]	2.46	6.43	8.54	66
QMC[d]	(2.46)	6.852	(8.98)	56±5
ACFDT-RPA[e]	(2.46)	6.68	(8.75)	48
Expt.	2.46[f]	6.70[f]	8.80[f]	52 ±5[g]

[a] Ref. [25]. [b] Ref. [62]. [c] Ref. [63]. [d] Ref. [22]. [e] Ref. [61]. [f] Ref. [64]. [g] Ref. [65].

al.[76] demonstrate by using the semi-empirical dispersion correction, that the structural parameters are significantly improved, and the agreement with the experiment becomes much better. Here we use vdW-DF to address the importance of the vdW interaction.

The trigonal selenium belongs either to $P3_121$ or $P3_221$ space group and has three atoms per unit cell (see Fig. 6.10). The atomic position in the cell can be described by the internal parameter x, which scales the distance from the screw axis to the atomic position. The structure of the trigonal selenium is also characterized by the shortest Se-Se distance in the same chain (ℓ_1) and the shortest Se-Se distance in different chains (ℓ_2). We used a $8 \times 8 \times 4$ MP k-point set, and plane wave cutoffs of 60 and 500 Ry for wave functions and electron density, respectively. The binding energy was calculated from the difference between the total energies of solid in the equilibrium and the isolated chain.

Calculated structural parameters and binding energy are summarized in Table 6.6. In general, the lattice constant along the chiral chain (c) is overestimated by all the functionals used in this study, while accuracy for the lattice constant a varies. LDA significantly underestimated a, while PBE significantly improves the description of a, in good agreement with previous studies. Both vdW-DF and vdW-DF2 overestimates

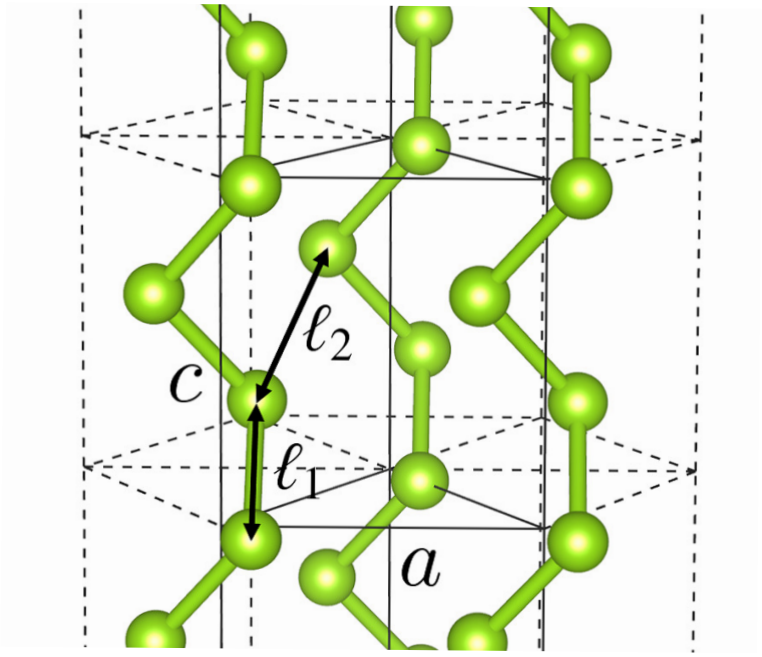

FIGURE 6.10: Trigonal structure of selenium.

a and c, while the use of the C09 exchange (vdW-DF$^{\mathrm{C09x}}$ and vdW-DF2$^{\mathrm{C09x}}$) leads to the underestimation of a. On the other hand, while c is slightly overestimated, rVV10 provides a balanced description of both the lattice constants. It is found from our results that there is a correlation between calculated a and c: if a is overestimated, the error in c tends to be smaller. Thus, in order to obtain accurate structural parameters for the trigonal selenium, it is very important to describe both covalent and vdW interactions accurately, suggesting that this material can be a good benchmark system for a vdW inclusive functional.

6.7 Dry ice

The solid form of carbon dioxide is called dry ice. Carbon dioxide has no dipole moment, and thus, the attractive vdW forces play an important role in the condensation. We chose this material as a representative application of our vdW-DF implementation to non-magnetic molecular crystals.

The crystalline dry ice has a cubic symmetry with the space group of $Pa3$ (see Fig. 6.11 for the structure). Plane wave cutoffs of 160 and 960 Ry were used for wave functions and electron densities, respectively. An $8 \times 8 \times 8$ MP k-point set was used for

TABLE 6.6: Optimized lattice parameters (a and c), equilibrium volume (V_0), internal parameter (x), shortest Se-Se distance in a chain (ℓ_1), shortest Se-Se distance in different chains (ℓ_2), and binding energy (ΔE_b) for trigonal selenium.

Functional	a (Å)	c (Å)	V_0 (Å^3/atom)	x	ℓ_1 (Å)	ℓ_2 (Å)	ΔE_b (meV/atom)
LDA	3.89	5.04	21.94	0.2540	2.40	3.06	395
PBE	4.51	4.97	29.16	0.2148	2.36	3.58	55
vdW-DF	4.70	5.04	32.15	0.2091	2.39	3.74	189
vdW-DF2	4.57	5.12	30.81	0.2177	2.42	3.62	228
vdW-DF$^{\mathrm{C09x}}$	3.96	5.11	23.08	0.2521	2.43	3.11	429
vdW-DF2$^{\mathrm{C09x}}$	3.99	5.10	23.42	0.2497	2.42	3.14	330
rVV10	4.24	5.11	26.54	0.2348	2.42	3.35	320
Expt.	4.366[a]	4.954[a]	27.261[a]	0.225[b]	2.373[a]	3.436[a]	

[a] Ref. [72]. [b] Ref. [73].

Brillouin zone sampling.

Optimized structural parameters and binding energy for the dry ice are given in Table 6.7, along with the MP2[77] and experimental (150K)[78] results. Our PBE equilibrium volume is in good agreement with the theoretical value obtained by Bonev *et al.*[80] (52.9 Å^3/CO_2) using the same functional. On the other hand, both the equilibrium volume and the binding energy obtained using vdW-DFs are in better agreement with the highly accurate MP2 and experimental (150K) results, suggesting the improvement over LDA and PBE. The maximum deviation of the equilibrium volume obtained using vdW-DF is 9.1 %, with respect to the low temperature experiment. The above results suggest that PBE overestimates the equilibrium volume because of the lack of the dispersion forces, and more accurate description of structure and energetics of dry ice is made possible by considering the dispersion forces with vdW-DF. Regarding the severe underestimation of the binding energy with vdW-DF2$^{\mathrm{C09x}}$, it has been found[81] from a systematic assessment using the S22 dataset that although it predicts reasonable inter-molecular separation (distance), the functional severely underestimates the binding energy, because the C09 exchange is too repulsive at a relatively large density gradient relevant to the intermolecular region. This result implies that vdW-DF2$^{\mathrm{C09x}}$ is inaccurate to describe the intermolecular vdW interaction.

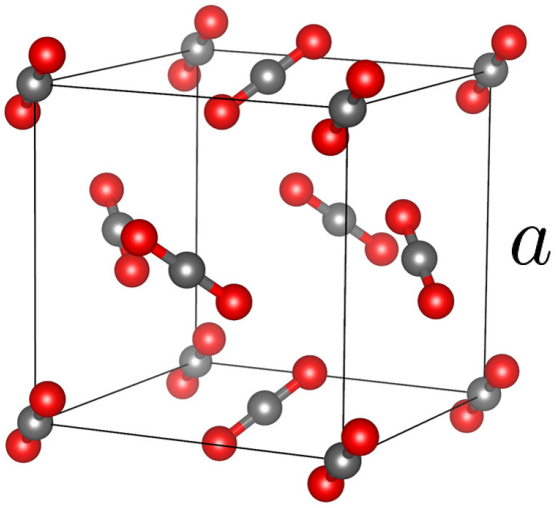

FIGURE 6.11: The cubic $Pa3$ structure of dry ice (solid CO_2).

TABLE 6.7: Equilibrium lattice parameter (a), volume (V_0), C-O bond length ℓ_b, and binding energy (ΔE_b) for the dry ice.

Functional	a (Å)	V_0 (Å^3/CO_2)	ℓ_b (Å)	ΔE_b (meV/CO_2)
LDA	5.28	36.88	1.165	370
PBE	6.04	55.11	1.175	103
vdW-DF	5.77	47.94	1.180	364
vdW-DF2	5.61	44.04	1.178	346
vdW-DF^{C09x}	5.53	42.17	1.176	339
vdW-DF2^{C09x}	5.79	48.42	1.176	155
rVV10	5.51	41.72	1.179	328
MP2[a]	5.46	40.69	1.17	290
Expt.	5.62 [b]	44.38[b]	1.155[b]	288[c]

[a] Ref. [77]. [b] Ref. [78]. [c] Ref. [79].

6.8 Solid oxygen in the α phase

The α-O_2 has an antiferromagnetic ground state with the crystal structure of the $C2/m$ space group, as shown in Fig. 6.12. There are four lattice parameters, a, b, c, and β, and the internal parameters of ℓ_b (bond length of O_2 molecule) and θ (tilted angle of molecular axis). The molecular axis is almost perpendicular to the ab-plane, and slightly tilted within the ac-plane. The angle of θ was reported to be ∼3 degree in the experiment.[82]. In the calculation, we used plane wave cutoffs of 160 and 960 Ry for wave functions and electron density, respectively, and an $8 \times 8 \times 8$ MP k-point set was used for the Brillouin zone sampling. During the structural optimization, the molecular

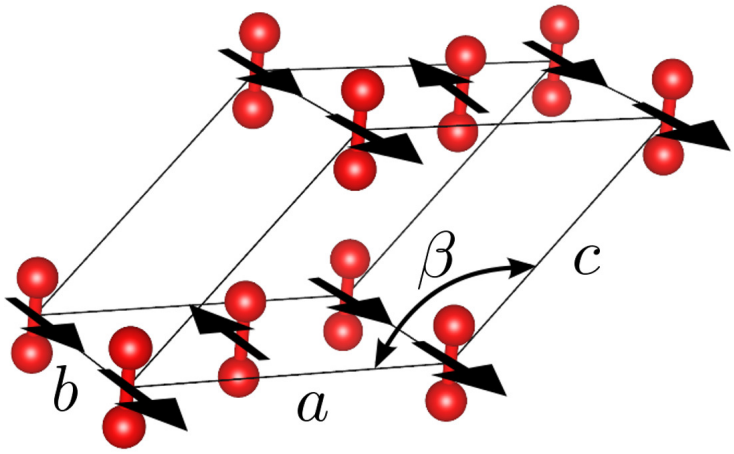

FIGURE 6.12: Crystal structure of the solid oxygen in α phase. The arrows on molecules represent the magnetic moment.

axis was fixed in the direction perpendicular to *ab*-plane, but the residual forces on atom were small, typically less than 0.001 eV/Å.

In Table 6.8, we report the structural parameters and binding energies obtained using different functionals. As expected, LDA severely underestimates the equilibrium volume by 42.8%, while PBE overestimates it, but the error is marginal (10.6%). However, this unexpectedly small error is because of the error cancellation of the errors in a (-15.0%) and b (14.6 %). The error in c is surprisingly small, but the trend in the lattice parameters with PBE is not systematic. On the other hand, all the vdW-DFs underestimate a and c, whereas b is overestimated, and as a result, the equilibrium volumes are consistently underestimated. The angle β is also consistently underestimated. Among vdW-DFs, original vdW-DF by Dion *et al.* predicts most accurate structural parameters, and inclusion of SGC further improves the structural parameters, which are in good agreement with the experiment, suggesting the importance of the spin polarization dependent gradient correction to the local correlation.

The nearest neighbor distance between O_2 molecules ($\ell_{\mathrm{mol}} \equiv \sqrt{a^2 + b^2}/2$) is a very important quantity in the α-O_2, as it strongly correlates with the antiferromagnetic interaction between O_2 molecules. We found that ℓ_{mol} is underestimated by LDA and PBE, but is increased using vdW-DF-SGC to the distance 3.05 Å toward the experimental value (3.20 Å). We also note that there is a correlation between β and c with vdW-DF, i.e., the smaller c is, the smaller β is. As discussed in the previous works,[42, 83] the distance between magnetic molecules is determined by a subtle balance between magnetic

TABLE 6.8: Optimized lattice parameters (a, b, c, and β), nearest neighbor distance ($\ell_{\rm mol} \equiv \sqrt{a^2+b^2}/2$), equilibrium volume ($V_0$), bond length ($\ell_{\rm b}$), magnetic moment ($M_a$) on oxygen atom, binding energy of molecule (ΔE_b). Experimental values are shown for comparison.

Functional	a (Å)	b (Å)	c (Å)	β (deg)	$\ell_{\rm mol}$ (Å)	V_0 (Å^3)	ℓ_b (Å)	M_a ($\mu_{\rm B}$)	ΔE_b (meV)
LDA	3.29	3.28	4.05	113.9	2.32	19.93	1.202	0.30	552
PBE	4.59	3.93	5.05	122.1	3.02	38.54	1.218	0.66	41
vdW-DF	4.68	3.68	4.70	125.2	2.98	33.05	1.231	0.66	221
vdW-DF-SGC	4.94	3.57	4.91	128.4	3.05	33.85	1.231	0.66	213
vdW-DF2	3.83	3.85	4.29	118.6	2.72	27.75	1.235	0.60	225
vdW-DF2-SGC	3.91	3.88	4.30	119.0	2.76	28.56	1.235	0.62	209
vdW-DF$^{\rm C09x}$	3.52	3.46	4.15	114.8	2.47	22.90	1.215	0.47	285
vdW-DF$^{\rm C09x}$-SGC	3.59	3.47	4.17	115.4	2.50	23.51	1.215	0.50	255
vdW-DF2$^{\rm C09x}$	3.66	3.56	4.34	115.1	2.55	25.51	1.216	0.52	95
vdW-DF2$^{\rm C09x}$-SGC	3.79	3.62	4.36	115.8	2.62	26.92	1.217	0.57	71
rVV10	3.71	3.62	4.18	117.2	2.59	24.94	1.225	0.56	240
Expt.[a]	5.403	3.429	5.086	132.3	3.200	34.85	1.29		

[a] Ref. [82].

TABLE 6.9: Magnetic energy for α-O_2 ($\Delta E^{\rm mag}$).

Functional	$\Delta E^{\rm mag}$ (meV)
PBE	95
vdW-DF	118
vdW-DF-SGC	87
vdW-DF2	304
vdW-DF2-SGC	251

and vdW interactions. In the solid state, not only the balance between magnetic and vdW interactions within the *ab*-plane, but also that between *ab*-planes (out of the plane direction) plays the decisive role: an complicated interplay amang the antiferromagnetic, ferromagnetic, and vdW interactions in the three-dimension determines the structure of α-O_2. The molecules in the *ab*-plane can be considered to form a triangle configuration. In the experimental structure, this configuration is very similar to an equilateral triangle, where the antiferromagneitc interaction between the neighboring molecules could destabilize the magnetic structure or distort the triangle to reduce the magnetic frustration. Based on this consideration and the knowledge acquired in the previous study[42], the underestimation of the nearest neighbor distance ($\ell_{\rm mol}$) in vdW-DF may be ascribed to

the overestimation of antiferromagnetic interaction between molecules with respect to the ferromagnetic one. Thus, in order to improve the description of α-O_2, it is necessary to develop more accurate exchange and correlation functionals, which predict balanced description of antiferromagnetic and ferromagnetic interactions.

Magnetic interaction J is proportional to $-t^2/\Delta E$, where t and ΔE are the transfer integral and the energy gap between spin-up and spin-down states just above and below the Fermi level. The antiferromagnetic states is over-stabilized as a result of underestimation of ΔE (overestimation of $|t|$ as well), because GGA is known to underestimate the energy gap for insulating and molecular systems. In order to capture a trend in the functionals on the magnetic interaction, we calculated the magnetic energy, defined by the energy difference between the ferromagnetic (F) and the antiferromagnetic(AF) states at the same AF crystal structure ($\Delta E^{\mathrm{mag}} = E^{\mathrm{F}} - E^{\mathrm{AF}}$). The results obtained using PBE, vdW-DF, and vdW-DF2 (with and without SGC) are summarized in Table 6.9. It is found that vdW-DF and vdW-DF-SGC, which predict more accurate structural parameter, yield small ΔE^{mag}, while the other vdW-DFs tend to give much larger values, supporting the above consideration.

6.9 Solid oxygen in the δ phase

The δ phase of solid oxygen appears in high pressure and low temperature state on solid oxygen. Recently, it was found that β phase has three type of magnetic structures depending on temperature, namely, LTC (low temperature commensurate), HTC (high temperature commensurate) and ITC (intermediate commensurate) phase [84]. Analysis based on first principle calculation is important to investigate the origin of these phase transitions. Figure 6.13 shows crystal and magnetic structure on the LTC and HTC phase. The LTC and HTC phase has $A-A-A$ and $A-B-A$ stacking structure on c axis, however the ITC phase has $1 \times 1 \times 2$ unit cell and $A-A-B-B-A$ stacking.

We investigated optimized crystal structure using LDA, GGA(PBE) and vdW-DF-SGC. Since vdW-DF-SGC gave a better crystal structure on the α phase, it functional is used on the δ phase analysis. The revPBE exchange functional which is employed on vdW-DF and vdW-DF-SGC tend to describe a repulsive interaction compared with other GGA functional. We used a $8 \times 8 \times 4$ MP k-point set, and plane wave cutoffs

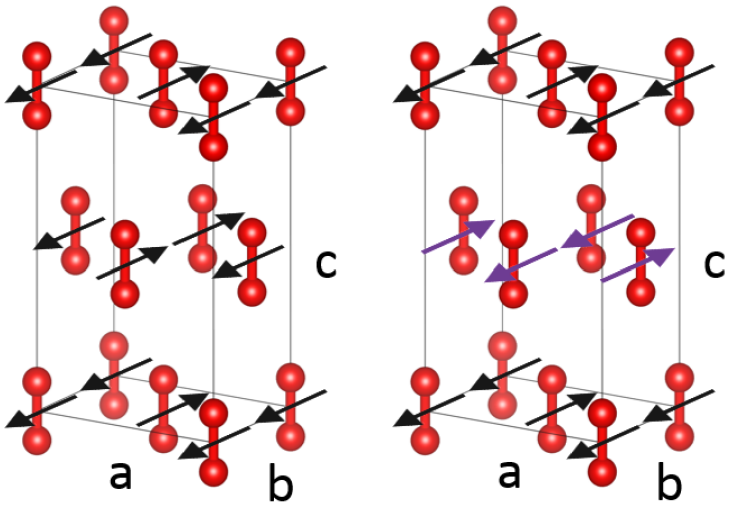

FIGURE 6.13: Crystal structure of the solid oxygen δ phase. Right (Left) figure shows LTC (HTC) phase. The arrows on molecules represent the magnetic moment.

TABLE 6.10: Optimized lattice parameters (a, b, c) on the solid oxygen δ phase at 6.2GPa.

Functional	a (Å)	b (Å)	c (Å)	V_0 (Å^3)
LDA	3.21	3.18	6.86	17.47
PBE	3.61	3.33	7.11	21.38
vdW-DF-SGC	3.93	3.23	7.08	22.47
Exp. [53]	4.33	3.06	6.83	22.62

of 160 and 960 Ry for wave functions and electron density, respectively. The magnetic structure is assumed as the LTC phase.

Optimized lattice parameters at 6.2GPa are shown in Table 6.10. Figure 6.14 shows pressure dependency of equilibrium volume using vdW-DF-SGC. LDA underestimated lattice constant and volume as well as the α phase. GGA(PBE) also underestimated volume even though it overestimate the α phase volume, however the layer distance is overestimated owing to the neglect of vdW force. vdW-DF-SGC volume is good agreement with the experiment value, and that error is less than 1%.

According to Fig. 6.14 vdW-DF-SGC was expected to describe accurate crystal structure on the δ phase. We carried out calculation for the HTC phase using several functionals. Computational conditions were same with LTC calculation. The Table 6.11 shows energy difference between the LTC and HTC phase. The LTC phase should be stabilized than the HTC phase because our calculation did not consider the temperature

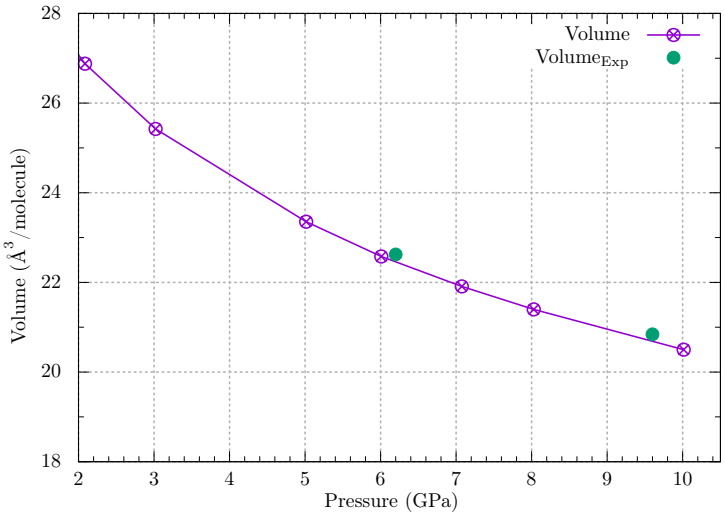

FIGURE 6.14: Pressure dependency of crystal volume on the δ (LTC) phase.

TABLE 6.11: Energy difference between the LTC and HTC phase.

	Optimization intermolecular distances	Optimization lattice constant	$\Delta E = E^{\mathrm{HTC}} - E^{\mathrm{LTC}}$ (meV/molecule)
PBE (ecalj)	No	No	-4
PBE	No	No	-3.6
vdW-DF-SGC	No	No	-3.8
vdW-DF-SGC	Yes	No	-1.0

effect. However we found that DFT calculation indicated the HTC phase has lower energy than LTC phase. The reason of this discrepancy is poor description for magnetic interaction. The difference between the LTC and HTC phase is magnetic orientation in the interlayer e.g.: $A-B-A$ layer stacking is LTC and $A-A-A$ layer stacking is the HTC phase. The interlayer atomic configuration can be represented as S-type molecular configuration at $\theta = 20$ in Fig. 6.4. Figure 6.7 indicate that vdW-DF-SGC method is poor at describing magnetic interaction, especially J around $\theta = 20$ is much overestimated. Therefore antiferromagnetic interaction has been overemphasized, stabilizing the HTC phase.

change of SGC term at the displacement of molecular distance in the ferromagnetic pair, whereas for the antiferromagnetic pair the repulsive behavior appeared from the SGC term, as discussed below. Thus, we propose to introduce $\alpha_{\rm GC}$ to optimize SGC term to reduce the difference between ferromagnetic and antiferromagnetic states, as one of improving methods. Note that the present functional is reduced to the original vdW-DF in the absence of spin polarization.

As another way, we propose to scale the relative spin polarization in order to optimize the antiferromagnetic interaction as follows:

$$\zeta \to \alpha_\zeta \zeta. \tag{7.3}$$

where α_ζ is scaling factor of ζ. This scale may be related with the fact that the averaged sub-lattice magnetic moment in antiferromagnetic systems is reduced from the elemental saturated value. In both the local correlation energy functional and SGC term, ζ is used as an argument of spin scaling function (SSF) $\phi(\zeta) = [(1-\zeta)^{2/3} + (1+\zeta)^{2/3}]/2$ which was derived within the random-phase-approximation [88]. As a consequence, scaled ζ is equivalent to what scales the SSF. Note that α_ζ does not exceed unity. In both of the parametrizations ($\alpha_{\rm GC}$ and α_ζ), we expect a negligible change in the potential energy curve for ferromagnetic pairs since the dependence of correlation energy functional is investigated, but not of exchange energy functional. Indeed, as reported later in the next section, there is no dependence on $\alpha_{\rm GC}$ and α_ζ in the potential energy curve.

In this work, we have examined effects of these two scaling parameters in H-type oxygen molecular dimer and solid oxygen at ambient pressure. We used plane wave basis set and ultrasoft pseudopotential [31, 32]. For exchange and local correlation energy functions, $E_{\rm x}$ and $E_{\rm c}^{\rm LSDA}$, we used the versions of revPBE and PW92, respectively [38, 17]. In the pseudopotential construction, we neglected the nonlocal correlation ($E_{\rm c}^{\rm nl}$) and employed the semilocal exchange and correlation functionals. This treatment has been justified, because the nonlocal correlation vanishes in spherical atomic calculation [89]. To compute the nonlocal correlation energy efficiently, we used an order N log N method [23, 24]. In the method, we used the cutoff of 8 a.u. for the wave number q_0 and 31 q_0 values (q_α), which were constructed by a logarithmic mesh except near $q_\alpha = 0$[43]. We have already confirmed a reliability of these parameters in the previous study[43].

The kinetic energy cutoffs of 40 Ry and 350 Ry were used for the wave functions and charge density, respectively, in the H-type cluster calculation. We used large energy cutoffs for the plane wave basis (160 Ry and 960 Ry) in the crystal calculation to achieve the convergence in the pressure tensor, since the potential energy surface is very sluggish in the solid oxygen. We optimized the lattice parameters of solid oxygen to converge within a pressure of 0.05 GPa. The cubic box with a dimension of 10.6 Å was used in the cluster calculation. In the cluster calculations, optimized bond length of the isolated molecule was used (1.232 Å), which is slightly larger than the experimental value (1.207 Å [47]).

First, we have investigated the scaling parameters $\alpha_{\rm GC}$ and α_ζ in the H-type oxygen molecular dimer. Figure 7.1 shows the $\alpha_{\rm GC}$ dependence of the binding energy as a function of the distance between centers of molecules (d) for both antiferromagnetic and ferromagnetic states. Using the original vdW-DF-SGC ($\alpha_{\rm GC} = \alpha_\zeta = 1$), the potential energy curve of antiferromagnetic pair has the equilibrium distance of 3.20 Å and the binding energy of 45 meV. The equilibrium distance agrees well with the accurate data from the quantum chemistry approaches but the binding energy is larger [49, 4]. For ferromagnetic pair, the potential energy curves have a slightly large equilibrium distance with a slightly high binding energy, compared with the quantum chemistry approaches [49, 4]. As implied in the previous study [43], the antiferromagnetic state is destabilized and the equilibrium distance becomes larger as $\alpha_{\rm GC}$ is increased, whereas the interaction energy curve for the ferromagnetic state is unchanged. Thus, the $\alpha_{\rm GC}$ plays a role to tune the stability of the antiferromagnetic state only. Figure 7.1 also shows the magnetization of oxygen atom. By increasing $\alpha_{\rm GC}$, atomic magnetic moment decreases, implying that the wave function extends more to the intermolecular region.

Figure 7.2 shows the magnetic coupling constant J, defined by the energy difference between ferromagnetic and antiferromagnetic states; $J = E_{\rm F} - E_{\rm AF}$. The figure indicates a stability of antiferromagnetic state in a wide range of $\alpha_{\rm GC}$'s and d's. The strength of J decreases as increasing $\alpha_{\rm GC}$ or d and becomes comparable to those estimated in the methods of quantum chemistry (CASSCF, RCCSD(T))[49, 4] when $\alpha_{\rm GC} = 8$ and $d = 3.3$ Å. Unlike the quantum chemistry approaches, there is a region where the ferromagnetic state is more stable (negative J) at the larger $\alpha_{\rm GC}$'s ($\alpha_{\rm GC} = 8, 12$) and larger d's in the present frame work of vdW-DF-SGC. Such ferromagnetic stability can come from

a direct exchange interaction between the orbitals on the molecules. However, these interactions should be very small at $d \sim 4$ Å.

Figure 7.3 shows the dependence of the binding energy curve on α_ζ for antiferromagnetic and ferromagnetic states. As α_ζ decreases, energy difference between antiferromagnetic and ferromagnetic states decreases. In this case the equilibrium distance does not change, but the repulsive nature of potential curves becomes strong. As shown in Fig. 7.3, the magnetic moment slightly increases when the antiferromagnetic state is destabilized. This is an opposite trend, compared with the case of $\alpha_{\rm GC}$.

Since magnetic energy of the electron correlation is estimated as a local relative spin polarization in Eq.(7.1), it is unable to distinguish stability between antiferromagnetic and ferromagnetic states by the local spin density. Nevertheless once the difference of spin densities in magnetic states is generated through self-consistent field calculations, the system can converge to the respective magnetic state.

Next, we have applied vdW-DF-SGC with $\alpha_{\rm GC}$ and α_ζ to the solid oxygen at ambient pressure. The crystal structure belongs to a $C2/m$ (monoclinic) space group and its magnetic unit cell contains two molecules with an antiferromagnetic coupling [90]. The molecular axis has been known to tilt from the z-direction perpendicular to ab plane by a few degrees within the ac-plane. This effect is tiny and is negligible for the present work. In Table 7.1, we report optimized structural parameters, crystal binding energy, and magnetic energy for typical sets of scaling parameters $\alpha_{\rm GC}$ and α_ζ. We have found that by applying $\alpha_{\rm GC}$, the lattice parameters are improved as compared with the previous theoretical result[43]. For example, by setting $\alpha_{\rm GC} = 4$ and $\alpha_\zeta = 1$, we obtain the nearest neighbor distance between molecules of 3.14 Å, which is larger than that of 3.05 Å with $\alpha_{\rm GC} = 1$ and $\alpha_\zeta = 1$. The effects on α_ζ appeared also in the lattice parameter a, but the detail trend depends largely on $\alpha_{\rm GC}$; when $\alpha_{\rm GC} = 2$ ($\alpha_{\rm GC} = 4$), a increased (decreased). However, the overall effect of α_ζ is not as large as that of $\alpha_{\rm GC}$.

The lattice parameter a is in excellent agreement with the experiment, when $\alpha_{\rm GC} = 8$ and $\alpha_\zeta = 1$. However, other lattice parameters deviate from the experimental values. In our optimization about $\alpha_{\rm GC}$ and α_ζ, the potential curves of ferromagnetic molecular pair do not change. This may limit a region of searching space for exchange and correlation energy functionals. In the previous works [36], the weak repulsive nature was realized by optimizing the exchange functional, whereas the original functional shows a stronger

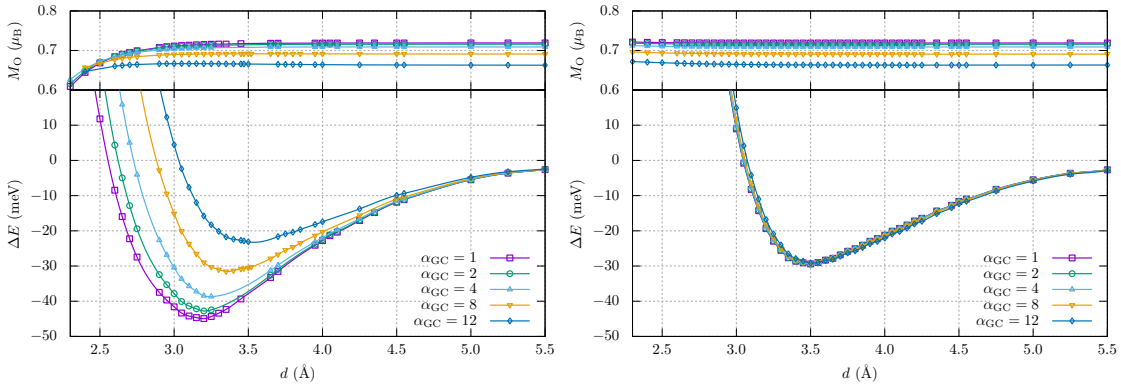

FIGURE 7.1: Binding energy (ΔE) curves for the oxygen molecular dimer in the H-Type configuration as a function of the distance connecting the center of molecules (d) for several α_{GC}'s and $\alpha_\zeta = 1$. The left and right panels show antiferromagnetic and ferromagnetic cases, respectively. The atomic magnetic moments (M_O) are shown on the upper parts.

repulsive nature at short distances [8]. The potential energy of ferromagnetic dimer is also important in determining the structural parameters in solid oxygen as well as those of antiferromagnetic dimer. Because there are ferromagnetic molecular pairs at the next nearest neighbors within *ab* plane, the structural details might depend on the ferromagnetic potentials of molecular pairs. Another importance in ferromagnetic potential of molecular pair may be related with the phase transition to δ phase at the high pressure, at which the nearest neighbor magnetic coupling between molecules of neighboring *ab* planes is changed from antiferromagnetic to ferromagnetic one [91].

The binding and magnetic energies, as expected from the results of H-type molecular dimer, were reduced as α_{GC} increases. In particular, the magnetic energy at $\alpha_{GC} = 8$ and $\alpha_\zeta = 1$ becomes about one-fourth (21 meV) of that at $\alpha_{GC} = \alpha_\zeta = 1$. This energy is consistent with the magnetic interaction energy of oxygen molecule (2 μ_B) under the large experimental magnetic field ($\sim$ 200 T)[54]; 23 meV. Structural properties at high magnetic fields are under consideration by taking into account a giant magneto-volume effect in solid oxygen [92].

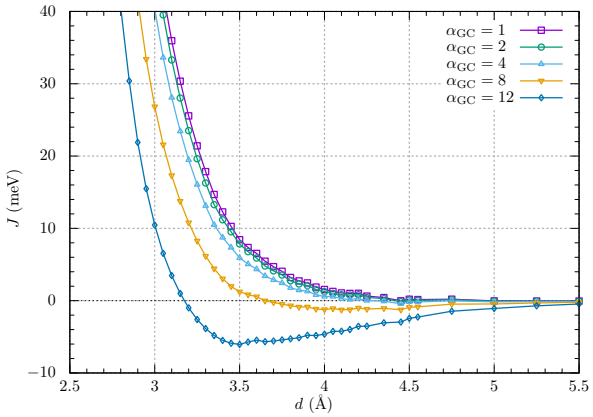

FIGURE 7.2: Magnetic interaction J ($= E_F - E_{AF}$) for the oxygen molecular dimer in the H-type configuration as a function of the distance between molecules for several α_{GC}'s and $\alpha_\zeta = 1$.

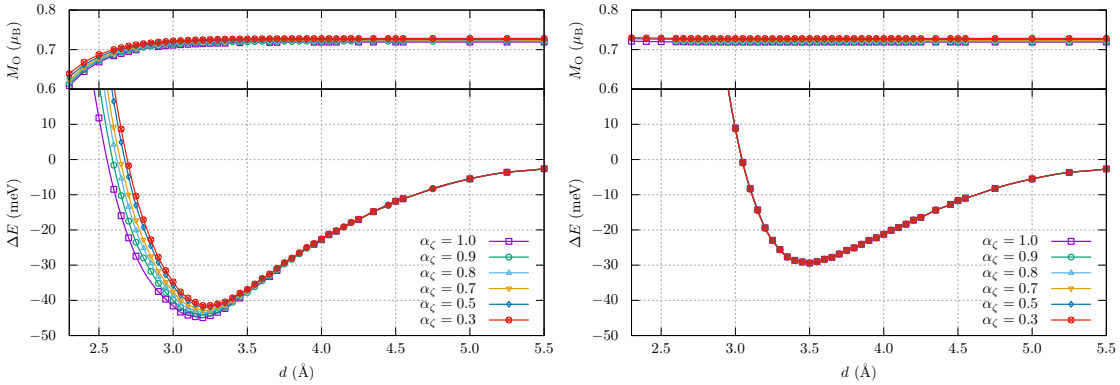

FIGURE 7.3: Binding energy (ΔE) curves for the oxygen molecular dimer in the H-Type configuration and atomic magnetic moment (M_O) as a function of distance of molecules for several α_ζ's and $\alpha_{GC} = 1$. The left and right panels show antiferromagnetic and ferromagnetic cases, respectively.

TABLE 7.1: Optimized lattice parameters (a, b, c, and β), equilibrium volume (V_0), binding energy of molecule (ΔE), and magnetic energy per molecule (ΔE^{mag}) for solid oxygen at ambient pressure. Experimental values are also shown for comparison.

α_{GC}	α_ζ	a (Å)	b (Å)	c (Å)	β (deg)	V_0 (Å^3)	ΔE (meV)	ΔE^{mag} (meV)	Ref.
0.0	1.0	4.68	3.68	4.70	125.2	33.05	221	118	[43]
1.0	1.0	4.94	3.57	4.91	128.4	33.84	213	87	[43]
2.0	1.0	5.04	3.59	4.85	127.4	34.86	207	69	
2.0	0.7	5.11	3.64	4.86	127.0	36.06	204	57	
2.0	0.5	5.14	3.62	4.85	127.5	35.76	204	54	
2.0	0.3	5.15	3.62	4.85	127.6	35.74	203	53	
4.0	1.0	5.13	3.63	4.94	128.5	36.02	196	51	
4.0	0.7	5.09	3.54	4.82	127.0	34.59	198	61	
4.0	0.5	5.06	3.54	4.78	126.8	34.27	200	63	
8.0	1.0	5.43	3.61	4.57	122.3	37.87	177	21	
		5.403	3.429	5.086	132.3	34.85			Expt. [82]

Chapter 8

Prospect

The van der Waals density functional (vdW-DF) approach, although it is called "van der Waals" correction, can describe nonlocal effect not only vdW effect in principle. The important benefit is that it does not require any adjustable parameter which depends on materials. Originally, vdW effect should depend on electron state owing to essential quantum effect. In such a reason, this approach is clearly different from some vdW correction methods using semi-empirical parameters. Therefore it is suitable for material design, analysis of phase transition, etc. We demonstrated that the vdW-DF-SGC method is a useful tool for studying weakly-bound magnetic systems.

It is well recognized that the density functional approach is serviceable method for material analyzing and designing. This is true regardless of spin-polarized and non-polarized systems. For non-polarized systems, many researches reported their works using non-empirical vdW force approach. This fact suggests that there are a lot of materials which had never been investigated owing to the lack of vdW force. As similar to non-polarized cases, the spin dependent vdW-DF approach can accelerate the research of weakly-bound systems such as organic-spintronics materials. We belive that spin dependent vdW-DF methods will be applied to the materials in these fields.

We found a new problem in the solid oxygen δ-phase. The problem was that even using vdW-DF-SGC approach to , the LTC phase could not be stabilized compared with the HTC phase. Although this problem comes down to the description of pair potential for antiferromagnetic and ferromagnetic states, we found that the LDA/GGA and vdW-DF approaches much overestimate the magnetic interaction owing to an underestimation of electronic excitation energy. Solving this problem, a more accurate spin dependent van der Waals functional approach is truly desirable.

The most important core of nonlocal correlation approach is, of course, the shape of kernel function. By some improvement of the kernel function, which seems to be the most straight-forward improvement approach, computational accuracy should increase. The kernel function depends on charge density in vdW-DF approach, but it should also depend on spin polarization. For example, nonlocal correlation energy will be written as

$$E_{\mathrm{c}}^{\mathrm{nl}}[n,\zeta] = \frac{1}{2}\int d\mathbf{r}d\mathbf{r}' n(\mathbf{r})\phi(\mathbf{r},\mathbf{r}',n(\mathbf{r}),n(\mathbf{r}'),\zeta(\mathbf{r}),\zeta(\mathbf{r}'))n(\mathbf{r}'), \tag{8.1}$$

where ζ is spin polarization function defined as $\zeta(\mathbf{r}) = (n_\uparrow(\mathbf{r}) - n_\downarrow(\mathbf{r}))/(n_\uparrow(\mathbf{r}) + n_\downarrow(\mathbf{r}))$. It is functional of density and spin polarization, not spin density, because correlation energy is essentially quantum effect except the exchange effect. This expression describe not only charge density fluctuation but also spin density fluctuation effect. The vdW-DF-SGC or svdW-DF may be one of approximations, being implied from Eq. 8.1.

Since the vdW force is smaller than the energy order that had been treated with conventional LDA/GGA, the subtle differences in the exchange or correlation energy functional and error of weak energy estimation are remarkably appear in the weakly bound material. We found that magnetic interaction is comparable with the vdW force and sometimes it is overestimated. The problem related with underestimation of band gap should be corrected by improving the exchange-correlation energy functional. For example, it is reported that this problem can be partly improved by self-interaction correlation [93].

Some exchange functionals have been proposed and the accuracy of these functionals has been investigated [35, 36, 39]. And the combination of exchange and correlation energy are also investigated because correlation energy using exchange functional estimated by charge density, not wave functions, should have a correction term to cancel the error of exchange energy. However, we found that the choice of functionals sometimes generates a large difference for the optimized structural parameters in crystal or molecular system. Although currently we should force to use a suitable functional for materials, universal approach is desirable for treating complex materials. As one possibility, nonlocal functional approach can be applied not only correlation but also exchange energy.

Then nonlocal exchange-correlation functional will be as follows:

$$E_{\mathrm{x}}^{\mathrm{nl}} = \frac{1}{2}\sum_{\sigma\sigma'}\int d\mathbf{r}d\mathbf{r}' n_\sigma(\mathbf{r})\phi_{\sigma\sigma'}(\mathbf{r},\mathbf{r}', n_\sigma(\mathbf{r}), n_{\sigma'}(\mathbf{r}'))n_{\sigma'}(\mathbf{r}'). \tag{8.2}$$

If kernel function is much smooth, the order $N\log N$ method can be applied for calculating Eq. 8.2. This is just expansion from LDA or GGA and it may solve the band gap problem. Since nonlocal correction approach is better than local density approximation, it will be a common approach instead of LDA/GGA.

Chapter 9

Conclusion

We had implemented the nonlocal correlation functional approach (vdW-DFs, rVV10) on plane wave basis DFT code, and the order $N\log N$ method was applied to reduce computational cost on nonlocal correlation energy. In order to test the vdW-DF energy, force, and stress implemented in our program code, we performed the calculations of solid argon in fcc and hcp phases, graphite, trigonal selenium, dry ice, in which the vdW interaction is supposed to be important. We could demonstrate that the nonlocal correlation approach is a useful technique to overcome the lacking of vdW force problem on local density approach.

We had proposed an extension (vdW-DF-SGC) to the spin polarized systems. We have investigated oxygen molecules and solid oxygen in the α-phase and δ-phase with the antiferromagnetic configuration by using the several variants of vdW-DF and the correction scheme for magnetic systems proposed. We have found that the vdW-DF shows overall improvement in the structure and energy of these materials over LDA and GGA and it is in good agreement with the previous studies available. In the case of antiferromagnetic solid oxygen, we have found that vdW-DFs consistently underestimate the lattice parameters, and the original vdW-DF by Dion et al. with our spin polarization dependent gradient correction scheme (vdW-DF-SGC) provides most accurate structural parameters among other functionals. We found that influence of spin by semi-local correlation effect plays an important role on antiferromagnetic state, involving the diluted and spread electron density on antiferromagnetic caused by lacking of Pauli exchange repulsion. We point out the competing nature of ferromagnetic, antiferromagnetic, and vdW interactions in the solid oxygen and balanced description of these interactions is decisively important for more accurate prediction of the structural properties of solid

oxygen.

We have introduced the scaling parameters α_{GC} and α_{ζ} to improve the description of the magnetic interaction in spin-polarized systems. It was found that our treatment reduces both binding energy and magnetic energy in the solid oxygen, indicating that the energy functional improves the description of spin-polarized vdW systems. The new approach developed in this work has adjustable parameters, and further investigation on the correlation energy functional may reveal applicability and limitation for an application range on real material.

We also investigated relation between vdW-DF-SGC and svdW-DF. The ideas in them are different between each other, but we found that there is no contradiction results in both techniques as a result. Although the svdW-DF correction from vdW-DF is still unclear in theoretically, our results indicate that it contains semilocal spin dependent gradient correction effects.

Appendix B

Electronic structure in the interface of ferroelectric and ferromagnetic materials

Recently, ferroelectric tunnel junctions are a focus of attention because the polar direction that can control electronic states in ferroelectric materials may be serviceable for application in electronic devices. The direction of spontaneous polarization of ferroelectric materials can be utilized to hold the digital bit information. Suck kind of nonvolatile device is expected owing to reducing power consumption

We pay attention to ZnO which is well-known as ferroelectric material. We investigated an interface between ferroelectric and ferromagnetic material, respectively. Pt_3Co and the ZnO are used for ferromagnetic material and ferroelectric material. For simplicity, we put Co and 3 Pt atoms on the ZnO surface that is terminated at oxygen atom and the 1×1 unit cell (inplane lattice constant is fixed as ZnO bulk value) is used for the dimensional translational periodicity. We used $24 \times 24 \times 1$ k-points and 30 Ryd and 300 Ryd for wave function and density energy cutoff.

The computational models are shown in Fig.B.1. $P+$ and $P-$ states indicate the direction of polarization. We considered three kinds of interface and found that the type B and C having similar atomic configuration, is more stable than the type A 1.4 eV on both of the polarization states. As evidenced by the Fig. B.1, the difference of these three structures is stacking order of Pt 3ML and Co 1ML on interface oxygen atom, namely, ABC, BCA and CAB stacking. The type B and C have same relative position of Co atom from interface oxygen atom and difference is the relative position of

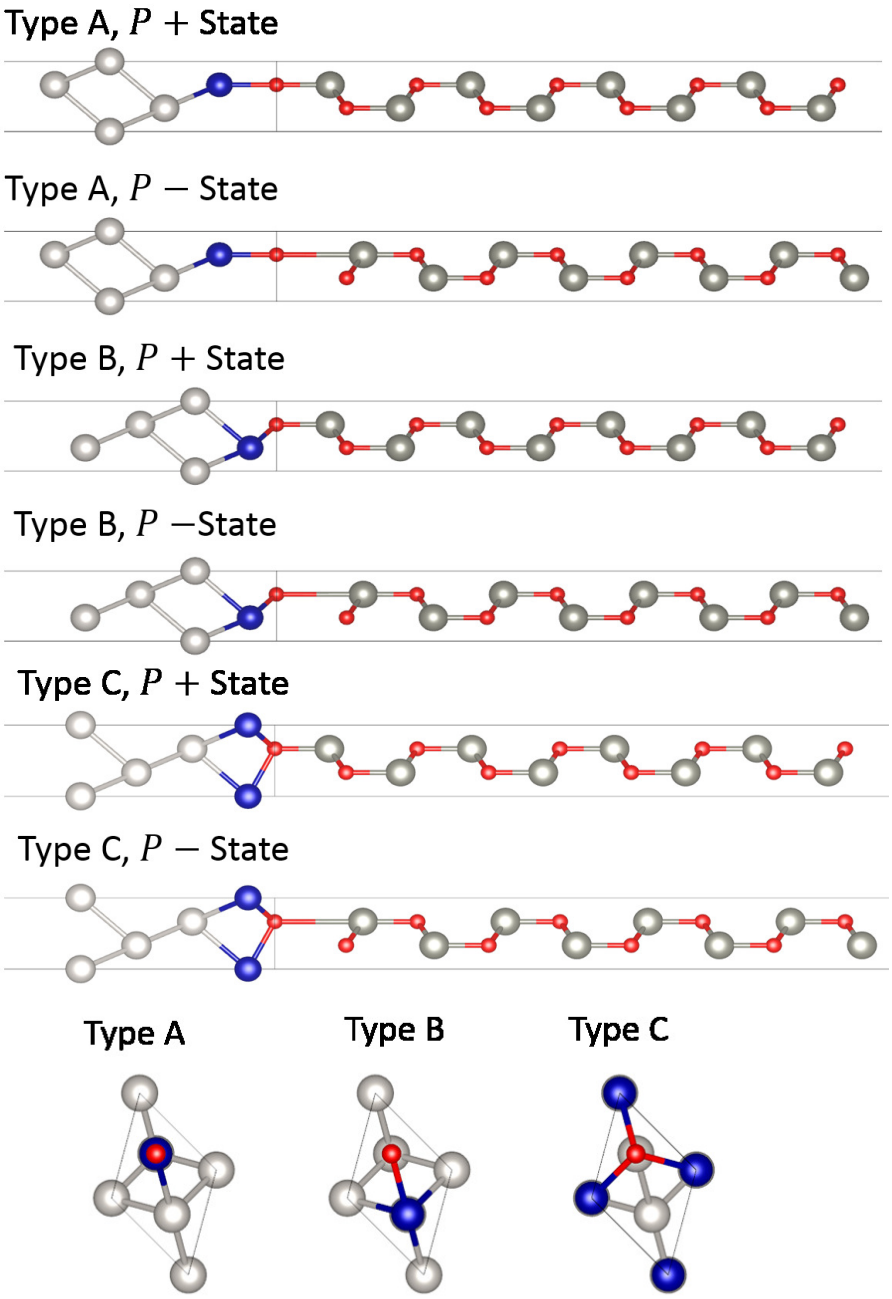

FIGURE B.1: Slab structures on Pt_3Co/ZnO. Top and bottom figures show side and top view from interface oxygen atom, respectively.

the second nearest neighbor oxygen atom with respect to the configuration of metallic layer. Since it seems to have no effect on the interface electronic state in these two types, and the difference between the total energies is very small (1 meV and 10 meV on $P+$ and $P-$ state, respectively), we focused the type B configuration in further analysis of electronic structures.

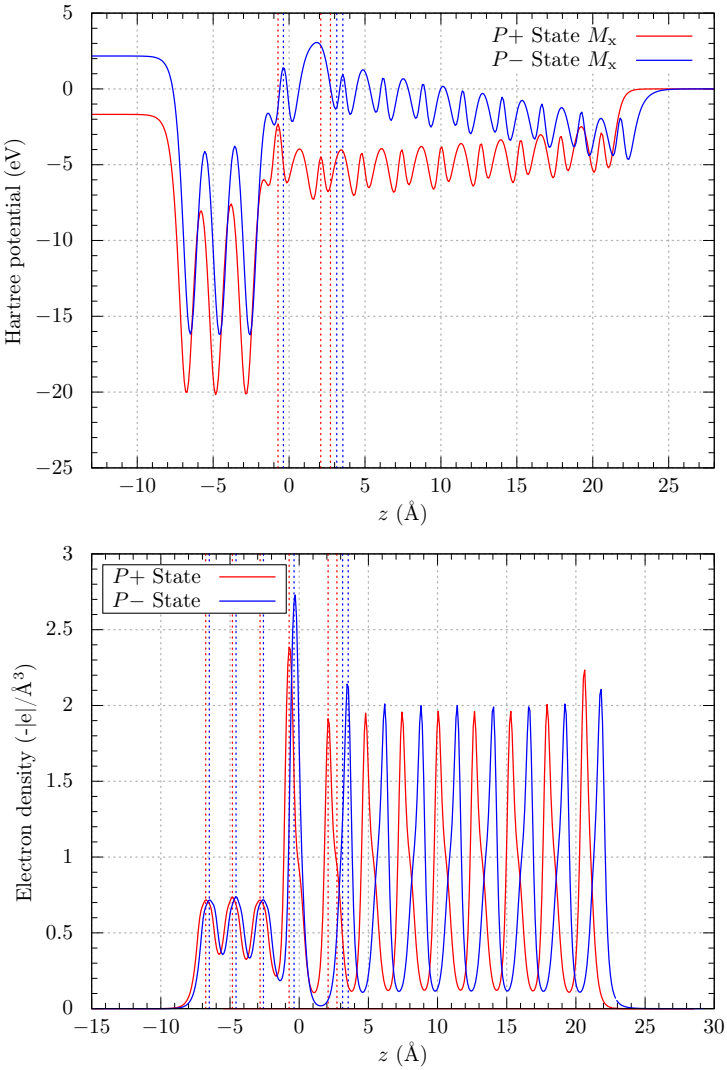

FIGURE B.2: Hartree potential and valence electron density.

Figure B.2 shows Hartree potential and valence electron density averaged over xy-plane and vertical dash lines indicate positions on some atoms ($z = 0$ is set to interface oxygen atom). We confirmed the gradient of Hartree potential in the ZnO film, indicating that existence of spontaneous polarization. According to Fig. B.2, $P-$ state has a high potential barrier on the Co and O interface which is caused by vanishing electron density, indicating that the tunneling resistance implies to increase. By changing the polarization direction from $P+$ to $P-$, interaction between Co/O and Zn becomes weak leading to get closer on Co/O interface

Bibliography

[1] T. Kotani, M. van Schilfgaarde, S. Faleev, Quasiparticle self-consistent GW method: A basis for the independent-particle approximation, Phys. Rev. B 76 (2007) 165106.

[2] M. van Schilfgaarde, T. Kotani, S. Faleev, Quasiparticle Self-Consistent GW Theory, Phys. Rev. Lett. 96 (2006) 226402.

[3] V. Aquilanti, D. Ascenzi, M. Bartolomei, D. Cappelletti, S. Cavalli, M. de Castro Vítores, F. Pirani, Quantum Interference Scattering of Aligned Molecules: Bonding in O4 and Role of Spin Coupling, Phys. Rev. Lett. 82 (1999) 69.

[4] M. Bartolomei, E. Carmona-Novillo, M. I. Hernández, J. Campos-Martínez, R. Hernandez-Lamoneda, Accurate *ab initio* intermolecular potential energy surface for the quintet state of the $O_2(^3\Sigma_g^-)$-$O_2(^3\Sigma_g^-)$ dimer, J. Chem. Phys. 128 (2008) 214304.

[5] P. Hohenberg, W. Kohn, Inhomogeneous electron gas, Phys. Rev. 155 (1964) B864.

[6] W. Kohn, L. Sham, Self-consistent equations including exchange and correlation effects, Phys. Rev. 385 (1965) A1133.

[7] S. Goedecker, Linear scaling electronic structure methods, Rev. Mod. Phys. 71 (1999) 1085.

[8] M. Dion, H. Rydberg, E. Schröder, D. C. Langreth, B. I. Lundqvist, Van der Waals Density Functional for General Geometries, Phys. Rev. Lett. 92 (2004) 246401.

[9] F. Djeghloul, F. Ibrahim, M. Cantoni, M. Bowen, L. Joly, S. Boukari, P. Ohresser, F. Bertran, P. Le Fèvre, P. Thakur, F. Scheurer, T. Miyamachi, R. Mattana, P. Seneor, a. Jaafar, C. Rinaldi, S. Javaid, J. Arabski, J.-P. Kappler, W. Wulfhekel,

N. B. Brookes, R. Bertacco, a. Taleb-Ibrahimi, M. Alouani, E. Beaurepaire, W. Weber, Direct observation of a highly spin-polarized organic spinterface at room temperature, Sci. Rep. 3 (2013) 1272.

[10] R. G. パール, W. ヤング, 狩野覚, 関元, 吉田元二, 原子・分子の密度汎関数法, シュプリンガー・フェアラーク東京, 1989.

[11] R. M. Martin, Electronic Structure Basic Theory and Practical Methods, CAMBRIDGE, 2004.

[12] D. Ceperley, B. Alder, Ground state of the electron gas by a stochastic method, Phys. Rev. Lett. 45 (1980) 566.

[13] J. White, D. Bird, Implementation of gradient-corrected exchange-correlation potentials in Car-Parrinello total-energy calculations, Phys. Rev. B 50 (1994) 4954.

[14] J. Perdew, K. Burke, M. Ernzerhof, Generalized Gradient Approximation Made Simple, Phys. Rev. Lett. 77 (1996) 3865.

[15] A. Becke, Density functional calculations of molecular bond energies, J. Chem. Phys. 84 (1986) 4524.

[16] A. Becke, Density-functional exchange-energy approximation with correct asymptotic behavior, Phys. Rev. A 38 (1988) 3098.

[17] J. Perdew, J. Chevary, S. Vosko, Atoms, molecules, solids, and surfaces: Applications of the generalized gradient approximation for exchange and correlation, Phys. Rev. B 46 (1992) 6671.

[18] O. Gunnarsson, B. Lundqvist, Exchange and correlation in atoms, molecules, and solids by the spin-density-functional formalism, Phys. Rev. B 13 (1976) 4274.

[19] D. Langreth, J. Perdew, Exchange-correlation energy of a metallic surface: Wavevector analysis, Phys. Rev. B (1977) 2884.

[20] J. Harl, G. Kresse, Cohesive energy curves for noble gas solids calculated by adiabatic connection fluctuation-dissipation theory, Phys. Rev. B 77 (2008) 045136.

[21] J. Harl, G. Kresse, Accurate Bulk Properties from Approximate Many-Body Techniques, Phys. Rev. Lett. 103 (2009) 056401.

[22] L. Spanu, S. Sorella, G. Galli, Nature and Strength of Interlayer Binding in Graphite, Phys. Rev. Lett. 103 (2009) 196401.

[23] G. Román-Pérez, J. Soler, Efficient Implementation of a van der Waals Density Functional: Application to Double-Wall Carbon Nanotubes, Phys. Rev. Lett. 103 (2009) 096102.

[24] J. Wu, F. Gygi, A simplified implementation of van der Waals density functionals for first-principles molecular dynamics applications, J. Chem. Phys. 136 (2012) 224107.

[25] R. Sabatini, T. Gorni, S. de Gironcoli, Nonlocal van der Waals density functional made simple and efficient, Phys. Rev. B 87 (2013) 041108.

[26] O. A. Vydrov, T. Van Voorhis, Dispersion interactions from a local polarizability model, Phys. Rev. A 81 (2010) 062708.

[27] F. Corsetti, E. Artacho, J. M. Soler, S. S. Alexandre, M.-V. Fernández-Serra, Room temperature compressibility and diffusivity of liquid water from first principles, J. Chem. Phys. 139 (2013) 194502.

[28] R. Car, M. Parrinello, Unified approach for molecular dynamics and density-functional theory, Phys. Rev. Lett. 55 (1985) 2471.

[29] T. Oda, A. Pasquarello, R. Car, Fully Unconstrained Approach to Noncollinear Magnetism: Application to Small Fe Clusters, Phys. Rev. Lett. 80 (1998) 3622.

[30] T. Oda, A. Pasquarello, *Ab Initio* Molecular Dynamics Investigation of the Structure and the Noncollinear Magnetism in Liquid Oxygen: Occurrence of O_4 Molecular Units, Phys. Rev. Lett. 89 (2002) 197204.

[31] D. Vanderbilt, Soft self-consistent pseudopotentials in a generalized eigenvalue formalism, Phys. Rev. B 41 (1990) 7892.

[32] K. Laasonen, A. Pasquarello, R. Car, C. Lee, D. Vanderbilt, Car-Parrinello molecular dynamics with Vanderbilt ultrasoft pseudopotentials, Phys. Rev. B 47 (1993) 142.

[33] J. Perdew, W. Yue, Accurate and simple density functinoal for the electronic exchange energy: Generalized gradient approximation, Phys. Rev. B 33 (1986) 12.

[34] E. D. Murray, K. Lee, D. C. Langreth, Investigation of Exchange Energy Density Functional Accuracy for Interacting Molecules, J. Chem. Theory Comput. 5 (2009) 2754.

[35] J. Klimeš, D. R. Bowler, A. Michaelides, Van der Waals density functionals applied to solids, Phys. Rev. B 83 (2011) 195131.

[36] I. Hamada, van der Waals density functional made accurate, Phys. Rev. B 89 (2014) 121103.

[37] J. Perdew, A. Zunger, Self-interaction correction to density-functional approximations for many-electron systems, Phys. Rev. B 23 (1981) 5048.

[38] Y. Zhang, W. Yang, Comment on "Generalized gradient approximation made simple", Phys. Rev. Lett. 165 (1998) 9007.

[39] V. R. Cooper, Van der Waals density functional: An appropriate exchange functional, Phys. Rev. B 81 (2010) 161104.

[40] L. Hedin, New Method for Calculating the One-Particle Green's Function with Application to the Electron-Gas Problem, Phys. Rev. 139 (1965) A796.

[41] O. A. Vydrov, T. Van Voorhis, Improving the accuracy of the nonlocal van der Waals density functional with minimal empiricism, J. Chem. Phys. 130 (2009) 104105.

[42] M. Obata, M. Nakamura, I. Hamada, T. Oda, Implementation of van der Waals Density Functional Approach to the Spin-Polarized System: Interaction Potential between Oxygen Molecules, J. Phys. Soc. Jpn. 82 (2013) 093701.

[43] M. Obata, M. Nakamura, I. Hamada, T. Oda, Improving the Description of Nonmagnetic and Magnetic Molecular Crystals via the van der Waals Density Functional, J. Phys. Soc. Jpn. 84 (2015) 024715.

[44] T. Thonhauser, S. Zuluaga, C. A. Arter, K. Berland, E. Schröder, P. Hyldgaard, Spin Signature of Nonlocal Correlation Binding in Metal-Organic Frameworks, Phys. Rev. Lett. 115 (2015) 136402.

[45] M. Obata, I. Hamada, T. Oda, Molecular Interactions for Modeling of Oxygen System Using van der Waals Density Functional Approach, JPS Conference Proceedings 5 (2015) 011011.

[46] T. Thonhauser, V. R. Cooper, S. Li, A. Puzder, P. Hyldgaard, D. C. Langreth, Van der Waals density functional: Self-consistent potential and the nature of the van der Waals bond, Phys. Rev. B 76 (2007) 125112.

[47] K. P. Huber, G. Herzberg, Molecular Spectra and Molecular Structure IV. Constants of Diatomic Molecules p.490, Van Nostrand Reinhold, New York, 1979.

[48] R. Hernández, R. Toumi, D. Clary, State-selected vibrational relaxation rates for highly vibrationally excited oxygen molecules, J. Chem. Phys. 9544 (1995) 9544.

[49] K. Nozawa, N. Shima, K. Makoshi, Theoretical Study of Structures of Solid Oxygen under High Pressure, J. Phys. Soc. Jpn. 71 (2002) 377.

[50] G. Ewing, Structure and properties of van der Waals molecules, Acc. Chem. Res. 1511 (1975) 1969.

[51] E. Hult, H. Rydberg, B. Lundqvist, D. Langreth, Unified treatment of asymptotic van der Waals forces, Phys. Rev. B 59 (1999) 4708.

[52] B. Bussery, P. E. S. Wormer, A van der Waals intermolecular potential for $(O_2)_2$, J. Chem. Phys. 99 (1993) 1230.

[53] I. Goncharenko, O. Makarova, L. Ulivi, Direct Determination of the Magnetic Structure of the Delta Phase of Oxygen, Phys. Rev. Lett. 93 (2004) 055502.

[54] T. Nomura, Y. Matsuda, S. Takeyama, A. Matsuo, K. Kindo, J. Her, T. Kobayashi, Novel Phase of Solid Oxygen Induced by Ultrahigh Magnetic Fields, Phys. Rev. Lett. 112 (2014) 247201.

[55] F. Tran, J. Hutter, Nonlocal van der Waals functionals: the case of rare-gas dimers and solids, J. Chem. Phys. 138 (2013) 204103.

[56] K. Rościszewski, B. Paulus, P. Fulde, H. Stoll, *Ab initio* coupled-cluster calculations for the fcc and hcp structures of rare-gas solids, Phys. Rev. B 62 (2000) 5482.

[57] O. Peterson, D. Batchelder, R. Simmons, Measurements of X-ray lattice constant, thermal expansivity, and isothermal compressibility of argon crystals, Phys. Rev. 60 (1966) 703.

[58] L. A. Schwalbe, R. K. Crawford, H. H. Chen, R. A. Aziz, Thermodynamic consistency of vapor pressure and calorimetric data for argon, krypton, and xenon, J. Chem. Phys. 66 (1977) 4493.

[59] J. Wittlinger, R. Fischer, S. Werner, J. Schneider, H. Schulz, High-Pressure Study of h.c.p. -Argon, Acta Cryst. B 53 (1997) 745.

[60] T. Ishikawa, M. Asano, N. Suzuki, K. Shimizu, Superconductivity of compressed solid argon from first principles, Phys. Rev. B 91 (2015) 064512.

[61] S. Lebègue, J. Harl, T. Gould, J. G. Ángyán, G. Kresse, J. F. Dobson, Cohesive Properties and Asymptotics of the Dispersion Interaction in Graphite by the Random Phase Approximation, Phys. Rev. Lett. 105 (2010) 196401.

[62] T. Björkman, A. Gulans, A. V. Krasheninnikov, R. M. Nieminen, van der Waals Bonding in Layered Compounds from Advanced Density-Functional First-Principles Calculations, Phys. Rev. Lett. 108 (2012) 235502.

[63] K. Berland, P. Hyldgaard, Exchange functional that tests the robustness of the plasmon description of the van der Waals density functional, Phys. Rev. B 89 (2014) 035412.

[64] Y. Baskin, L. Meyer, Lattice Constants of Graphite at Low Temperatures, Phys. Rev. 253 (1955) 1953.

[65] R. Zacharia, H. Ulbricht, T. Hertel, Interlayer cohesive energy of graphite from thermal desorption of polyaromatic hydrocarbons, Phys. Rev. B 69 (2004) 155406.

[66] K. Lee, É. D. Murray, L. Kong, B. I. Lundqvist, D. C. Langreth, Higher-accuracy van der Waals density functional, Phys. Rev. B 82 (2010) 081101.

[67] I. Hamada, M. Otani, Comparative van der Waals density-functional study of graphene on metal surfaces, Phys. Rev. B 82 (2010) 153412.

[68] R. E. Mapasha, a. M. Ukpong, N. Chetty, *Ab initio* studies of hydrogen adatoms on bilayer graphene, Phys. Rev. B 85 (2012) 205402.

[69] G. Graziano, J. Klimeš, F. Fernandez-Alonso, A. Michaelides, Improved description of soft layered materials with van der Waals density functional theory, J. Phys. Condens. Matter 24 (2012) 424216.

[70] P. Lazić, N. Atodiresei, M. Alaei, V. Caciuc, S. Blügel, R. Brako, *JuNoLo* – Jülich nonlocal code for parallel post-processing evaluation of vdW-DF correlation energy, Comput. Phys. Commun. 181 (2010) 371.

[71] M. Callsen, N. Atodiresei, V. Caciuc, S. Blügel, Semiempirical van der Waals interactions versus ab initio nonlocal correlation effects in the thiophene-Cu(111) system, Phys. Rev. B 86 (2012) 085439.

[72] H. Swanson, N. T. Gilfirch, G. Ugrinic, National Bureau of Standerds Circular 539, Vol. 5, U. S. Government Printing Office, Washington, D. C., 1955.

[73] P. Cherin, P. Unger, The Crystal Structure of Trigonal Selenium, Inorg. Chem. 6 (1967) 1589.

[74] A. D. Corso, R. Resta, Density-functional theory of macroscopic stress: Gradient-corrected calculations for crystalline Se, Phys. Rev. B 50 (1994) 4327.

[75] G. Kresse, J. Furthmüller, J. Hafner, Theory of the crystal structures of selenium and tellurium: The effect of generalized-gradient corrections to the local-density approximation, Phys. Rev. B 50 (1994) 13181.

[76] T. BucÌko, J. Hafner, Improved description of the structure of molecular and layered crystals: ab initio DFT calculations with van der Waals corrections, J. Phys. Chem. A 114 (2010) 11814.

[77] O. Sode, M. Keçeli, K. Yagi, S. Hirata, Fermi resonance in solid CO_2 under pressure, J. Chem. Phys. 138 (2013) 074501.

[78] A. Simon, K. Peters, Single-crystal refinement of the structure of carbon dioxide, Acta Cryst. B 2 (1980) 112750.

[79] A. Otero-de-la Roza, E. R. Johnson, A benchmark for non-covalent interactions in solids, J. Chem. Phys. 137 (2012) 054103.

[80] S. Bonev, F. Gygi, T. Ogitsu, G. Galli, High-Pressure Molecular Phases of Solid Carbon Dioxide, Phys. Rev. Lett. 91 (2003) 065501.

[81] I. Hamada, unpublished (2013).

[82] R. Meier, R. Helmholdt, Neutron-diffraction study of α-and β-oxygen, Phys. Rev. B 29 (1984) 1387.

[83] M. Santoro, F. Gorelli, L. Ulivi, R. Bini, H. Jodl, Antiferromagnetism in the high-pressure phases of solid oxygen: Low-energy electronic transitions, Phys. Rev. B 64 (2001) 064428.

[84] S. Klotz, T. Strässle, A. L. Cornelius, J. Philippe, T. Hansen, Magnetic Ordering in Solid Oxygen up to Room Temperature, Phys. Rev. Lett. 104 (2010) 115501.

[85] F. Mittendorfer, A. Garhofer, J. Redinger, J. Klimeš, J. Harl, G. Kresse, Graphene on Ni(111): Strong interaction and weak adsorption, Phys. Rev. B 84 (2011) 201401.

[86] P. L. Silvestrelli, A. Ambrosetti, van der Waals corrected DFT simulation of adsorption processes on transition-metal surfaces: Xe and graphene on Ni(111), Phys. Rev. B 91 (2015) 195405.

[87] M. Obata, I. Hamada, T. Oda, First principles study on solid oxygen using van der Waals density functional, Phys. Procedia 75 (2015) 771.

[88] Y. Wang, J. P. Perdew, Spin scaling of the electron-gas correlation energy in the high-density limit, Phys. Rev. B 43 (1991) 8911.

[89] M. Callsen, I. Hamada, Assessing the accuracy of the van der Waals density functionals for rare-gas and small molecular systems, Phys. Rev. B 91 (2015) 195103.

[90] Y. Freiman, H. Jodl, Solid oxygen, Phys. Rep. 401 (2004) 1.

[91] I. Goncharenko, Evidence for a Magnetic Collapse in the Epsilon Phase of Solid Oxygen, Phys. Rev. Lett. 94 (2005) 205701.

[92] K. Katsumata, S. Kimura, U. Staub, Y. Narumi, Y. Tanaka, S. Shimomura, T. Nakamura, S. W. Lovesey, T. Ishikawa, H. Kitamura, The giant magneto-volume effect in solid oxygen, J. Phys. Condens. Matter 17 (2005) L235.

[93] A. Filippetti, C. D. Pemmaraju, S. Sanvito, P. Delugas, D. Puggioni, V. Fiorentini, Variational pseudo-self-interaction-corrected density functional approach to the *ab initio* description of correlated solids and molecules, Phys. Rev. B 84 (2011) 195127.

[94] K. Ullakko, J. K. Huang, C. Kantner, R. C. O'Handley, V. V. Kokorin, Large magnetic-field-induced strains in Ni_2MnGa single crystals, Appl. Phys. Lett. 69 (1996) 1966.

[95] O. Velikokhatnyi, I. Naumov, Electronic structure and instability of Ni_2MnGa, Phys. Solid State 41 (1999) 617.

[96] S. Özdemir Kart, M. Uludoğan, I. Karaman, T. Çağin, DFT studies on structure, mechanics and phase behavior of magnetic shape memory alloys: Ni_2MnGa, Phys. Stat. Sol. 205 (2008) 1026.

[97] N. Xu, J.-M. Raulot, Z. Li, J. Bai, Y. Zhang, X. Zhao, L. Zuo, C. Esling, Oscillation of the magnetic moment in modulated martensites in Ni_2MnGa studied by ab initio calculations, Appl. Phys. Lett. 100 (2012) 084106.

[98] M. Cococcioni, S. de Gironcoli, Linear response approach to the calculation of the effective interaction parameters in the LDA + U method, Phys. Rev. B 71 (2005) 035105.

[99] B. Himmetoglu, V. M. Katukuri, M. Cococcioni, Origin of magnetic interactions and their influence on the structural properties of Ni_2MnGa and related compounds, J. Phys. Condens. Matter 24 (2012) 185501.

[100] S. J. J. Clark, M. D. Segall, C. J. J. Pickard, P. J. J. Hasnip, M. I. J. Probert, K. Refson, M. C. Payne, First principles methods using CASTEP, Zeitschrift für Krist. 220 (2005) 567.

Publication

Referee reading : First author

- Masao Obata, Makoto Nakamura, Ikutaro Hamada, and Tatsuki Oda "Implementation of van der Waals Density Functional Approach to the Spin-Polarized System: Interaction Potential between Oxygen Molecules" J. Phys. Soc. Jpn. 82 (2013) 093701.

- Masao Obata, Makoto Nakamura, Ikutaro Hamada, and Tatsuki Oda "Improving the Description of Nonmagnetic and Magnetic Molecular Crystals via the van der Waals Density Functional" J. Phys. Soc. Jpn. 84 (2015) 024715.

- Masao Obata, Ikutaro Hamada, and Tatsuki Oda, "Molecular Interactions for Modeling of Oxygen System Using van der Waals Density Functional Approach" JPS Conference Proceedings 5 (2015) 011011(1-7). Proceedings of Computational Science Workshop 2014 (CSW2014).

- Masao Obata, Ikutaro Hamada, and Tatsuki Oda, "First principles study on solid oxygen using van der Waals density functional", Physics Procedia 75 (2015) 771-778 . Proceedings of ICM 2015(20th International Conference on Magnetism).

Referee reading : Collaborative works

- Indra Gunawan, Masao Obata, Makoto Nakamura, Muhamad A. Martoprawiro, and Tatsuki Oda "Implementation of Parallel Matrix Diagonalization for Ab-Initio Molecular Dynamics Program using ScaLAPACK" Recent Development in Computational Science (ISSN 2223-0785), 4 (2013) 39-43.

- Nurul Ikhsan, Yuusaku Taguchi, Masao Obata, Makoto Nakamura, Suprijadi, and Tatsuki Oda "Magnetic, structural, and electronic properties of Co doped Fe/MgO

interface: Density functional approach" Recent Development in Computational Science (ISSN 2223-0785), 4 (2013) 95-104.

- Sasfan Arman Wella, Makoto Nakamura, Masao Obata, Suprijadi, and Tatsuki Oda "Tight-Binding Molecular Dynamics with Fermi Operator Expansion: Application to Vacancy Defects in Silicon" Recent Development in Computational Science (ISSN 2223-0785), 4 (2013) 145-154.

- Makoto Nakamura, Masao Obata, Tetsuya Morishita, and Tatsuki Oda "An ab initio approach to free-energy reconstruction using logarithmic mean force dynamics" J. Chem. Phys. 140 (2014) 184110(1-10).

- Daiki Yoshikawa, Masao Obata, Yusaku Taguchi, Shinya Haraguchi, and Tatsuki Oda "Possible origin of non-linear magnetic anisotropy variation in electric field effect in a double interface system" App. Phys. Express 7 (2014) 113005(1-4).

- Daiki Yoshikawa, Masao Obata, and Tatsuki Oda "First-principles study on structural and electronic properties in Fe/MgO double interface" JPS Conference Proceedings 5 (2015) 011012(1-7). Proceedings of Computational Science Workshop 2014 (CSW2014).

- Naoshiro Kitagawa, Masao Obata, and Tatsuki Oda "Density functional study on positively charged six-coordinate FeO_2 porphyrin complex for a trigger of O_2 dissociation" Chem. Phys. Let. 643 (2016) 119.

- Mohamed Belmoubarik, Muftah Al-Mahdawi, Masao Obata, Daiki Yoshikawa, Hideyuki Sato, Tomohiro Nozaki, Tatsuki Oda, and Masashi Sahashi "Tunneling electroresistance of MgZnO-based tunnel junctions" submitted for publication (2016).

Presentation

Oral Presentations on International Conference

- Masao Obata, Ikutaro Hamada, Tatsuki Oda, ”Implementation and application of van der Waals density functional to the systems of oxygen molecules” E-MRS (European Materials Research Society) 2014 Fall Meeting 15th-19th September Warsaw Poland (Oral presentation, Symposium K 3-2)

- Masao Obata, Ikutaro Hamada, Tatsuki Oda, ”Non-empirical Study on Oxygen Molecular and Crystal Systems Using Van der Waals Density Functional Approach” International Symposium on Computational Science 2015 (17-18th February 2015), Kanazawa University, Kanazawa (Japan), 17th February 2015 (Oral presentation, 17th Morning session 2-4)

- Masao Obata, Ikutaro Hamada, Tatsuki Oda, ”Effects of van der Waals force and electron correlation in molecular crystals” International Symposium on Computing Energy Landscape in Material Science and particles Physics (ISCEL-MS&PP) (19th -20th February 2016), Kanazawa University, Kanazawa (Japan), (Oral presentation, First Session-4)

Poster Presentations on International Conference

- Masao Obata, Ikutaro Hamada, Tatuki Oda, ”Non-empirical Study on Oxygen Molecular Systems Using Van der Waals Density Functional Approach” Computational Science Workshop August20th - 22th, 2014 Epocal Tsukuba, (Poster Presentation No. PA-32)

- Masao Obata, Ikutaro Hamada, Tatsuki Oda, ”First principles study on solid oxygen using van der Waals density functional” Poster Presentation Paper number:

1033.00 TH.C-P59 ICM 2015(20th International Conference on Magnetism), (5-10th July 2015) Barcelona, Spain

Oral Presentations on Domestic Conference

- 小幡正雄、中村慎、濱田幾太郎、小田竜樹、「 ファン・デル・ワールス密度汎関数法の実装と分子複合体への応用」、日本物理学会 2013 年秋季大会、徳島大学常三島キャンパス、2013 年 9 月 27 日 (口頭発表、講演番号 27aDF-5)
- 小幡正雄、中村慎、濱田幾太郎、小田竜樹、「ファン・デル・ワールス密度汎関数法を用いた固体酸素の第一原理的研究」、日本物理学会第 69 回年次大会、東海大学湘南キャンパス、2014 年 3 月 28 日 (口頭発表、講演番号 28pAM-10)
- 小幡正雄、中村慎、濱田幾太郎、小田竜樹、「ファン・デル・ワールス密度汎関数法を用いた固体酸素の第一原理的研究 II」、日本物理学会第 69 回秋季大会、中部大学春日井キャンパス、2014 年 9 月 7 日 (口頭発表、講演番号 7aAL-5)
- 小幡正雄、濱田幾太郎、小田竜樹、 「ファン・デル・ワールス密度汎関数法を用いた固体酸素の圧力依存性」、日本物理学会第 70 回年次大会、日本物理学会 2015 年秋季大会関西大学千里山キャンパス、 2015 年 9 月 18 日 (口頭発表、講演番号 18pAF-1)

Poster Presentations on Domestic Conference

- 小幡正雄、中村慎、濱田幾太郎、小田竜樹「ファン・デル・ワールス密度汎関数に基づく電子状態計算手法の実装」、文部科学省科学研究費新学術領域研究「コンピューティクスによる物質デザイン:複合相関と非平衡ダイナミクス」平成 25 年度第 1 回研究会、ポスター番号 P39、東京大学本郷キャンパス武田先端知ビル、 2013 年 7 月 8 日
- 小幡正雄、中村慎、濱田幾太郎、小田竜樹「ファン・デル・ワールス密度汎関数の磁性物質への適応」 第 7 回物性科学領域横断研究会凝縮系科学の最前線、ポスター番号 P2-1、東京大学本郷キャンパス武田先端知ビル 2013 年 12 月 1 日
- 小幡正雄、中村慎、濱田幾太郎、小田竜樹「ファン・デル・ワールス密度汎関数の磁性物質への適応」、 物性件スパコン共同利用・CMSI 合同研究会「計算物質科学の

過大と展望」、ポスター番号 P-29、東京大学柏キャンパス物性研究所大講義室 2013 年 12 月 11 日

- 小幡正雄、北川直裕、吉川大輝、 ヌルルーイクサン、中野博斗、小田竜樹「スピントロニクス材料界面ノ磁気異方性、電子状態、超並列計算」、第 6 回 計算物質科学イニシアティブ CMSI 研究会、ポスター番号 P-33、東京大学 本郷キャンパス 小柴ホール、 2015 年 12 月 7 日-8 日

Acknowledgements

The finishing of my doctoral study would have not been possible without the support of many people, especially, my supervisor Prof. Tatsuki Oda and collaborator Dr. Ikutaro Hamada. I express my sincere thanks to them for coaching and helping to my research. Thanks to their powerful guidance and much discussion, I was able to finish the my doctoral study on time. I would like to acknowledge all the professor in computational science department, especially, Mineo Saito, Masahide Sato, Shinichi Miura and Fumiyuki Ishii, for fruitful discussions and benefit advices. I gratefully acknowledge the support of my current and previous members of our laboratory. I acknowledge JSPS Research Fellowships for Young Scientists (Grant No. 27-4610). I want to thank all of the people who have been involved with me.